POLITECNICO DI MILANO

School of Industrial and Information
Engineering Master of Science in Materials
Engineering & Nanotechnology
Chemistry, Materials and Chemical Engineering Department "Giulio Natta"

Fluorinated liposome nanovector for ^{19}F-MRI and gene delivery applications

Supervisor: Prof. Francesca BALDELLI BOMBELLI
Co-supervisor: Dr. Giulia NERI

Master Thesis of:

Mani Nivedha
ID 899233

Academic Year 2018 - 2019

Table of Contents

Table of Contents

List of Figures

List of Figures

List of Figures

List of Figures

Abstract

Micro ribonucleic acid (miRNA) has recently emerged as a potential therapeutic tool for the treatment of a variety of human diseases such as cancer, cardiovascular disease, diabetes, mental disorder and viral infection. miRNA is a group of small, non-coding RNA molecules with 20-22 nucleotides in length that can control the activity of up to 30% of all protein-coding genes in mammals. When compared with other conventional therapeutics, it affords high specificity, resulting in improved efficacy and decreased side effects. However, many hurdles in effective clinical application, including low intracellular delivery and poor in vivo stability. These drawbacks can be improved by using lipids for nucleic acid delivery. Liposomes are spherical vesicles consisting of an aqueous core surrounded by a phospholipid bilayer, thus able to encapsulate hydrophobic molecules in the membrane. Because of polyanionic nature of miRNA, the cationic liposome (DOTAP) is used. Moreover, cationic liposomes are commonly employed in gene delivery due to their electrostatic interaction with oligonucleotides. Since cationic lipids are more toxic than zwitterionic, a formulation of cationic liposomes (DOTAP) with Zwitterionic liposomes employed for the preparation of positively charged liposomes to effectively transfer of miRNA into neuronal cells. The aim of this research work focuses on delivery of miRNA by using Cationic and Zwitterionic lipids in 3:7 molar ratio and be trackable by ^{19}F-MRI with the help of superfluorinated contrast agent called PERFECTA. ^{19}F-MRI used as a complementary diagnostic technique to ^{1}H-MRI. ^{19}F-MRI provides non-invasive in-depth in vivo detection, higher sensitivity, real-time response, and can be coupled to ^{1}H-MRI to provide selectively high-contrast images of the nanovector in vivo. Characterization was accomplished by Dynamic Light Scattering, ^{19}F- Nuclear Magnetic Resonance, Zeta Potential, Transmission Electron Cryomicroscopy and Small Angle X-ray Scattering. The result seems satisfactory with positive surface charge, and high ^{19}F atoms and excellent magnetic properties to be visible in ^{19}F-MRI.

Key words: cationic liposomes, ^{19}F-MRI, fluorinated contrast agents, mi-RNA

Abstract
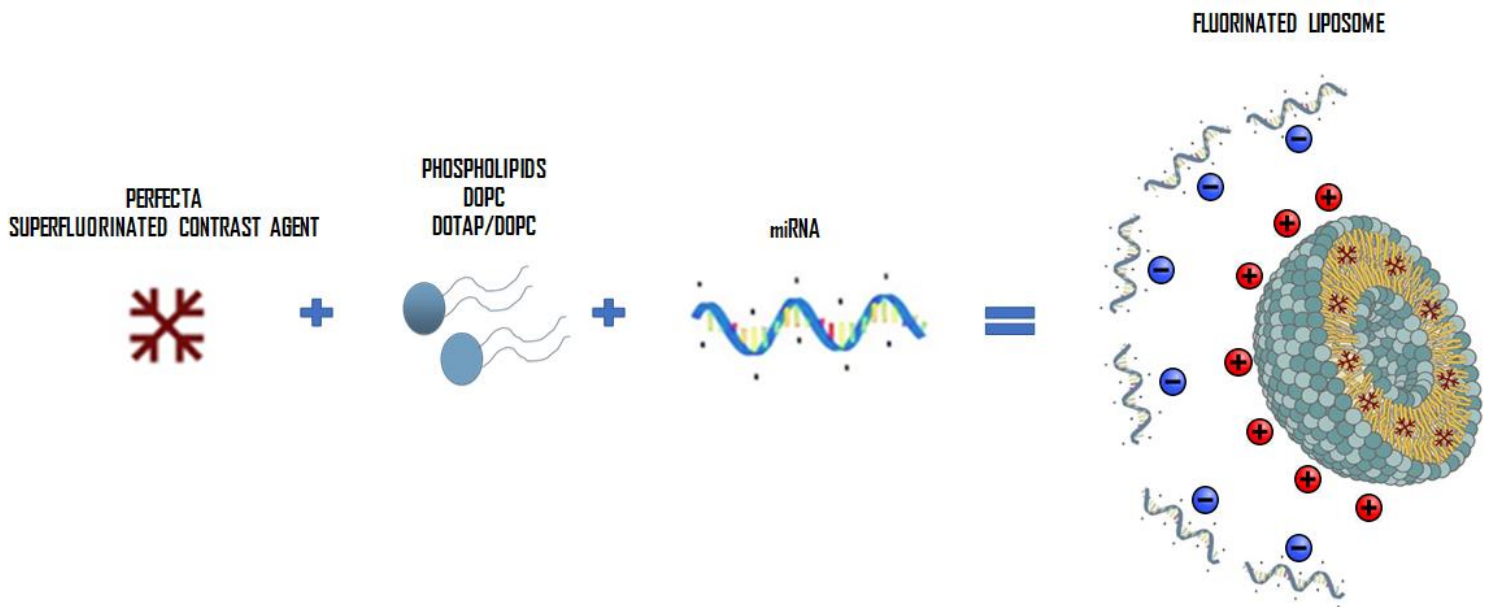
The schematic representation for effective delivery of miRNA with liposomal nanocarrier. The formation of fluorinated liposomes was prepared using a superfluorinated contrast agent and different lipid substrates.

Aim of the project

This research TRANS-ALS (2015-0023) project, funded by the "Fondazione Regionale Biomedica" is focused on the study of Amyotrophic Lateral Sclerosis (ALS) the most prevalent adult onset form of motor neuron disease. ALS is a fatal neurodegenerative disease; it is proved that miRNA as a biomarker to study the mechanism of neural differentiation in ALS. miRNA are small non-coding RNAs that bind to the complementary target sequences is altered in the ALS patients, thus miRNA is determined to have a new therapeutic approach to the disease. In this work, we synthesized a liposome nanocarrier which consist of a mixture of both neutral (DOPC) and cationic liposomes (DOTAP) with the molar ratio 3:7 to effectively transfer miRNA into neuronal cells and be trackable by ^{19}F-MRI with the help of superfluorinated contrast agent called PERFECTA, has high fluorine density, low toxicity, chemical stability which produces a single sharp NMR peak.

Liposomes are generally considered to be pharmacologically inactive with minimal toxicity, as they are composed of natural phospholipids (Koning and Storm, 2003; Metselaar and Storm, 2005; Ding et al., 2006; Hua and Wu, 2013). Liposomal formulations are characterized by properties such as particle size, charge, number of lamellae, lipid composition and surface modification- which govern their stability in vitro and in vivo. ^{19}F-MRI used as a complementary diagnostic technique to ^{1}H-MRI. ^{19}F-MRI provides non-invasive in-depth in vivo detection, higher sensitivity, real-time response, and can be coupled to ^{1}H-MRI to provide selectively high-contrast images of the nanovector in vivo. Future studies focus on the gene transfer property of developed liposomes into the neuronal cells.

1.1 Nanotechnology and Nanomedicine

"Nanotechnology is the understanding and control of matter at dimensions of roughly 1 to 100 nanometers, where unique phenomena enable novel applications. At this level the physical, chemical and biological properties of materials differ in fundamental and valuable ways from the properties of individual atoms and molecules or bulk matter". It has been shown that nanotechnology bridges the obstacle of biological and physical science by implementing nanostructures and nanophases in different areas of science [1]; particularly in nanomedicine and Nano-based drug delivery systems where particles are of significant interest [2, 3]. Nanomaterials can be well defined as material with dimensions varying from 1 to 100 nm, influencing the tissue engineering boundaries of nanomedicine beginning with biosensors, microfluidics, drug delivery and microarray testing [4, 5, 6]. Nanotechnology utilizes Nano-scale healing agents to produce nanomedicine. The field of biomedicine includes nanobiotechnology, drug delivery, nanoparticulated biosensors and tissue engineering [7]. Since nanoparticles consist of materials designed at the atomic or molecular level, they are usually nanospheres of small size [8]. Therefore, compared to larger products, they can move more freely in the human body.

Particles of nanoscale size have unique structural, chemical, mechanical, magnetic, electrical and biological characteristics. In latest times, nanomedicines have become well valued as nanostructures can be used as delivery agents by encapsulating drugs or by attaching therapeutic drugs and delivering them exactly with a controlled release to target tissues [9, 10]. Nanomedicine is an evolving area of application of nanoscience understanding and methods in medical biology and prevention and bioremediation of diseases. It involves the use of Nano-dimensional materials, including nanorobots, Nano sensors for diagnostic, delivery, and sensory purposes, and the action of materials in live cells (Figure 1.1). For Example: A technique based on nanoparticles has been created that combines both cancer diagnosis therapy and imaging modalities [11]. The first generation of treatment based on nanoparticles included lipid structures such as liposomes and micelles, now approved by the FDA [12]. There are inorganic nanoparticles such as gold or magnetic nanoparticles in these liposomes and micelles [13]. These characteristics allowed the use of inorganic nanoparticles to increase with

emphasis on drug delivery, imaging and therapeutic functions. Furthermore, nanostructures are reported to assist prevent the tarnishing of drugs in the gastrointestinal region and help deliver sparingly water-soluble drugs to their target place. Nanodrugs show greater oral bioavailability as they display typical absorptive endocytosis take-up processes.
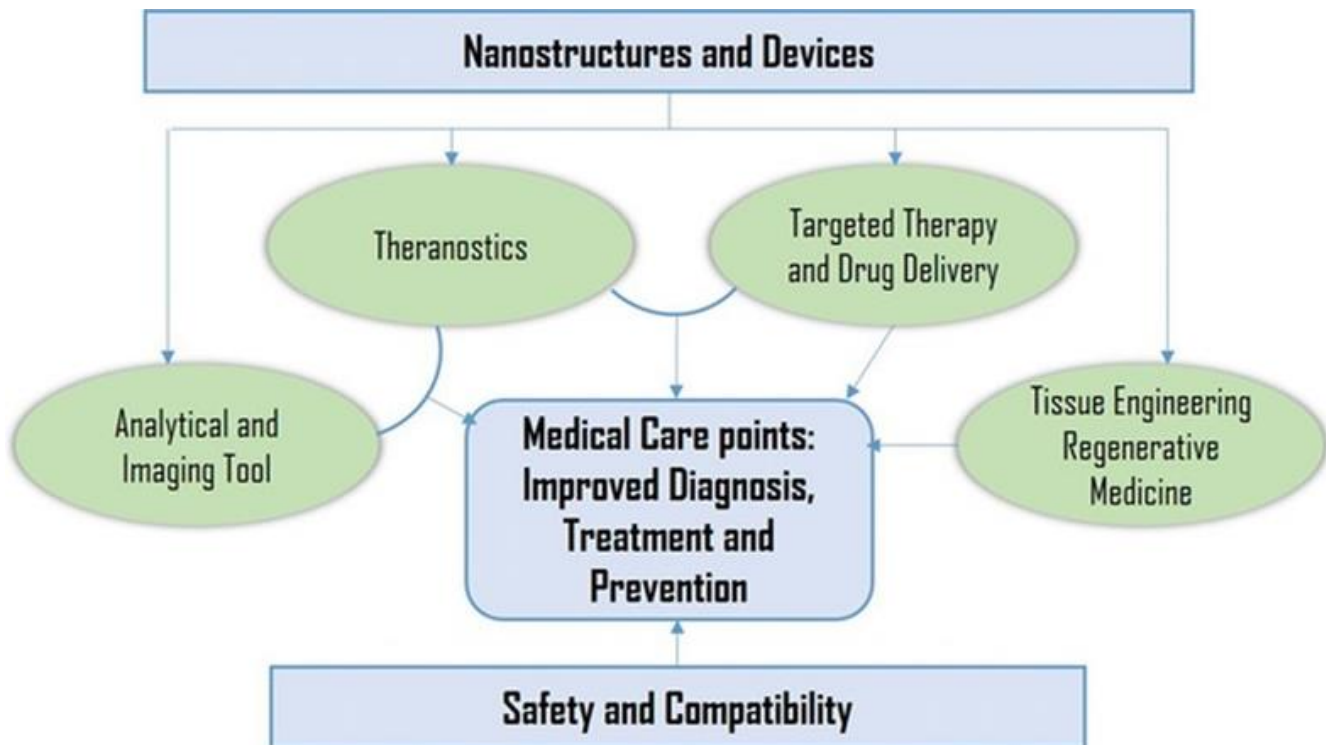
Figure 1.1: Application and goals of nanomedicine in different sphere of biomedical research [12]

Nanostructures remain in the circulatory system of the blood for a longer period and allow the drug to be released according to the dose specified. They thus have fewer negative effect-reducing plasma fluctuations [14]. Because they are nanosized structures, they can penetrate the tissue system, promote simple cell drug uptake, allow effective drug delivery, and guarantee action at the targeted place. Cell absorption of nanostructures is much greater than that of big particles of 1 to 10 μm size [7, 15]. Therefore, they communicate directly with enhanced effectiveness and decreased side effects to treat the diseased cells.

Due to their use in countless novel assays to treat and diagnose illnesses, nanoparticles have been discovered to be helpful in obtaining data at all clinical phases. These nanoparticles primary advantages relate to their surface characteristics; as different proteins can be attached to the surface. Au nanoparticles, for example, are used as biomarkers and tumor labels for various procedural tests for biomolecule detection.

In developing the target-specific drug delivery systems, metallic, organic, inorganic and polymeric nanostructures, including dendrimers, micelles, and liposomes are often regarded. In specific, these nanoparticles are marked with medicines with poor solubility with lower absorption capacity [7, 16]. However, the efficacy of these nanostructures as drug delivery vehicles varies depending on the size, shape, and other inherent biophysical/chemical characteristics. Very helpful in targeted drug delivery are compact lipid nanostructures and phospholipids including liposomes and micelles.

The use of the ideal Nano-drug delivery system is chosen mainly based on the biophysical and biochemical characteristics of the drugs chosen for treatment [17]. However, the use of nanomedicine cannot ignore issues such as the toxicity of nanoparticles. More lately, nanoparticles were mostly used to reduce toxicity problems in conjunction with natural products. Additionally, adjustments in the size, shape, hydrophobicity, and surface modifications of nanostructures may further improve these nanomaterials bioactivity. Thus, nanotechnology provides numerous advantages in the site-specific and targeted delivery of drugs in the treatment of human illnesses.

1.2 Gene delivery

Gene therapy is defined as the treatment of human disease by the transfer of genetic material into specific cells of the patient [18]. Advances in molecular biology and biotechnology, and the completion of the Human Genome Project, have led to the identification of numerous disease-causing genes. It is not difficult to envision treatment of genetic diseases such as hemophilia [19], muscular dystrophy [20] or cystic fibrosis [21] through replacement of errant genes within the affected cells. Gene therapies are also being developed for cardiovascular, neurological [22-24] and infectious dis-eases [25], wound healing [26] and cancer [27-29] by delivering genes to augment the naturally occurring proteins, to alter the expression of existing genes, or to produce cytotoxic proteins or prodrug-activating enzymes — for example, to kill tumor cells [30] or inhibit proliferation of endothelial cells to prevent restenosis [31]. Finally, it has been shown that expression of viral genes can result in immune responses, which has led to the concept of DNA vaccines [32]. Because of its broad potential, gene therapy has been heavily investigated during the past 15 years. The first clinical trial of gene therapy, for the treatment of severe combined immunodeficiency (SCID), was initiated in 1990 [33]. Gene therapy requires the identification of a therapeutic gene and transfer of that gene, often specifically to target cells, with high efficiency. Although short-term gene expression is enough for some applications, such as cancer therapies, long-term expression is needed for the treatment of chronic conditions, including most genetic diseases. For many applications it will be crucial to tightly regulate gene expression levels. Finally, one must obviously accomplish each of these tasks in a way that is safe for the patient. Both toxicity/pathogenicity of the delivery vehicle and immune responses to the treatment must be considered. A key limitation to development of human gene therapy remains the lack of safe, efficient and controllable methods for gene delivery [34].
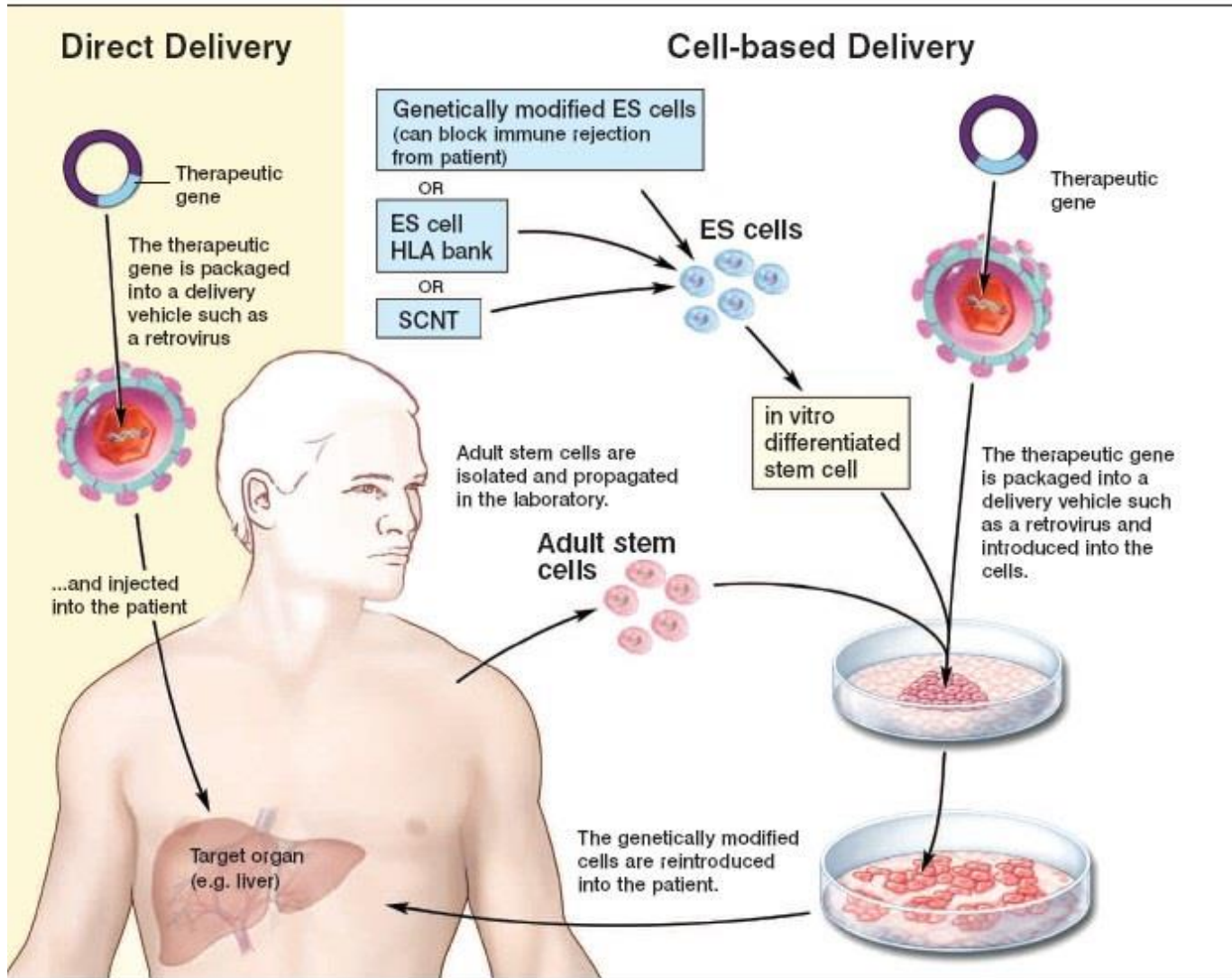
Figure 1.2: Strategies for delivering therapeutic transgenes into patients This figure illustrates the steps involved in direct delivery of a therapeutic transgene (left panel, in yellow) and for cell-based delivery of a therapeutic transgene (right panel). In direct delivery, the therapeutic gene is packaged into a delivery vehicle, such as a retrovirus, and injected into the patient. For cell-based delivery, the therapeutic genes are again packaged into a delivery vehicle [32].

1.2.1 Gene expression and regulation:

Gene expression is the process by which the genetic code - the nucleotide sequence - of a gene is used to direct protein synthesis and produce the structures of the cell. Genes that code for amino acid sequences are known as 'structural genes'. The process of gene expression involves two main stages:

- **Transcription:** the production of messenger RNA (mRNA) by the enzyme RNA polymerase, and the processing of the resulting mRNA molecule.
- **Translation**: the use of mRNA to direct protein synthesis, and the subsequent post-translational processing of the protein molecule.

10

Some genes are responsible for the production of other forms of RNA that play a role in translation, including transfer RNA (tRNA) and ribosomal RNA (rRNA).

A structural gene involves several different components:
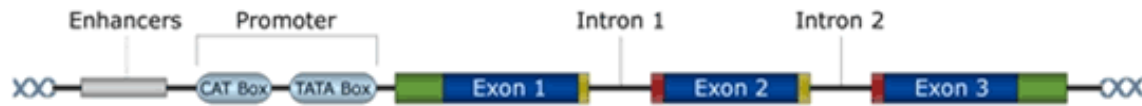
Figure 1.3: Gene structure which involves different components such as Introns, Exons, Promoters, Enhancers and Silencers [32].

- Exons: Exons code for amino acids and collectively determine the amino acid sequence of the protein product. It is these portions of the gene that are represented in final mature mRNA molecule.

- Introns: Introns are portions of the gene that do not code for amino acids and are removed (spliced) from the mRNA molecule before translation.

Gene control regions:

- **Start site**: A start site for transcription.

- **A promoter**: A region a few hundred nucleotides 'upstream' of the gene (toward the 5' end). It is not transcribed into mRNA but plays a role in controlling the transcription of the gene. Transcription factors bind to specific nucleotide sequences in the promoter region and assist in the binding of RNA polymerases.

- **Enhancers**: Some transcription factors (called activators) bind to regions called 'enhancers' that increase the rate of transcription. These sites may be thousands of nucleotides from the coding sequences or within an intron. Some enhancers are conditional and only work in the presence of other factors as well as transcription factors.

- **Silencers**: Some transcription factors (called repressors) bind to regions called 'silencers' that depress the rate of transcription.
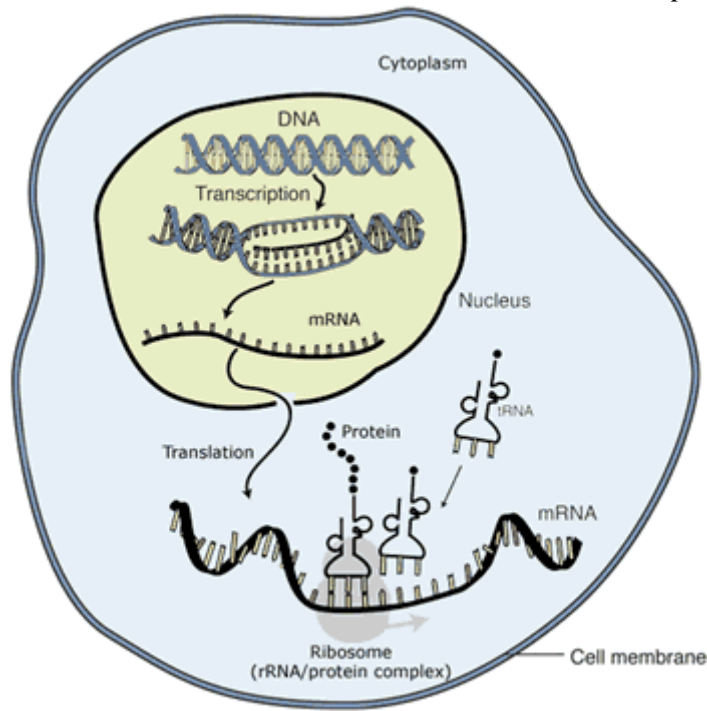
Figure 1.4: Transcription Process involving steps like Initiation, Elongation, Termination and Processing [32].

Transcription involves four steps:

1. **Initiation.** To shape a tiny open complex, the DNA molecule unwinds and divides. RNA polymerase connects the template strand promoter.

2. **Elongation.** RNA polymerase passes along the strand of the template to synthesize a molecule of mRNA. RNA polymerase is a holoenzyme made up of several subunits in prokaryotes, including a sigma factor (transcription factor) that recognizes the promoter. There are three RNA polymerases in eukaryotes: I, II and III. A proofreading mechanism is included in the process.

3. **Termination.** There are two methods of terminating transcription in prokaryotes. A protein factor called "Rho" is accountable for disrupting the complex comprising the template strand, polymerase RNA, and molecule RNA in Rho-dependent termination. A loop is formed at the end of the RNA molecule in Rho-independent termination, causing it to detach itself. Termination in eukaryotes is more complex, with extra adenine nucleotides being added to the RNA transcript 3' (a process called polyadenylation).

4. **Processing.** The RNA molecule is processed in various ways after transcription: introns are separated, and the exons spliced together to create a mature mRNA

consisting of a single protein-coding sequence. RNA synthesis involves the normal base pairing rules, but the base thymine is replaced with the base **uracil**.
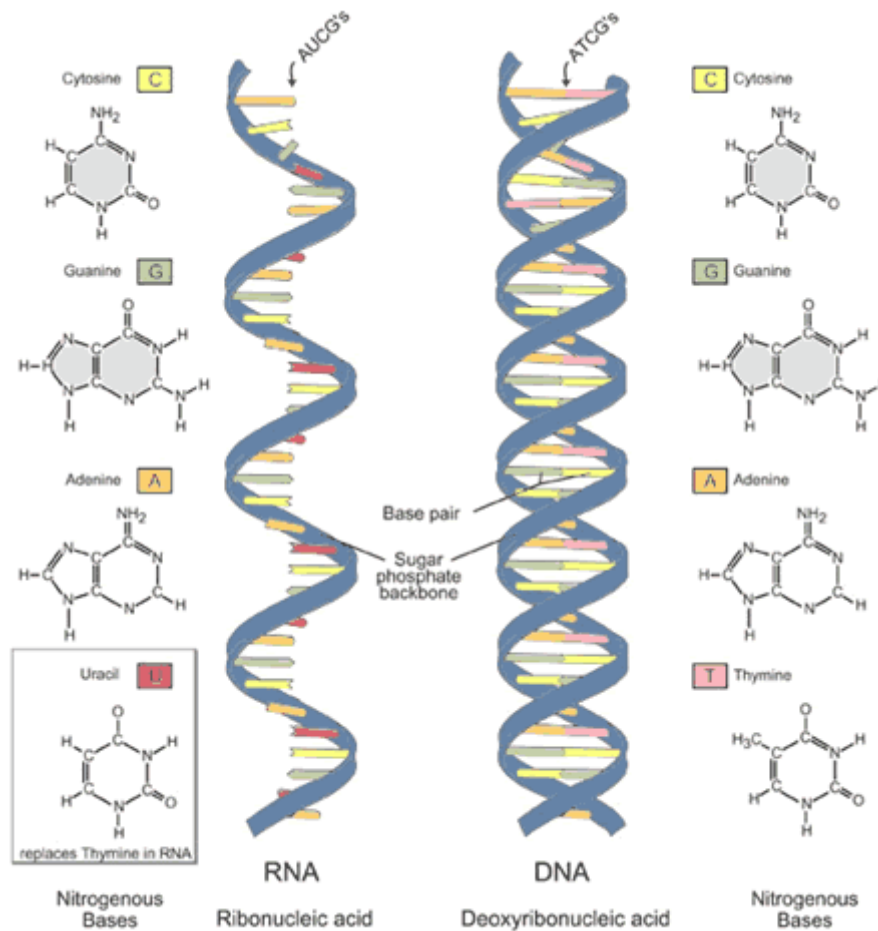
Figure 1.5: A Comparison of the Helix and Base Structure of RNA and DNA. They are both linear polymers, consisting of sugars, phosphates and bases, but there are some key differences which separate the two [34]**.**

Translation:

The mature mRNA molecule is used as a template in translation to assemble a series of amino acids to create a polypeptide with a sequence of amino acids. The complex that happens in the cytoplasm is called a ribosome. Ribosomes are a combination of ribosomal and ribosomal RNA (rRNA) proteins, consisting of a large subunit and a small subunit.
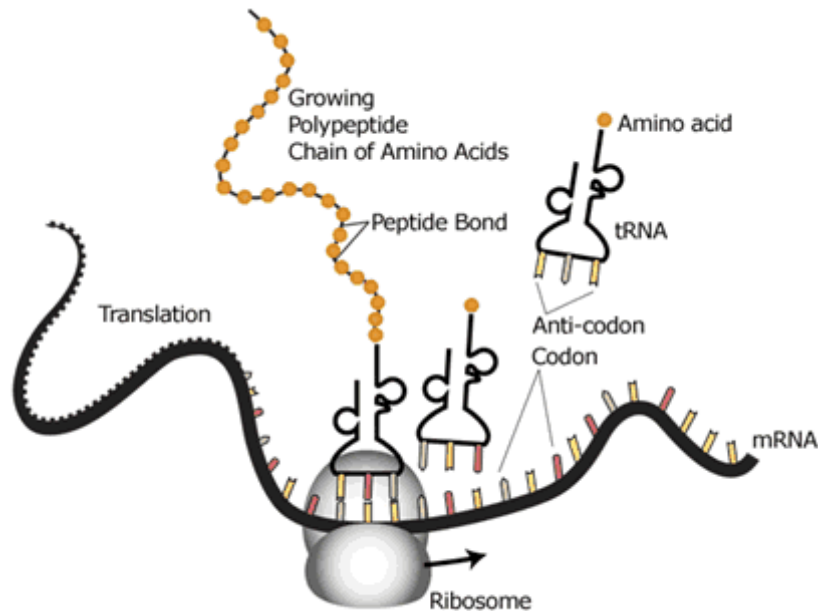
Figure 1.6: Translation Process which involves Initiation, Elongation, Termination and Post-translation process [34].

Four steps are involved in translation:

- Initiation. At the 5' end of the mRNA molecule, the ribosome's tiny subunit connects and moves in a 3' direction until it meets a start codon (AUG). It then forms a complex with the ribosome complex's big unit and a molecule of tRNA initiation.

- Elongation. Following codons on the mRNA molecule determine which amino acid-connected tRNA molecule connects to the mRNA. An enzyme peptidyl transferase uses peptide bonds to link the amino acids together. The method continues to produce an amino acid chain as the ribosome moves along the molecule of the mRNA.

- Termination. Once the ribosomal complex has achieved one or more stop codons

- Post-translation processing of the protein

Gene regulation:

Gene regulation is a label for the cellular processes that control the rate and manner of gene expression. A complex set of interactions between genes, RNA molecules, proteins (including transcription factors) and other components of the expression system determine when and where specific genes are activated, and the amount of protein or RNA product produced. Some genes are expressed continuously, as they produce proteins involved in basic metabolic functions; some genes are expressed as part of the process of cell differentiation; and some genes are expressed as a result of cell differentiation.

Mechanisms of gene regulation include:

- Regulating the rate of transcription. This is the most economical method of regulation.

- Regulating the processing of RNA molecules, including alternative splicing to produce more than one protein product from a single gene.

- Regulating the stability of mRNA molecules.

- Regulating the rate of translation.

Transcription factors are proteins that play a role in regulating the transcription of genes by binding to specific regulatory nucleotide sequences.

1.2.1.1 miRNA biogenesis and potential biomarker for ALS:

Amyotrophic lateral sclerosis (ALS) is one of the most prevalent adult onset form of motor neuron disease. As a result of progressive death of motor neurons in the primary motor cortex, brainstem and spinal cord, there is atrophy of muscles that are innervated by these neurons. This results in the muscle weakness and paralysis with death usually occurring within 3–5 years. Over the last decade, significant progress has been made in identifying the genes responsible for familial cases of ALS (fALS). Of these, the most frequently mutated genes are chromosome 9 open reading frame 72 (C9orf72), superoxide dismutase 1 (SOD1), TAR DNA-binding protein 43 (TARDBP; TDP-43), and FUS RNA binding protein (FUS), accounting for over 70% of fALS cases [35]. Nevertheless, fALS constitutes approximately 10% of all the cases, with the genetic

underpinnings of sporadic ALS (sALS) mostly unknown, though C9orf72 is known to account for 5% of sALS cases. In the last years, research has been focused on the identification of potential biological markers to use in the diagnostic procedure and clinical practice.

Recently, among the different categories of potential biomarkers, miRNAs have aroused great interest in several fields of research. miRNAs are short (about 22 nucleotides in length) non-coding RNA molecules that play an important role as endogenous regulators of gene expression acting at the post-transcriptional level. miRNAs are synthesized from the primary miRNAs, which are transcribed in the nucleus. Primary miRNAs are processed into pre-miRNAs by Drosha and then exported to the cytoplasm. Pre-miRNAs are eventually processed by the Dicer complex, resulting in mature miRNAs, which form RNA-induced silencing complexes [36]. miRNAs have a tissue-specific expression and this knowledge can help to better understand a normal and a disease development of the respective tissue [37]. miRNAs are known to play important roles in many physiological and pathological processes, including tumorigenesis [38], metabolism [39], immune function [40], and several neurodegenerative disorders [41], such as Parkinson's disease, Alzheimer's disease, Huntington's disease [42] and ALS [43].
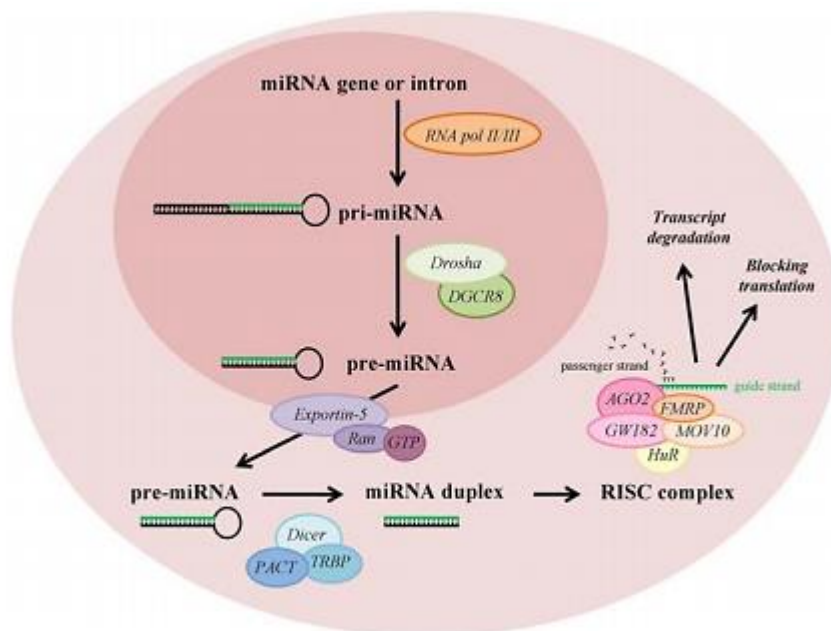
Figure 1.7: MiRNA biogenesis. The biogenesis process of miRNAs starts in the nucleus with the formation of pri-miRNA. This pri-miRNA is processed by Drosha and transported in the cytoplasm by Exportin-5. In the cytoplasm, Dicer binds premiRNA, forming the miRNA duplex. At this point, the guide strand of the duplex is incorporated into the RISC complex, whereas the other strand is typically degraded [36].

One class of molecules increasingly investigated as the potential biomarkers are short ncRNA species (those under 100 nucleotides long), which include tRNA, rRNA, piwi-RNA (piRNA), and microRNA (miRNA). MiRNA have been the main focus of most studies to date, driven by a good understanding of their biogenesis and function, high specificity, an ease in profiling their expression with a range of techniques including microarray, RNA-seq, and RT-qPCR, a relatively simple structure, increased stability from RNase degradation and freeze-thaw cycles, and a presence in a range of biofluids including blood, cerebrospinal fluid (CSF), and urine [44,45]. To date, several studies have shown that miRNAs are differentially expressed (downregulated) in ALS patients when compared to controls in a variety of biofluids, including CSF, and in the blood-derived components plasma and serum [46-60]. Thus, miRNA is proved to be a promising biomarker for ALS early diagnosis.

	qRT-PCR	Microarray	NGS	nCounter
Sensitivity	+++	+/++	++	++
Specificity	+++	+/++	+++	++
Throughput	+/++	+++	+++	++
Identification of novel miRNAs	no	no	yes	no
Validation data	no	yes	yes	yes
Normalization	yes	no	no	yes
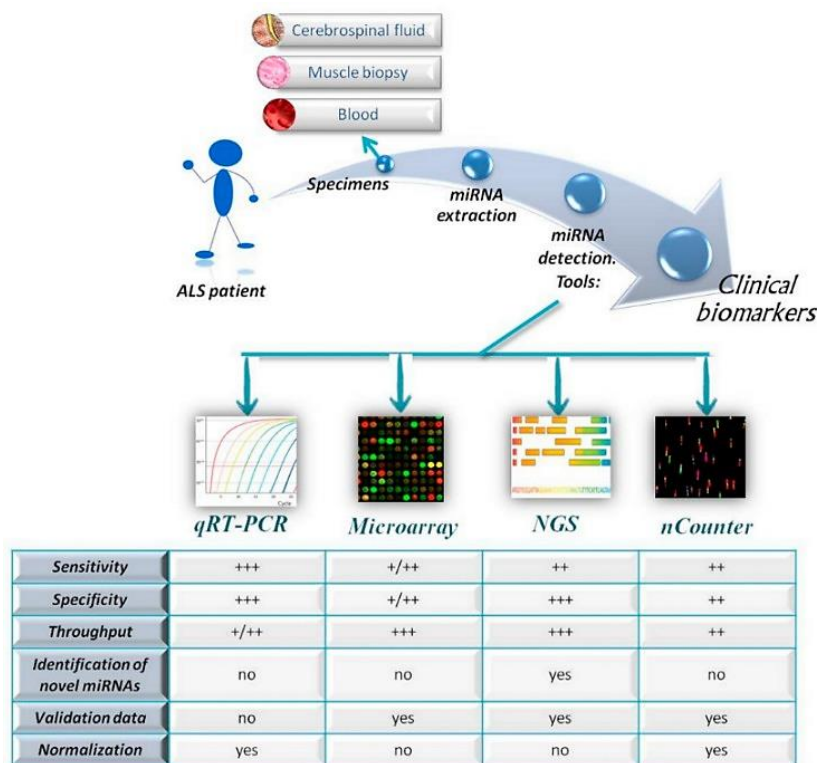
Figure 1.8: MicroRNA (miRNA)-based biomarkers in amyotrophic lateral sclerosis (ALS) patients. Schematic workflow to identify possible miRNAs as biomarkers starting from ALS patients' sample using different quantitative approaches. The comparison among the common characteristics of miRNA detection platforms is summarized in the figure. Sensibility, specificity and throughput are classified as follows: +++ (very high), ++ (moderate), +/++ (moderate to low) and + (low). Abbrevations: qRT-PCR, quantitative Real-Time Polymerase Chain Reaction; NGS, Next Generation Sequencing [46].

1.2.2 Gene transfer nanovesicles

Gene therapy is done using vectors like viral vectors and non-viral vectors, in spite of significant successes with viral vectors in nucleic acid delivery, several chemical non-viral methods are currently being explored. This is because viral vectors (lentivirus, retrovirus, adenovirus) are associated with risk of adverse immune effects and insertional mutagenesis. Considerable progress has also been achieved in non-viral delivery using physical methods (iontophoresis, electroporation, nucleofection, gene gun) with the advantage of low immunogenicity and toxicity [35]. However, physical methods are also associated with low expression efficiency which limits their use. In recent years, nanotechnology-based chemical methods have received increasing attention for achieving the delivery of nucleic acid [11].
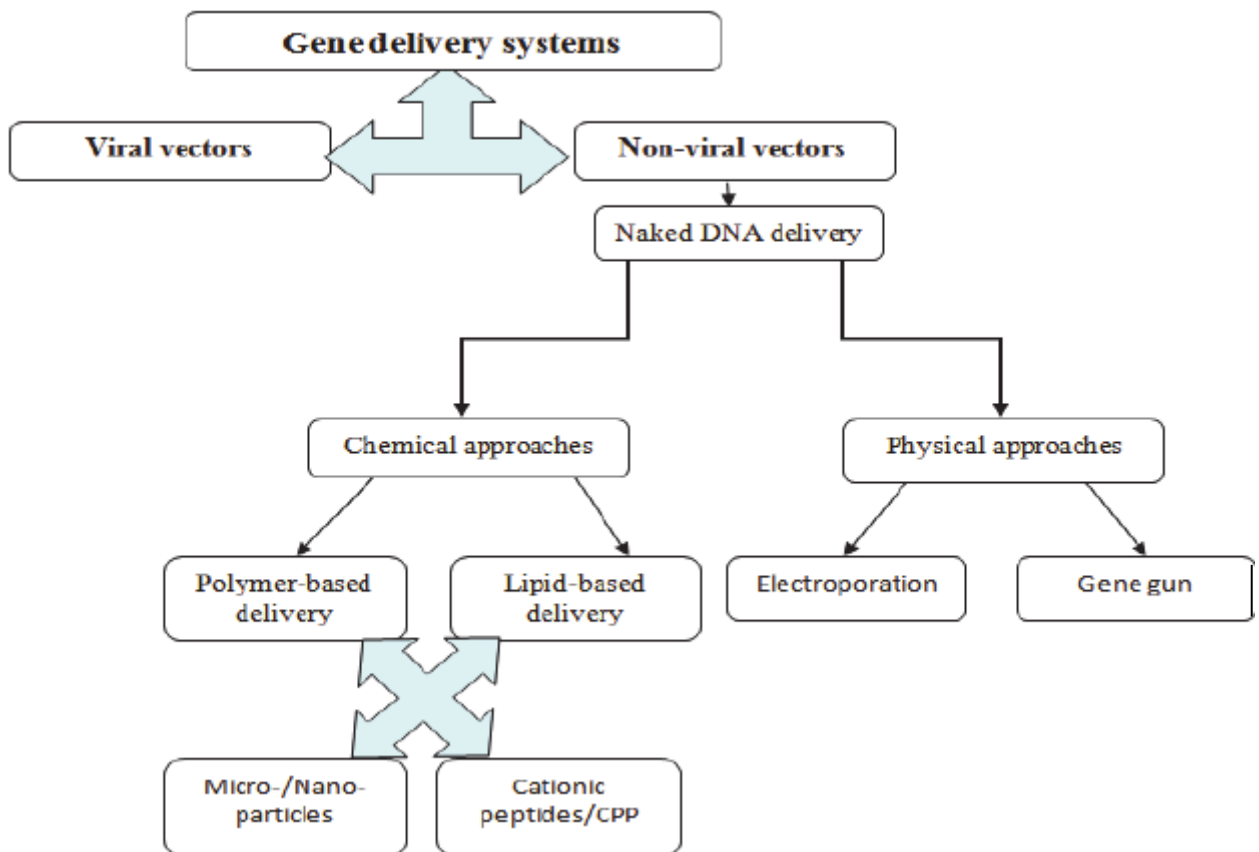
Figure 1.9: Summary of the main methods of gene delivery systems using viral and a non-viral vector [11].

Nanocarriers have high gene-carrying capacity, low risk of immunogenicity, and relatively low cost. These nanocarriers termed as "Nano-vectors" can be thought of as completely "synthetic viruses" whose composition is well defined and completely controlled (unlike actual viral vectors). Several Nano-vectors have been developed to enhance the delivery of nucleic acids [11]. The formation of complex between nucleic acid and the Nano-vector is based on electrostatic interaction between negatively charged nucleic acid at physiological pH and cationic Nano-vector. The positive surface charge of the Nano-vector facilitates its attachment to the cell surface and subsequent endocytosis. The cationic lipids in the form of liposomes [36] and lipid nanoparticles [37], cationic polymers are in the form of micelles [39], polyplexes [40] and polymeric nanoparticles [41] peptides as compacted DNA nanoparticles [42] and dendrimers [43] have improved the cellular uptake of nucleic acids with variable success *in vitro* and *in vivo*.

Viral vector	Genetic material	Advantages	Disadvantages
Retroviral vectors	dsRNA	Insert capacity for transgene <7–8kb Stable integration into host DNA Low immunogenicity Broad cell tropism of infectivity Prolonged expression	Difficult targeting of viral infection Transfect only proliferating cells Concern of insertional mutagenesis
Lentiviral vectors	dsRNA	Infect proliferating and non-proliferating cells Stable gene expression	Potential insertional mutagenesis No clinical trials
Adenovirus vectors	dsDNA	High transfection efficiency Efficient targeted transfection Infects dividing and non-dividing cells	Immune response to viral proteins Insert size limit of 7.5kb Transient gene expression
Herpes virus vectors	dsDNA	Infects a wide variety of cell types Insertion capacity of up to 50kb Generation of high virus titres	Possible toxicities Risk of recombination
Poxvirus vectors	dsRNA	High insertion capacity High expression levels	Possible cytopathic effects
Adeno-associated virus (AAV)	dsDNA	Infect dividing and non-dividing cells Very prolonged expression Low immunogenicity Non-pathogenic	Insert size limit of 4.5kb Insufficient clinical trials Requirement of adenovirus or herpes virus for AAV replication

dsDNA, double-stranded DNA.

Table 1.1 - The main studied viral systems for gene delivery with their advantages and flaws are reported.[16]

Nanoparticles   **Polymeric micelles**   **Liposomes**

5-200 nm   20 nm   40-400 nm

Dendrimers   **Polymer-drug conjugates**

1-10 nm   6-15 nm
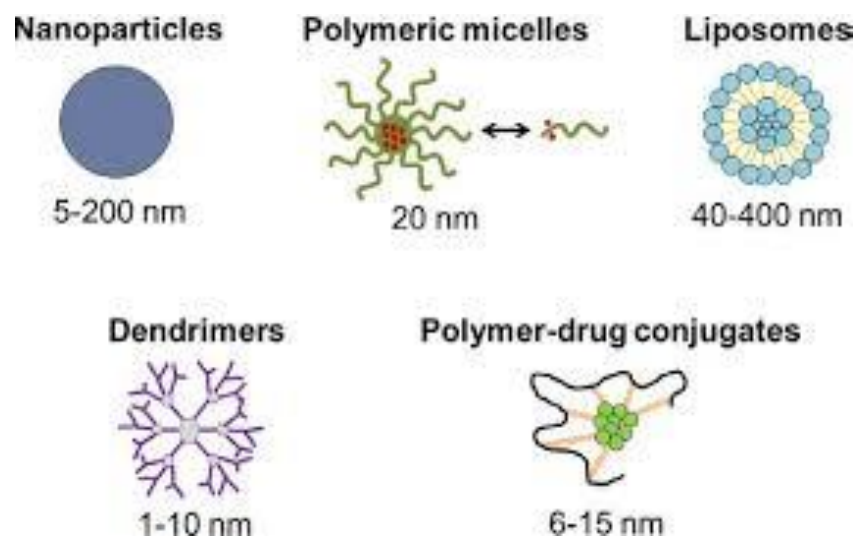
Figure 1.10 – Nano-vectors used for gene delivery: Nanoparticles, polymeric micelles, Liposomes, Dendrimers, Polymer-drug conjugates. [34, 35]

In general, an ideal carrier should [61]:

- be able to protect RNA from nuclease degradation;
- be stable and biocompatible upon administration;
- have high transfection efficiency (enhance cellular uptake, escape the endocytic pathway, release genes so they can be transcribed into the nucleus)
- have low cytotoxicity;
- be preferentially functionalized for allowing cell-targeted delivery or even *in vivo* tracking by imaging;
- be reproducible and controllable in size and structure so that large scale production is feasible, starting from simple components using robust methods and resulting in a cost-effective procedure.

The ideal vector should be taken up efficiently and extensively in the concerned tissue with minimal ectopic uptake or expression. Levels of gene expression should not induce toxicity but should be high enough to promote phenotypic improvement. Gene expression should start rapidly after treatment delivery and persist throughout the life of the organism. The vector should be able to be delivered by a safe non-invasive method, should be well tolerated and should not cause significant inflammation, immune response, toxicity, or adverse physiological conditions [35].

Nanomaterial	Advantages	Disadvantages
Liposomes	Controlled release, reduced toxicity, improved stability	Distribution and removal mechanisms, breakage in invivo.
Polymers	Variety, controllable molecular weight	Inflammatory response, degradation pathway
Micellar nanoparticles	Simple prescription, Passive targeting	Scale-up production, Cytotoxicity
Inorganic nanomaterials	Multifunctional, modifiable, ability to combine diagnosis and treatment	Metal toxicity, Stability And storage
Dendrimers	Nanosized cavity, controlled release, self-assembly	Immunoreaction, hematological toxicity

Table 1.2 – Nanomaterials as drug carriers: Advantages and disadvantages [35]

1.3 Liposomal Drug Delivery:

Drug carriers are usually required in pharmaceutical formulations for several reasons: first, most of therapeutic agents are scarcely soluble in aqueous environments, such as the body fluids or the cell interior; secondly, many drugs, as well as proteins or DNA, need to be protected from undesired interactions which could yield hydrolysis, enzymatic degradation or loss of the native structure and, consequently, of their activity. Finally, drugs may be toxic and must be compartmentalized until they reach the target tissue. At the same time, carriers can be engineered to include surface functionalities, such as targeting ligands, to improve the selectivity of delivery.

Moreover, both vectors and their load may undergo chemical and physical modifications, that affect the structure of the system, its loading and release capacity, interfacial properties, and, eventually, biodistribution [61, 62]. In some cases, the drug itself triggers these modifications, and may also destabilize the starting system. Therefore, a physical and chemical characterization of loaded vector is necessary, to fully understand the biological efficiency.

In 1965, some researchers published the first description of swollen phospholipid systems. Within a few years, a various enclosed phospholipid bilayer structures consisting of single bilayers, initially 'bangosomes' and then 'liposomes', were described. The early pioneers such as Gregoriadis and Perrie have established the concept that liposomes can entrap drugs and can be used as drug delivery systems [70]. The In vivo activity of liposome-entrapped drugs in animal models were first demonstrated by using the anti-cancer drug cytosine arabinoside to demonstrate significant increases in the survival times of mice bearing L1210 leukemia [71]. From then it became a popular 'model system' for testing the effects of a wide variety of liposome characteristics on therapeutic outcomes.
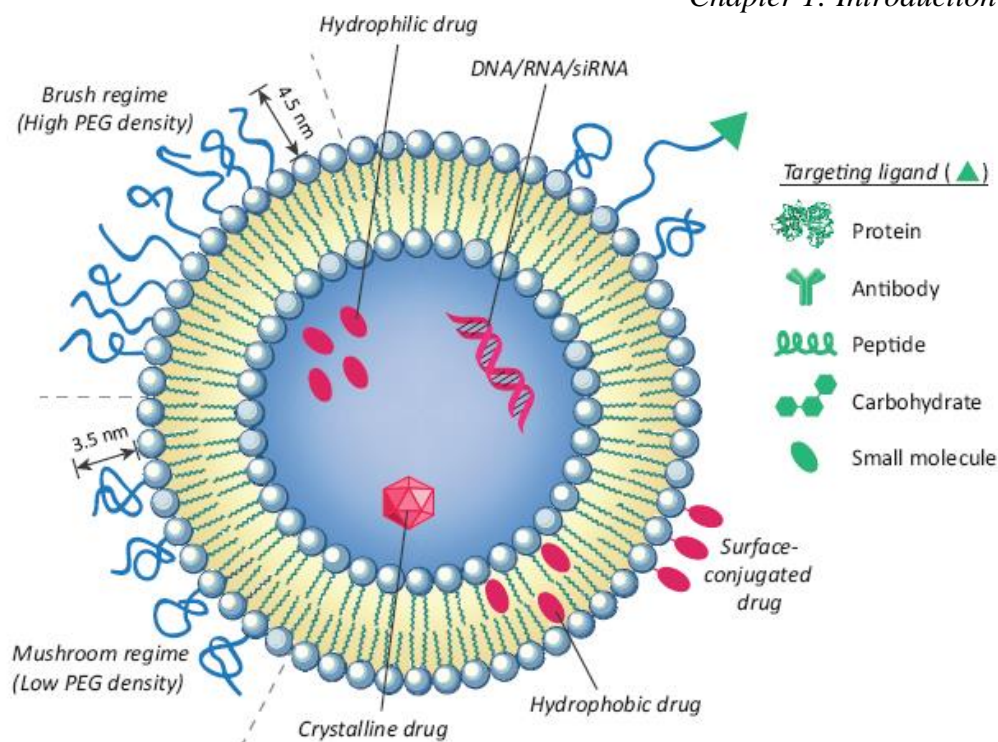
Figure 1.11: Structural and design considerations for liposomal drug delivery. Liposomes can be surface functionalized to endow stealth through PEGylation and to promote receptor-mediated endocytosis by using targeting ligands such as antibodies, peptides, proteins, carbohydrates, and various other small molecules. PEGylation extends liposomal circulation half-life in vivo by reducing clearance, immune recognition, and the non-specific absorption of serum proteins. Polyethylene glycol (PEG) density determines its structure at the liposome surface, with densities below 9% adopting a mushroom-like globular structure and those above 9% adopting a more rigid, extended, brush-like morphology. Chemotherapeutics or diagnostics can be encapsulated into the aqueous lumen, incorporated into the lipid bilayer, or conjugated to the liposome surface [58].

Liposomes are versatile carriers formed by molecules that self-assemble and were first proposed as drug delivery vehicles by Georgiadis more than 30 years ago [64]. Since then, liposomes have been extensively used for various delivery and imaging applications, including commercially available products [65-69]. Liposomes are phospholipid vesicles consisting of one or more concentric lipid bilayers enclosing discrete aqueous phase. The unique ability of liposome to entrap both hydrophilic and lipophilic compound enables a wide range of drugs to be encapsulated by these vesicles. Furthermore, the large aqueous center and biocompatible lipid exterior permits thedelivery of macromolecules, such as DNA, proteins and imaging agents (Ulrich, 2002; Monteiro et al., 2014). Liposomes offer several advantages including biocompatibility, capacity for self-assembly, ability to carry large drug payloads, and a wide range of physicochemical and biophysical properties that can be modified to control their biological characteristics (Koning and Storm, 2003;

Metselaar and Storm, 2005; Ding et al., 2006; Hua and Wu, 2013). For delivery of nucleic acids cationic liposomes are used and it has several advantages. Cationic lipids have a common structure of a positively charged head group and one or two hydrophobic tail region(s) made of hydrocarbon chains or steroid structure, so it is easier for nucleic acids to bind to cationic lipids.

Designing of liposomes is done to achieve the following optimized properties:

1. Drug loading & control of drug release rate
2. Overcoming the rapid clearance of liposomes
3. Intracellular delivery of drugs
4. Receptor-mediated endocytosis of ligand-targeted liposomes
5. Triggered release
6. Delivery of nucleic acids and DNA
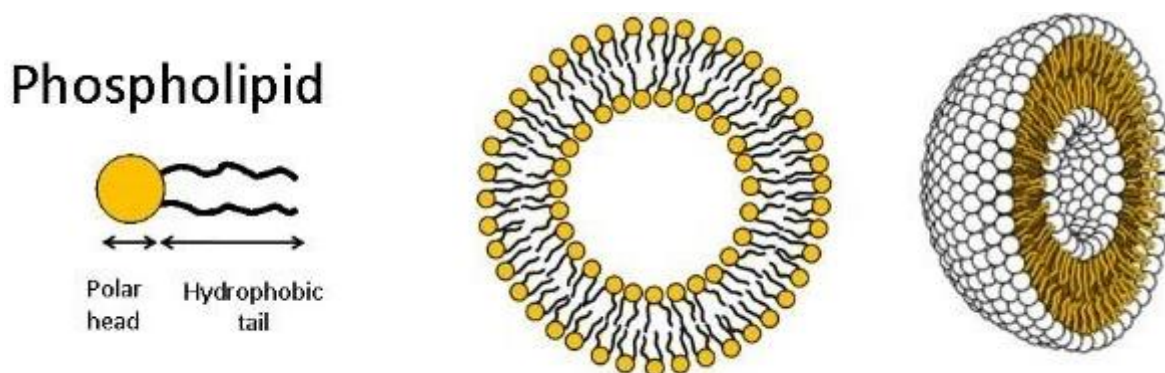
Figure 1.12: Schematic of a liposome. (A) A schematic of a phospholipid showing the hydrophilic and hydrophobic parts. (B) A cross section in a unilamellar liposome vesicle showing the two leaflets of the lipid bilayer which has a thickness of 5 nm [56]

Lipids are amphiphilic molecules that contain a hydrophobic (non-polar) tail and a hydrophilic (polar) head. Due to their amphiphilic nature, lipid molecules self-assemble in water minimizing interactions between their hydrophobic moieties and water, as well as maximizing those with their hydrophilic heads. [35, 56] Depending on their molecular structure and on the solvent properties (pH, ionic strength, etc.), lipids can self-assemble in different structures such as spherical micelles, cylindrical micelles, liposomes, etc. [57] Phospholipids, the main component of the cellular membranes, are amphiphilic lipids composed of a glycerol molecule substituted by one or two fatty acids and one additional polar group. [58]

1.3.1 Mechanism for Liposome formation:

Liposomes are formed by phospholipids (amphiphilic molecules having a hydrophilic head and hydrophobic tail). The hydrophilic part is mainly phosphoric acid bound to water-soluble molecule whereas the hydrophobic part consists of two fatty acid chains with 10-24 carbon atoms and 0-6 double bonds in each chain. They form lamellar sheets when dispersed in the aqueous medium by aligning themselves in such a way that the polar head group faces outwards the aqueous region while fatty acid groups face each other forming a spherical, vesicle like structures called as liposomes [72]. The polar fraction remains in contact with the aqueous region along with the shielding of the non-polar part. When the phospholipids are hydrated in water, along with the input of energy like sonication, shaking, heating, homogenization, etc. It is the hydrophilic/ hydrophobic interactions between lipid-lipid, lipid-water molecules that lead to the formation of bilayer

vesicles in order to achieve a thermodynamic equilibrium in the aqueous phase. Phospholipids are the main components of the cell membrane hence they possess excellent biocompatibility with amphiphilic properties. The amphiphilicity provide the property of self-assembly, emulsifying and wetting characteristics. When phospholipids introduced into aqueous medium, they self-assemble, and it generates different structures with specific properties at different conditions. For example, the phospholipids have a natural tendency to form liposomes, which can be employed as drug targeting molecules [73]. They also have good emulsifying property to stabilize the emulsions. In addition to the wetting property, this can be used in coating of drug to provide hydrophilicity to hydrophobic drugs [74]. These three properties are employed in various drug designing. Variation in aliphatic chains and alcohols lead to the occurrence of varieties of phospholipids. Additionally, different sources of phospholipids enhance varieties of phospholipids.

The reason for bilayer formation includes:
- The unfavorable interactions created between hydrophilic and hydrophobic phase which can be minimized by folding into closed concentric vesicles.

- The large free energy difference existing between the hydrophilic and hydrophobic environment is reduced by the formation of large vesicle formation. Since spherical structures have minimum surface tension and maximum stability. Hence there is maximum stability of self-assembled structure by forming vesicles.

At neutral pH, the fatty acid carboxyl ions provide better electrostatic interaction with repulsion which makes the liposomes stable at lamellar phase; At acidic pH, fatty acid carboxyl groups are protonated leading the formation of HII phase which leads to unstable liposomes and easy to aggregate, fuse and of releasing the contents [73]. Hence the pH sensitive liposomes are prepared for different usage for the drug delivery.

Liposomes have characteristic TC (transition temperature), at which they transit from gel phase to liquid crystalline phase. The encapsulated drugs are release at crystalline phase [73]. Liposomes formation is possible only if the temperature is above transition temperature. For pure liposomes the transition temperature is 41.4°C, whereas lipids from natural origin like lecithin exhibit broad transition temperature [74] The upper limit of temperature for liposome formation is the Krafft point for lecithin it is 58°C and therefore temperature range between 41.4°C and 58°C is ideal for liposome formation e.g. thermosensitive liposomes [75]. Hence the size of vesicles of the liposomes is dependent on the concentration of the phospholipid. Phospholipids with shorter and compact tails form micelles while phospholipids with longer tails tend to form liposomes.
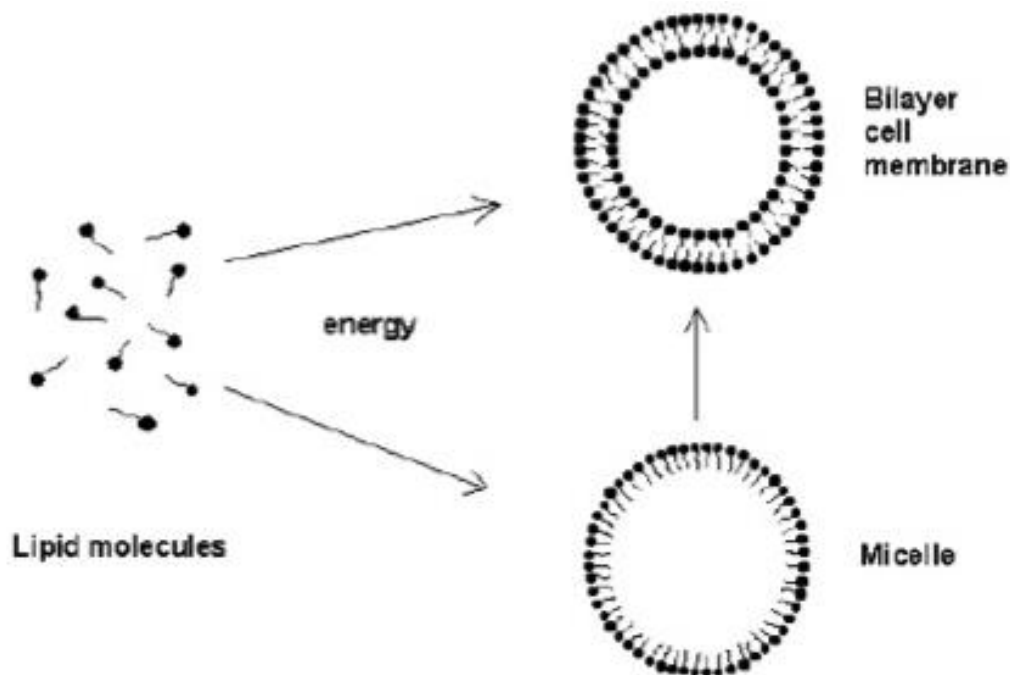
Figure 1.13: Mechanism of Liposome Formulation: Input energy (provided by sonication, heating, homogenization, etc) results in the arrangement of lipid molecules in the form of bilayer vesicles [75].

1.3.2 Classification of Liposomes:

Liposomes can be classified based on size and number of bilayers. They are classified as multilamellar vesicles (MLV), large unilamellar vesicles (LUV) and small unilamellar vesicles (SUV). Unilamellar vesicles can also be classified into two categories: large unilamellar vesicles (LUV) and small unilamellar vesicles (SUV). In unilamellar liposomes, the vesicle has a single phospholipid bilayer sphere enclosing the aqueous solution. In multilamellar liposomes, vesicles have an onion structure. Classically, several unilamellar vesicles will form on the inside of the other with smaller size, making a multilamellar structure of concentric phospholipid spheres separated by layers of water [36]. Based on composition, they are classified as conventional liposomes (CL), pH-sensitive liposomes, cationic liposomes, long circulating liposomes (LCL) and immuno-liposomes. Based on the method of preparation, they are classified [71] as reverse phase evaporation vesicles (REV), French press vesicles (FPV) and ether injection vesicles (EIV).
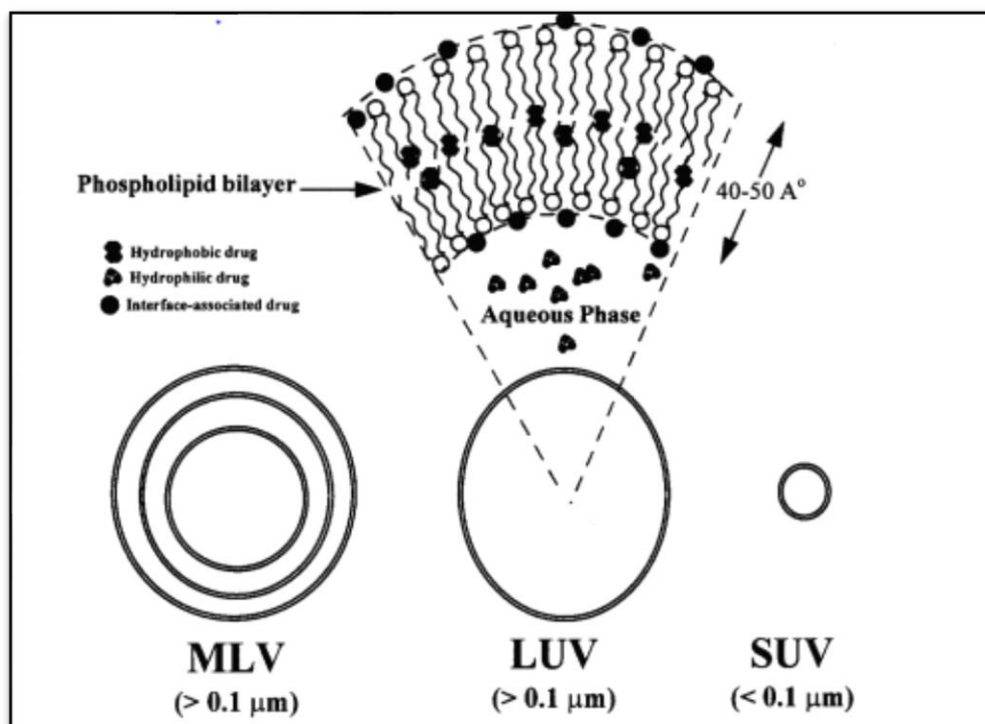
Figure 1.14: Types of Liposomes depending on size and number of lamellae [71].

1.3.3 Cationic Liposomes:

Cationic liposome is one of the most commonly used non-viral gene delivery vectors and it is widely used as a standard gene vector especially for in vitro transfection (Ozpolat et al., 2014). The low toxicity, low immunogenicity, high loading capacity, and easy preparation contributed to the wide application of cationic liposomes. Cationic liposomes are prepared from at least one cationic phospholipid mainly used for gene delivery applications.

Cationic lipids facilitate DNA and siRNA delivery into cells (Chesnoy and Huang, 2000; Hirko et al., 2003; Liu et al., 2003). The basic structure of cationic lipids consists of a positively charged head group and one or two hydrocarbon chains. The

charged head group governs the interaction between the lipid and the phosphate backbone of the nucleic acid and facilitates DNA condensation. Often, cationic lipids are formulated with a neutral co-lipid or helper lipid, followed by extrusion or microfluidization, which results in a unilamellar liposomal structure with a positive surface charge when in water.

The positive surface charge of the liposomes mediates the interaction of the nucleic acid and the cell membrane, allowing for fusion of the liposome/nucleic acid transfection complex with the negatively charged cell membrane. The transfection complex is thought to enter the cell through endocytosis. Endocytosis is the process where a localized region of the cellular membrane uptakes the DNA-Liposome complex by forming a membrane bound/intracellular vesicle.

Once inside the cell, the complex must escape the endosomal pathway, diffuse through the cytoplasm, and enter the nucleus for gene expression. Cationic lipids are thought to facilitate transfection during the early steps of the process by mediating DNA condensation and DNA/cellular interactions.
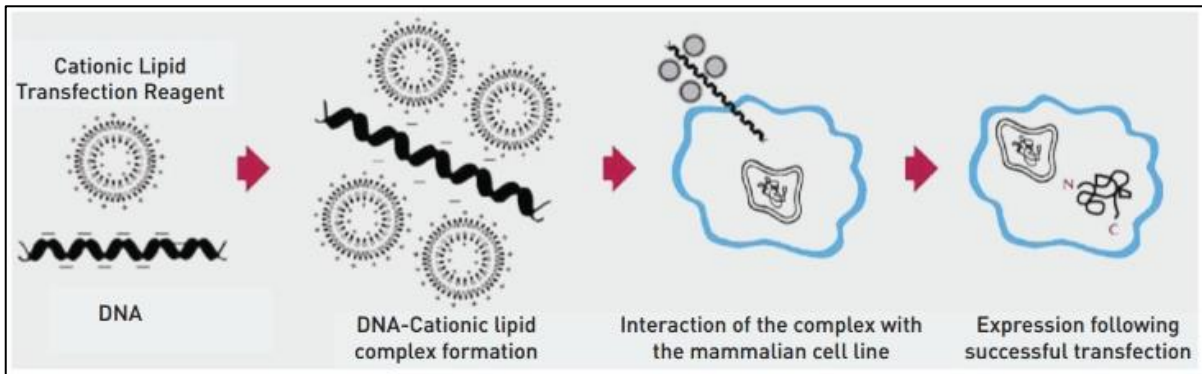
Figure 1.15: Mechanism of cationic lipid-mediated delivery [71]

Problems with Traditional Transfection methods:

- low efficiency of DNA delivery
- poor reproducibility
- cell toxicity
- inconvenience

In contrast, lipid mediated transfection:
- Yields high and previously unattainable transfection efficiencies
- Works in a wide variety of eukaryotic cells
- Is simple to perform
- Ensures consistently reproducible results

The advantages of cationic lipid-mediated transfection are the ability to transfect a broad range of cell lines with high efficiency, its applicability to high-throughput screens, and the ability to deliver DNA of all sizes, as well as RNA and proteins. In addition, this method can be applied to both stable and transient expression, and unlike other chemical methods, it can be used for in vivotransfer of DNA and RNA to animals and humans. Since using cationic liposomes alone is toxic to the cells, we used a mixture of DOTAP (cationic lipids) and DOPC (neutral lipids) with the molar ratio of (3:7) in our research work.
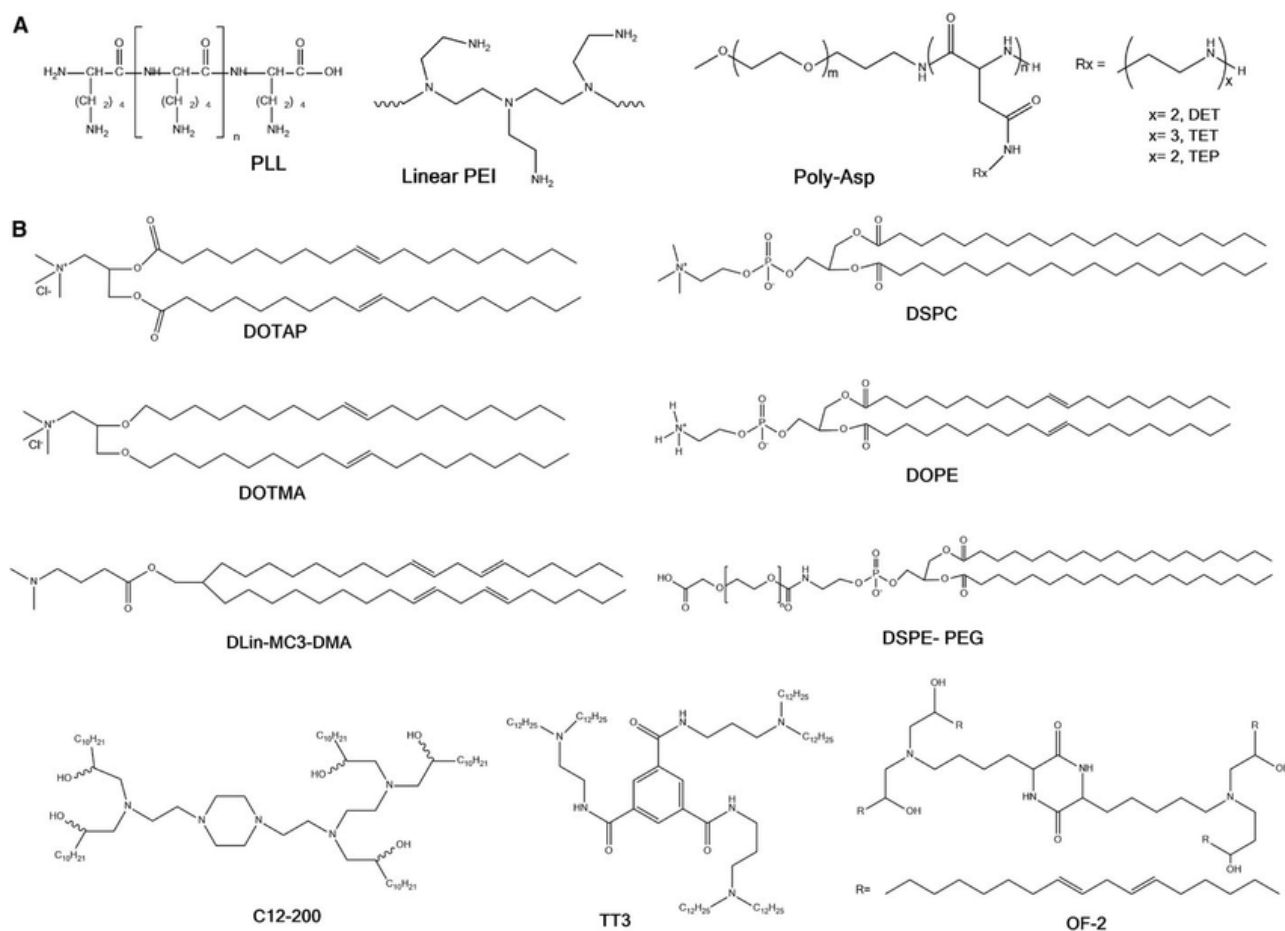
Figure 1.16: Structures of (A) polycations and (B) lipid and lipid-like materials developed for in vivo [71]

Type	Composition	Characteristics
Conventional liposomes	Neutral and or negatively charged phospholipids + cholesterol	Subject to coated-pit endocytosis, contents ultimately delivered to lysosomes if they do not fuse from the endosomes, useful for RES targeting; rapid and saturable uptake by RES; short circulation half life; dose dependent pharmacokinetics.
PH sensitive liposomes	Phospholipids such as phosphatidyl ethanolamine, dioleoyl phosphatidyl ethanolamine with either CHEMS[1] or OA[2].	Subject to coated-pit endocytosis at low pH, fuse with cell or endosome membrane and release their contents in cytoplasm; suitable for intracellular delivery of weak base and macromolecules; biodistribution and pharmacokinetics similar to conventional liposomes.
Cationic liposomes	Cationic lipids	Possibly fuse with cell or endosome membranes; suitable for delivery of negatively charged macromolecules (DNA, RNA); ease of formation; structurally unstable; transfection activity decreases with time; toxic at high dose, mainly restricted to local administration.
Long circulating liposomes (or) Stealth liposomes	Neutral high transition temperature, lipid, cholesterol+ 5-10% of PEG-DSPE[3], GMI[4], HPI[5]	Hydrophilic surface coating, low opsonisation and thus low rate of uptake by RES; long circulating half life (40 hrs); dose independent pharmacokinetics upto 10micromoles/mouse lipid dose.
Immuno-liposomes	Conventional or long circulating liposomes with attached Ab or recognition sequence.	Subject to receptor-mediated endocytosis; cell specific binding (targeting); can release contents extracellularly near the target tissue and drugs diffuse through plasma membrane to produce their effects
Magnetic liposomes	Phosphatidyl choline, cholesterol, small amounts of a linear chain aldehyde and colloidal particles of magnetic iron oxide	Liposomes that indigenously contain binding sites for attaching other molecules like antibodies on their exterior surface. Can be made use of by an external vibrating magnetic field in their deliberate, on site, rupture and immediate release of their components.
Temperature (or) heat sensitive liposomes	dipalmitoyl phophatidylcholine	Vesicles showed maximum release at 41°Y, the phase transition temperature of dipalmitoyl phophatidylcholine Liposomes released the entrapped content at the target cell surface upon a brief heating to the phase transition temperature of the liposome membrane

Table 1.3 – "Liposome classification based on composition and mode of drug delivery" [46]

1.4 Medical Imaging

Medical imaging is widely used in the hospitals and biomedical research for visualizing the internal organs and the early detection of diseases. It is a multidisciplinary field which conceives concept from molecular biology, chemistry, bioinformatics, biophysics, nanotechnology, biotechnology, pharmacology, bioengineering and clinical sciences. There is an increasing growth in the development of imaging techniques for the past few decades. Imaging techniques helps to identify the pathological regions, study the disease mechanism, and assess the treatment process. There are different imaging modalities such as X-rays, Computed Tomography (CT), Magnetic Resonance Imaging (MRI), Positron Emission Tomography (PET), Single Photon Emission Computed Tomography (SPECT), Optical imaging and ultrasounds for disease diagnosis which are depicted in the Figure below. Each modality differs in their energy source, resolution, penetration depth, sensitivity and so on. The spatial resolution of the molecular imaging techniques should be increased, so that the in vivo studies with extremely detailed three-dimensional resolution can be obtained. The type of radiation and materials used for various imaging modalities are tabulated in the Table 1.4 given below. MRI techniques are used for various cancer. The detailed discussion on MRI is given below.

Imaging modalities	Equipment's	Type of radiation	Materials used
PET	PET PET/CT PET/MRI	High energy ọ-rays (511 keV)	Radio isotopes (^{11}C, ^{15}O, ^{18}F, ^{131}I, ^{99m}Tc, ^{111}In)
SPECT	SPECT SPECT/CT SPECT/MRI	Gamma rays (20–300 keV)	Radio isotopes (^{123}I, ^{99m}Tc, ^{133}Xe, ^{201}Tl, and ^{18}F)
MRI	Closed and open type MRI Functional MRI Magnetic resonance angiography (MRA) 3D MRI Hybrid MRI	Radio waves (1–100 MHz)	Magnetic nanoparticles (Iron oxide, Gadolinium oxide, Manganese oxide)
Optical microscopy	Fluorescent microscopy Bioluminescence	Visible or near IR light (659–900 nm)	Organic dye, dye-doped silica, quantum dots, lanthanide atom, carbon nanotube
X-ray CT	Spiral CT Computed tomography angiography (CTA) Multislice computed tomography	X-rays (70 keV energy)	Iodine, gadolinium, gold nanoparticle, bismuth sulfide nanoplate
Ultrasound	Echocardiography 3D ultrasound imaging Doppler ultrasound imaging	High frequency sound (2–15 MHz)	Microbubbles

Table 1.4: Different imaging modalities used in molecular medicine [71]
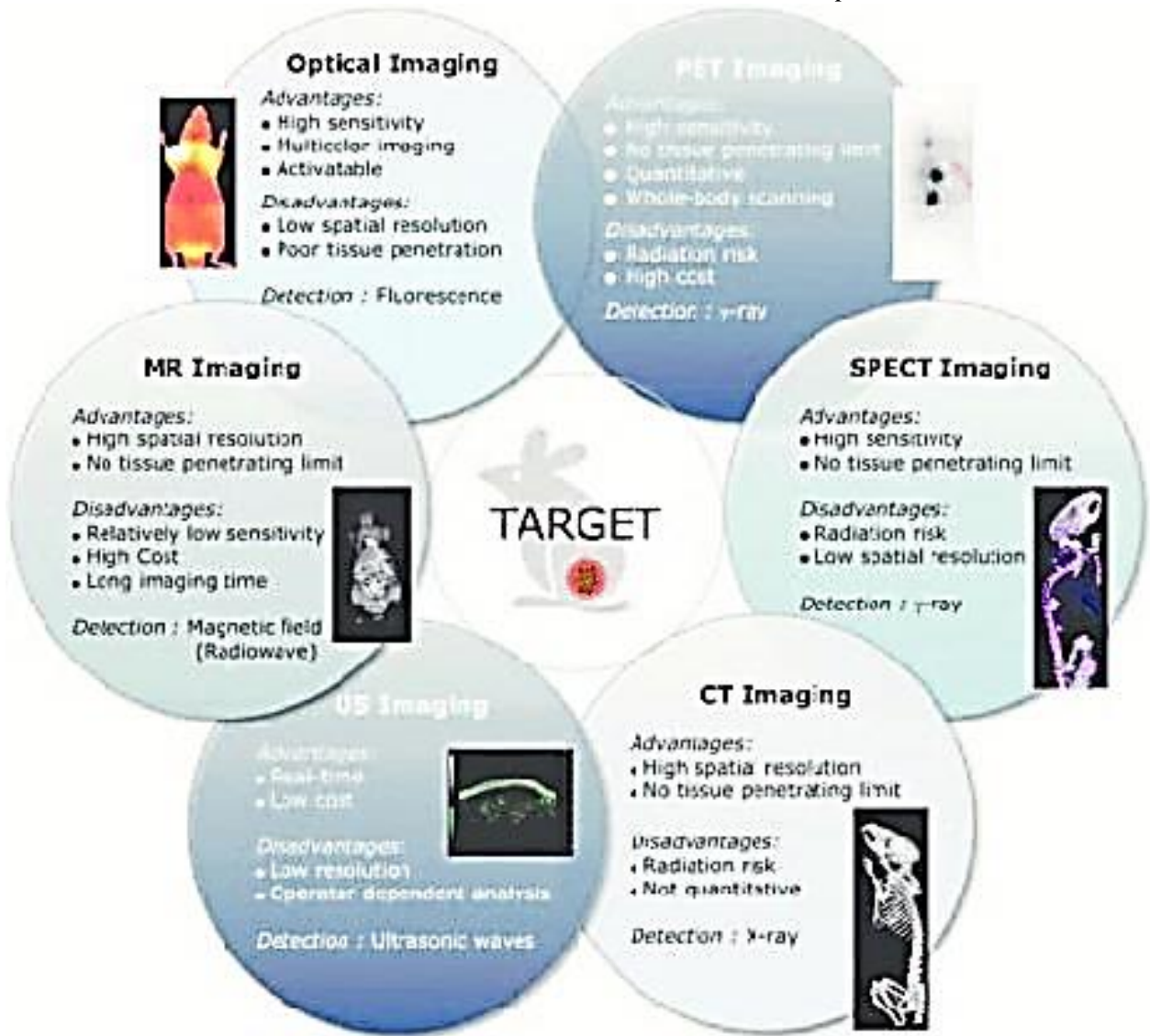
Figure 1.17: Different imaging modalities used in Molecular medicine with the advantages and disadvantages of each imaging modality [71]

1.4.1 Magnetic Resonance Imaging (MRI)

The essence of magnetic resonance imaging (MRI) is spectroscopy, specifically nuclear magnetic resonance (NMR) spectroscopy. The technique had enormous influence and has generated more than one Nobel prize. From the first development in NMR awarded to Felix Bloch (Bloch, 1946) and Edward Mills Purcell (Bloembergen, 1948) in the 1952 Physics prize to the latest recognition of Paul C. Lauterbur (Lauterbur, 1986) and Sir Peter Mansfield (Mansfield and Maudsley, 1977) in the 2003 prize for Physiology or Medicine. At its core, NMR utilizes the absorption and emission of radiofrequency electromagnetic radiation (RF) by nuclei made susceptible by placement in a magnetic field. If the nuclei of interest have a non-zero quantum of nuclear spin, its placement into a magnetic field will cause it to align either with or against the applied field, as it approximates a rotating charge.

This applied magnetic field then forces the nuclei of interest into one of several energy levels, the proton, by way of example, falls into one of two energy levels. The difference in energy levels, termed Zeeman splitting (after Pieter Zeeman, 1902 Nobel Laureate in Physics), provides for the possibility of radiative absorption or emission by the nuclei as they are passed from one energy level to another. By slight modulation of the applied field using the magnetic field gradient coils present in the scanner, it is possible to measure a different specific absorption and emission frequency and phase for many small volumes within the bore of the scanner. These small volumes are commonly termed voxels, to specify a three-dimensional unit of resolution similarly as the term pixel specifies a two-dimensional unit of resolution.

While the precise physics of nuclear spin resonance are deserving of a treatise in and of themselves (Lambert and Mazzola, 2004), it is useful to have some specific understanding of the concepts central to MRI. When a suitable RF pulse is applied to the nuclei within the magnetic field, the populations at the susceptible energy levels are altered. Due to the slight predominance of nuclei in the lower energy state, as predicted by the Boltzmann distribution, a net absorption of radiation occurs. Depending on the length of the RF pulse, the precession frequencies of the nuclei are brought into phase and deflected all or partially into the magnetization plane transverse to the applied field. As

time passes, various effects contribute to the eventual relaxation of this magnetic moment back to equilibrium. The two types of relaxation commonly measured by MRI are termed T1 and T2 relaxation. T1, or longitudinal, relaxation is governed by so-called spin-lattice interactions. That is, the inverted susceptible nuclei transfer their energy to the surrounding milieu, or lattice, thereby relaxing back into a lower energy state. Classically, this may be conceived of as the angles of the spin axis of the nuclei gradually realigning with the direction of the applied magnetic field. The energy of the nuclei is absorbed by the lattice often in the form of increased molecular rotational or vibrational energy, which, if sustained for an excessive period, can be observed as an increase in temperature. T2, or transverse, relaxation is governed by so-called spin-spin interactions. In spin-spin interactions, energy is transferred directly between two susceptible nuclei with similar precession frequencies. As the spins simply reverse orientation relative to the external magnetic field, no net change in T1 occurs. The drop in T2 is due to the loss of phase coherence when the transfer occurs.
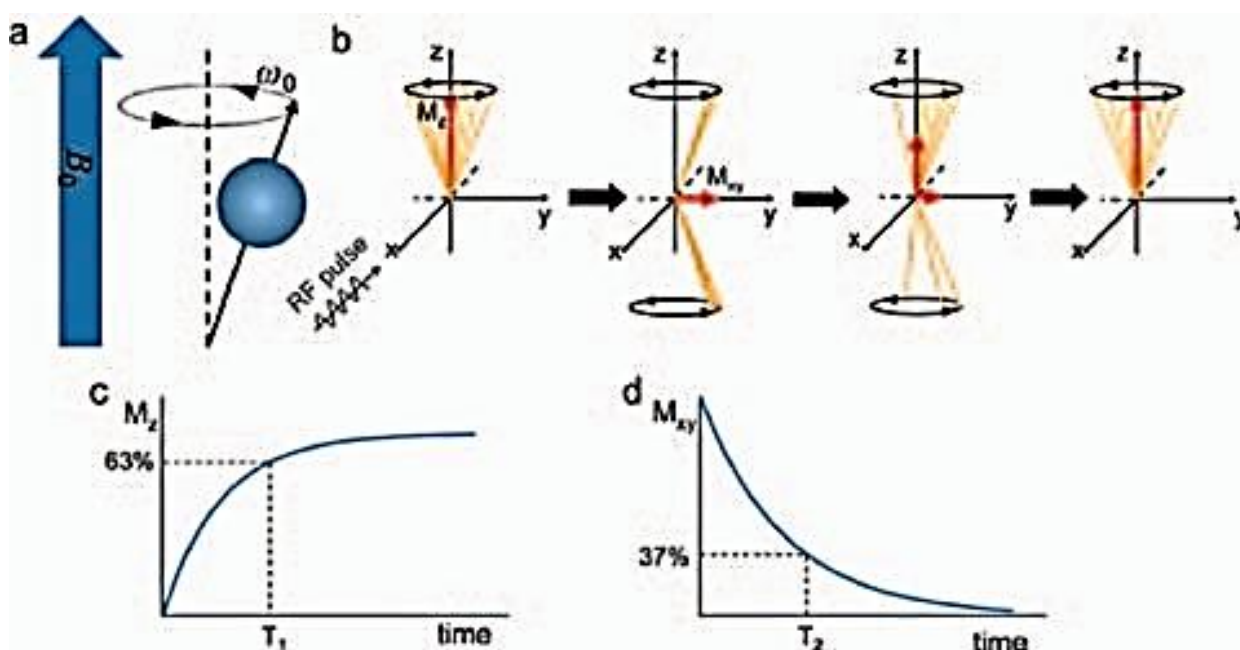
Figure 1.18: Principles of magnetic resonance imaging (MRI). (a) In magnetic field, the hydrogen nuclear spins align with (parallel) or against (antiparallel) the external magnetic field. (b) Irradiation of resonant RF results in decrease in longitudinal magnetization and generation of transverse magnetization. Subsequently, the nuclear spins return to their initial state, referred to as relaxation. (c and d) T1 is the time required for longitudinal magnetization to recover to 63% of its equilibrium (c), and T2 is the time required for transverse magnetization to drop to 37% of its initial magnitude (d). Reproduced from [47], N. Lee and T. Hyeon, Chem. Soc. Rev. 41, 2575 (2012). © 2012

In discussion of MRI pulse sequences, particularly the gradient echo which finds common use in fMRI, the term T2* is often encountered. In actual measurement, the signal decays much faster than would normally be predicted by T2 relaxation. The source of this additional speed is relaxation from the spins of the individual nuclei dephasing as they encounter local fluctuations in the magnetic field and is designated as the T2* rate of relaxation.

Every human cell contains hydrogen atoms (protons with spin property). When a patient is placed within a magnetic field, these protons align like tiny magnets. When radiofrequency (RF) pulses producing an electromagnetic field are transmitted in a plane perpendicular to the magnet, these protons become excited. When such protons return to their original state, i.e. relax, energy is produced, which can be received and translated into images [61]. MRI scanning can discriminate between body substances based on their physical properties, for example, differences between water and fat containing tissues. MRI scanning is therefore particularly useful at providing highly detailed images of soft tissues. MRI scanning can also provide images in various planes without the movement of the patient. On an MRI scan some tissues appear to be brighter or darker than others. Brightness might depend on the density of protons in that area (an increased density being associated with a brighter area). Relaxation times for the hydrogen protons can vary and two times are commonly measured: Longitudinal relaxation time, known as T1, and transverse relaxation time, known as T2. Relaxations time properties are routinely used to show contrast between different soft tissues.

Figure 1.19: Magnetic Resonance Image showing a vertical (sagittal) cross section through a human head [71].

1.4.1.1 ^{19}F-MRI:

The first ^{19}F observations were attempted with NMR in 1942,81 followed by MRI in the 1970s.82 Since then, ^{19}F imaging agents have been used for a variety of purposes, such as to measure the intracellular partial pressure of oxygen83 and as a gastrointestinal contrast agent by proton displacement [77] .Nuclear magnetic resonance signal from ^{19}F has been used to investigate lung structure and drug pharmokinetics. Unlike with iron oxide agents, nuclear magnetic resonance signal from the ^{19}F atoms are directly detected and there is no disruption to the underlying proton image contrast. Once the detection threshold has been reached, the signal produced is linearly proportional to the number of ^{19}F atoms, allowing for quantification [78]. A drawback of this direct detection is the relative insensitivity of the nuclear magnetic resonance signal. As discussed in previous Section, signal in MRI is governed by the surplus of spins in alignment with the main magnetic field. With standard MRI this is not a concern, due to the high abundance of ^{1}H in biological tissue. For ^{19}F-MRI, many additional ^{19}F atoms must be introduced to the cell in order to produce enough NMR signal to be detectable. This requires mM concentrations (~ 1015 ^{19}F atoms) per voxel for imaging.[79] However, due to the near-absence of native ^{19}F-atoms in biological tissue no background signal is observed, providing excellent imaging specificity.

The first application of ^{19}F-MRI for cell tracking was demonstrated in 2005 by Ahrens et al. [80] In this study, immunotherapeutic DCs were tracked following subcutaneous injection to the draining popliteal lymph node.[81]Cells were labeled in vitro by coincubation with an emulsified perflurocarbon (PFC), which was internalized through phagocytosis. Anatomical localization was achieved by overlaying the ^{19}F image onto a traditional proton MR image. In the 11 years since this first study, the field has grown at an exponential rate, [82] with significant advances in hardware,88–90 image acquisition and data processing. [83] To date, most of this work has been performed at high-field strengths (>7 T), to improve sensitivity of ^{19}F-MRI. Studies have demonstrated ^{19}F can be added to cells in culture and used to track stem cells from hematopoietic, neuronal and mesenchymal progenitors; [84] as well as a variety of immune cells, such as: DCs, [85] NK cells, 99 T-cells,100 and macrophages. [86] PFC uptake has been observed in both T- and B-cells, which have been historically difficult to label with SPIO-based agents. [87]

Dendritic cells have been by far the most frequently imaged cell type with ^{19}F-MRI. Besides the natural phagocytic ability allowing for high intracellular label uptake in the range of 1012 ^{19}F atoms/ cell; DC do not undergo mitotic cell division preventing the diffusion of label. Finally, the known migratory pathway to the draining lymph nodes provides the perfect translation model for assessing in vivo functionality with imaging.

Building on previous work by Dr. Ahrens, in 2010 Helfer et al. introduced the first commercial ^{19}F imaging agent by imaging the migration of DCs to the draining popliteal lymph node. In this study, extensive work was performed to show that labeling did not negatively affect the expression of surface markers, DC maturation, and T-cell stimulatory function. [88]. In 2011, a German group led by Dr. Waiczies showed that the labeling efficiency of DCs increased with the PFC particle size, up to a maximum of 560nm diameter. Interestingly, their work showed improved T-cell activation following ^{19}F-loading of DCs; [89] suggesting heavy intracellular 19F-uptake may act to induce DC maturation processes.

With these promising results, the clinical feasibility of detecting DCs in vivo was first explored in 2011 by Bonetto et al. [90] In this work, they showed an intracellular uptake of 1.7x1013 19F/cell, the highest reported labeling efficiency to date. Using a spin density weighted SE sequence on a 7T system, a minimum of 2000 cells/voxel could be detected in phantoms. These results were extrapolated to provide an estimation of a minimum detection threshold of 30,000 cells/voxel on a clinical 3T MRI,102 or around 5x1017 ^{19}F atoms.
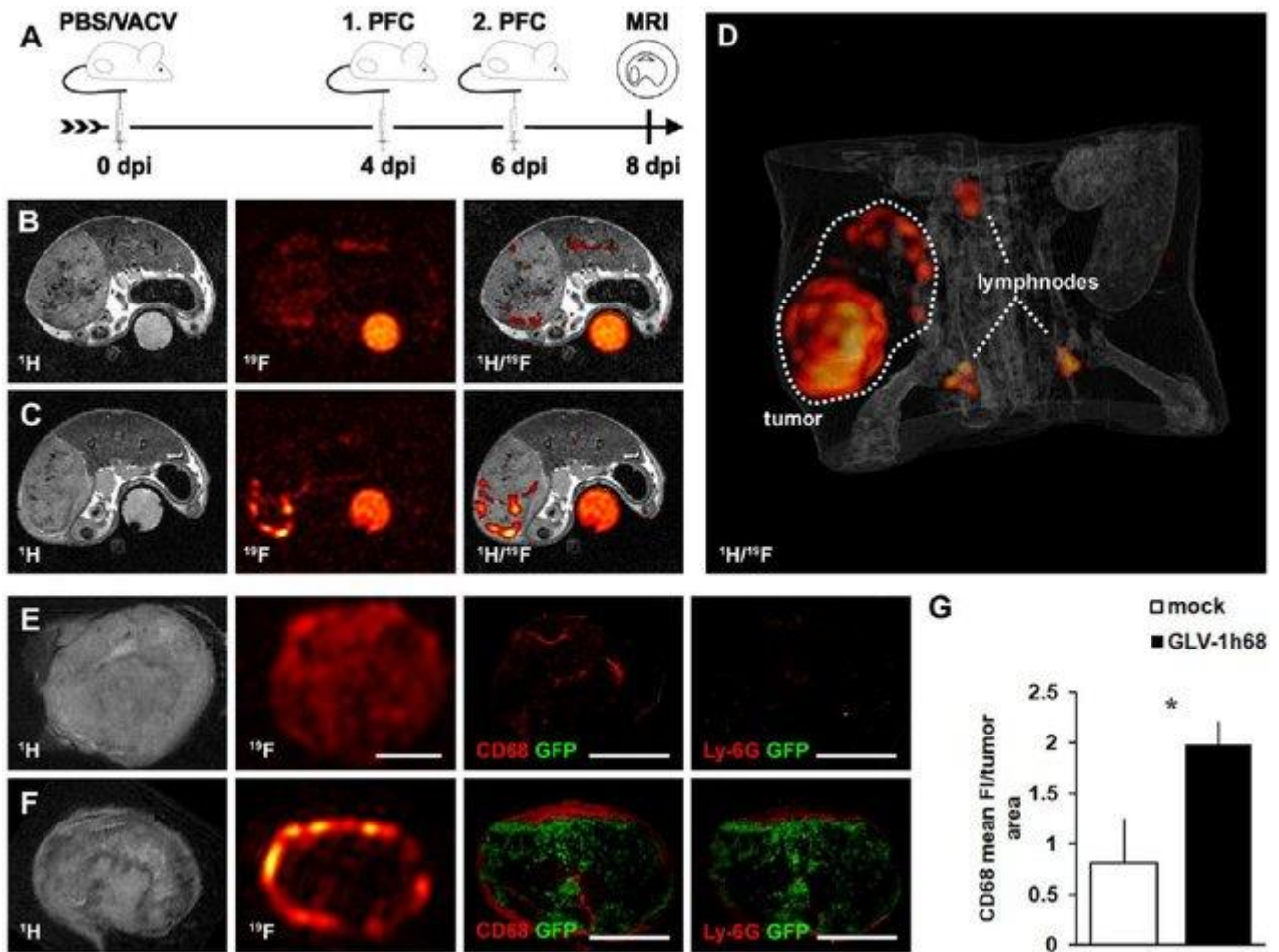
Figure 1.20 –Visualization of viral tumor colonization by 19 F MRI-based imaging of inflammation. (A) timeline - 1936-MEL melanoma- bearing athymic nude mice were i.v. injected with either 1 6 10 7 pfu of GLV-1h68 or PBS as control. Emulsified PFC was i.v. administered at day 4 and 6 [71]

40

1.5 PERFECTA

Recently a new superfluorinated molecular probe, called PERFECTA (from suPERFluorinatEdContrasT Agent), was designed to develop a small molecule containing the higher possible amount of equivalent ^{19}F atoms. In specific, this molecule varies from PFCs as it has a polar hydrocarbon nucleus surrounded by 36 equal ^{19}F atoms, developed because of tetra replacement on pentaerythritol with perfluoro-t-butanol equivalent CF_3 groups. Figure 1.21–PERFECTA (left) synthetic strategy and PERFECTA (correct) single-crystal X-ray structure.
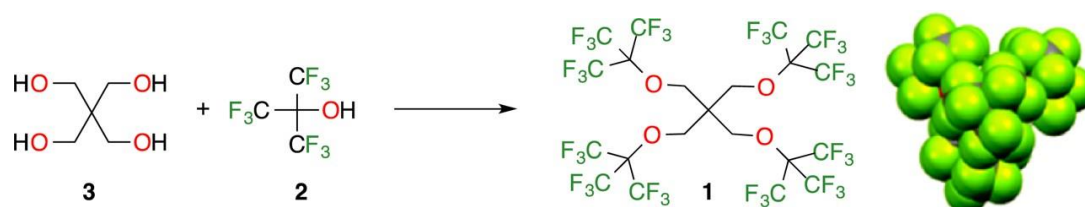
Figure. 1.21– Synthetic strategy of PERFECTA (left) and single crystal X-ray structure of PERFECTA (right) [102]

Pentaerythritol and perfluoro-t-butanol are acquired from PERFECTA in a single step via a Mitsunobu reaction, which happens with excellent yield. The molecule appears as a white crystalline powder and is insoluble in water as well as in the most prevalent organic solvents such as acetone, chloroform and methanol. However, PERFECTA can be developed in homogeneous emulsions by dispersing a certain quantity of PERFECTA in an aqueous solution of Lecithin and Safflower Oil (75 mg PERFECTA, 4% Lecithin and 4% Safflower Oil in an aqueous solution of 1 mL. Full characterization has been performed, showing that the PERFECTA emulsion has a long shelf life (6 weeks at room temperature and 7 weeks at 4 ° C), is perfectly compatible with cellular viability even at high concentrations (9.92 mM) and long incubation times (up to 8 hours). Because of its very elevated fluorine concentration (1,61 ± 0,04x 1021 ^{19}F atoms per mL of emulsion), PERFECTA displays a single intense resonance peak at both ^{19}F-NMR and MRI methods [102]. Not only its spectral characteristics, but also the relaxation times and the signal-to-noise ratios showed that the fresh molecule is an optimal contrast agent for ^{19}F-MRI. Not only its spectral characteristics, but also the relaxation times and the signal-to-noise ratios showed that the fresh molecule is an optimal contrast agent for ^{19}F-MRI.

Chapter 2: Materials and Methods

2.1 Materials and Equipment

1,2-dioleoyl-sn-glycero-3-phosphocholine (DOPC) ($C_{44}H_{84}NO_8P$) and 1,2-dioleoyl-3-trimethylammonium-propane (chloride salt) (DOTAP) ($C_{42}H_{80}NO_4Cl$) in form of powder was dissolved in chloroform (25 mg/mL) were purchased from Avanti Polar Lipids®. Tetra(perfluorotertbutyl)pentaerythritol (PERFECTA) was synthetized in the SupraBioNanoLab (SBNLab) at Politecnico di Milano according to the protocol optimized by Tirotta et al. Chloroform ($CHCl_3$, ≥99.8%) purchased from Sigma-Aldrich®.
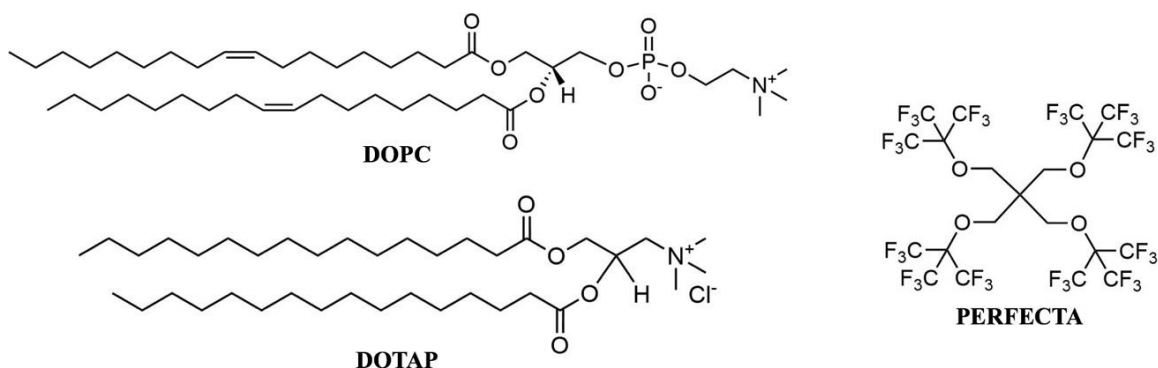
Figure 2.1 – The chemical structures of PERFECTA, DOPC, DOTAP are reported. [102,71]

Extrusion was carried out using an Avanti Mini Extruder supplied by Avanti Polar Lipids ®, fitted with two 1 mL volume Gas Tight syringes. Avanti Polar Lipids ® has also bought filter supports and polycarbonate membranes (pore diameter size equal to 200 nm and 100 nm) for its operation. The Dynamic Light Scattering (DLS) configuration involves an ALV device fitted with an ALV-5000/EPP correlator, a unique optical fiber detector and a compact goniometer ALV / CGS-3. The source of light is a laser He-Ne (π= 633 nm) with output energy of 22 mW. Zeta Potential (ZP) experiments were conducted using a Zetasizer Nano ZS (Malvern Instrument, Malvern, Worcestershire, UK), equipped with a 633 nm red laser and 173 ° angle measurement of the dispersed light. A Bruker AV400 spectrometer registered NMR spectra

2.2 Methods

2.2.1 Liposomes preparation

In the development of new liposomal formulations, scientists also came up with various new methods appropriate for ensuring their simple and effective production. As a result, a wide range of preparation techniques for liposomes are now recognized. Classical modalities include thin-film hydration or "Bangham process," inverted evaporation phase, solvent injection methods, and dialysis of detergents [103]

2.2.1.1 Liposomes formation

The classical thin-film hydration technique has been used in our study activity. The method can be outlined briefly in three steps: I lipid dissolution in an organic solvent, (ii) solvent evaporation with lipid film formation, and (iii) lipid hydration in aqueous media [104].Due to their chemical structure, consisting of hydrophobic tails and hydrophilic heads as outlined in the prior chapter, phospholipids are deposited on the surface layer in the form of bilayers during the removal of the organic solvent. Hydration then triggers the formation of spherical-shaped vesicles under a powerful hydrodynamic flow. Indeed, if the phospholipid bilayer is a finite patch, it has a certain amount of energy associated with its edge, where the hydrophobic tails are exposed to water [105]. This energy is therefore proportional to the perimeter of the patch and can be minimized by removing the edge, i.e. by folding the bilayer patch into the spherical vesicle. However, the bending action needs an original quantity of energy proportional to the sphere radius square. The pattern of liposome formation energy can therefore be defined as follows: it rises at the start owing to the demand for energy to bend the layer but, as quickly as the edges meet, it decreases steadily. [105] In fact, since the hydration rate is rapid, multi-lamellar vesicles (MLVs) are created. The resulting liposome particle size is big (1–5 μm) and it also has a wide distribution. The thin-film hydration technique is generally accompanied by post-processing granulation to guarantee the required size, lamellarity, and homogeneity characteristics of the produced liposomes.

A Disc

Edge energy $= 2\Pi R_d \lambda$

$\lambda = 1 \times 10^{-4} J/m$

$\Pi R_d^2 = 4\Pi R_v^2$

$2\Pi R_d \lambda = 4\Pi \left(2K_b + K_G\right)$

Bending energy $= 4\Pi \left(2K_b + K_G\right)$

Vesicle

$R_d = 2R_v$

$R_v = \dfrac{1}{\lambda}\left(2K_b + K_G\right)$

B

Phospholipid molecules

Stack of lipid bilayers

Hydration of lipid bilayers

Slow bilayer separation

High shear flow

Multilamellar vesicle (MLV)

No shear flow

Fast bilayer separation

Unilamellar vesicle (UV)
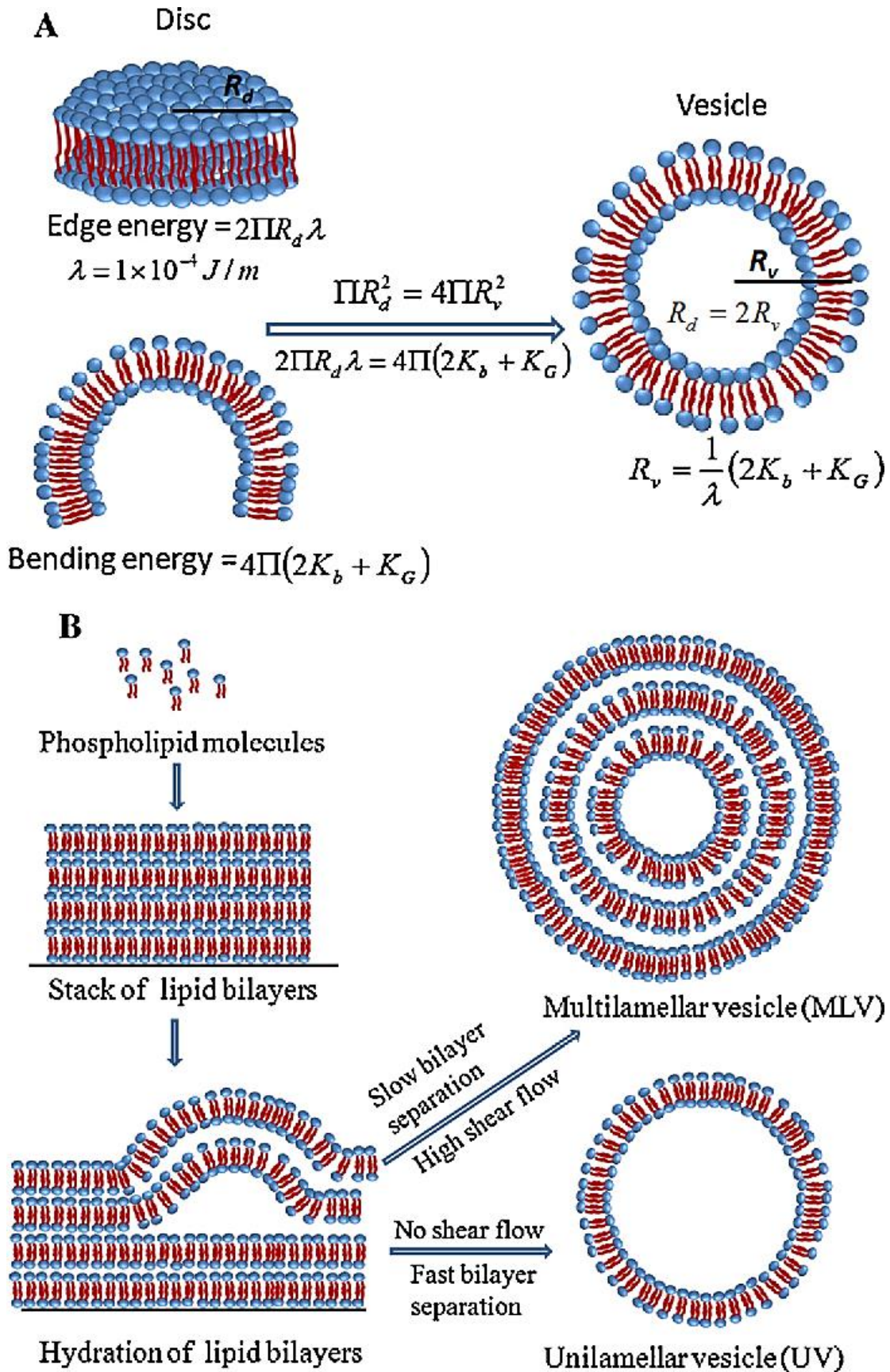
Figure 2.2 – "Schematic illustrating phospholipid self-assembly involved in liposome formation. The smallest liposome is formed when the edge energy first exceeds the bending energy" [105]

2.2.1.2 Post-formation processing

French press, sonication, homogenization and membrane extrusion are common methods for converting MLVs into either tiny or big uni-lamellar vesicles (SUVs and LUVs respectively). MLVs suspensions are compelled at elevated pressures to pass through a tiny orifice and are lowered to SUVs (30-50nm) [106]. On the other side, due to ultrasonic waves, sonication breaks MLVs. The resulting liposomes have a size of approximately 25 nm [107], lower than those obtained by French press. However, only small volumes of polydisperse SUVs are captured in sonication and this, along with the potential damage to phospholipids and encapsulated drugs, limits the use of sonication technique. [108] At the industrial level, the size and lamellarity of lots of liposomes are reduced by homogenization: the suspension of MLVs is pumped through the orifice at high pressure and impacts the wall of stainless steel. Indeed, because of the need for very elevated working pressure, this method is costly. [105] Finally, the membrane extrusion is the most commonly used technique of downsizing MLVs. It comprises of extruding the suspension of MLVs by pushing it to constantly cross a polycarbonate membrane's uniform cylindrical pores. They can deform to some extent when liposomes are pressed through a pore of a diameter smaller than their own.

Anyway, the distinction between the pressure on the opposite sides of the membrane at some stage leads the vesicle to break. The bilayers tend to recover the spherical shape instantly, forming smaller vesicles that can now pass through the pore. Extrusion therefore gives a monodispersed vesicle population, the size of which varies on the trans-membrane pressure and the number of extrusion cycles. Finally, the diameter of the liposomes in the polycarbonate membrane approaches the diameter of the pores. This technique is particularly valued as it is an economically useful reproducible method and does not cause liposomal degradation or impurity. [105]

Thin-film hydration technique has been used in our study to prepare liposomes. Chloroform-dissolved lipids were dried under vacuum. Hydration was performed by adding to the thin-film and vortexing the volume of the selected aqueous buffer for 20 minutes and bath sonicated at 40 ° C, 59 kHz frequency, 100% energy for 15 minutes. On the other side, extrusion was conducted through an extruder with an inner framework like the one shown in Figure below. When the pressure was particularly high between the two sides of the membrane, it was helpful to heat the sample at 40 ° C before extruding. On each side of the polycarbonate membrane, two filter supports were

placed. Before extruding, the device was pre-wetted with 1 mL of the same aqueous solvent used to hydrate the lipid film to decrease the dead volume (10 passages from one syringe to the other). The extrusion of the MLV solution could be conducted after checking the lack of leakages. Each sample was subjected to two stages of extrusion: the first using a 200 nm diameter pores membrane, while the second with a 100 nm diameter pores membrane. Each cycle accounts for 21 membrane-wide passages.
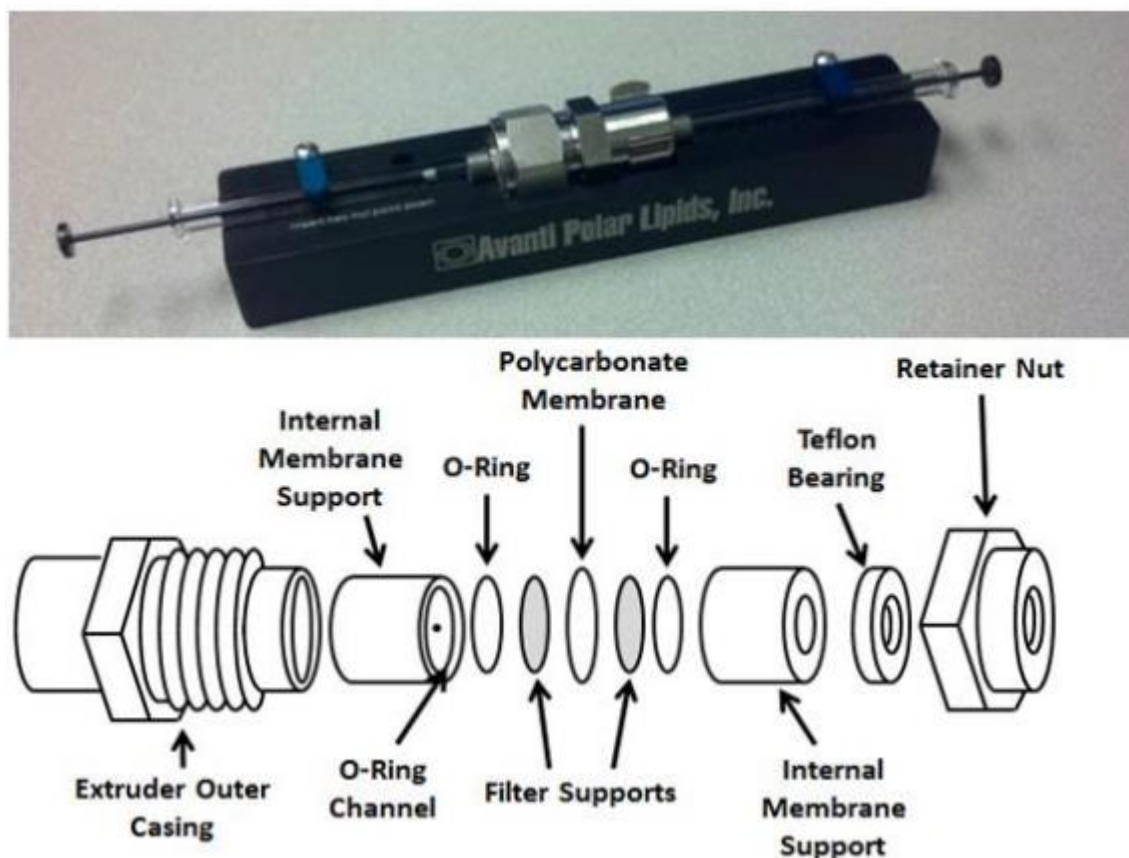
Figure 2.3 - Picture of the Avanti Mini Extruder and schematic sketch of its internal structure. [109]

2.2.2 Physical-chemical analysis

Particle size and surface charge are two of the most important parameters to be evaluated when dealing with nanovesicles of drug delivery as they are factors that are responsible for a multitude of biological effects including cellular uptake, toxicity and dissolution. In our research, the particle size distribution was determined using Dynamic Light Scattering (DLS) measurements, while the assessment of Zeta Potential Allowance (ZP), Small Angle X-ray Scattering (SAXS), Transmission Electron Cryomicroscopy (CryoTEM) was also conducted and the chemical composition of the macromolecule was conducted using NMR.

2.2.2.1 Dynamic Light Scattering

DLS is a well-established, non-invasive technique used to determine liposome size. DLS is also called PCS (Photon Correlation Spectroscopy) or QELS (Quasi-Elastic Light Scattering) for measuring the size of typically sub-micron molecules, nanoparticles or colloids. All spherical particles within a solution undergoes Brownian motion. Brownian motion is random movement of particles due to collisions with solvent molecules that surrounds them. The size of the particle is defined from how fast the fluctuations from these collisions fade out using the autocorrelation function. For a large particle the movement is slow, and its velocity can be related to a diffusion coefficient D. The particles will move faster with increasing temperature. When the particle stops diffusing, they start to sediment, which is the upper limit of the method and depends on the density of the particle measured.
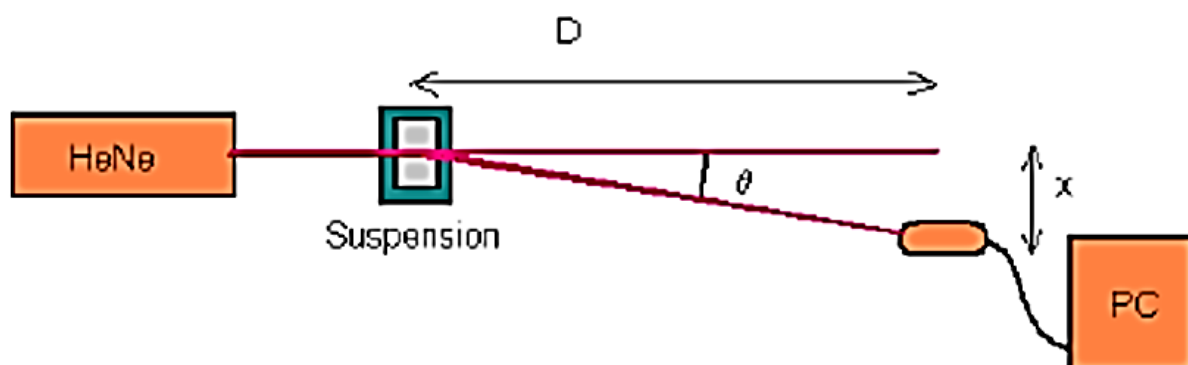
Figure 2.4: A typical Dynamic Light Scattering (DLS) experimental setup [107]

Monochromatic light (4 mW 633 nm HeNe, laser) hits the cuvette containing the particle solution. The detector measures the fluctuations in light intensity of back-scattered light, angle 173° from particles passing by. Small particles moving quickly will cause more rapid light intensity fluctuations over time than large particles. The velocity of the particle is related to the diffusion coefficient D in Stoke-Einstein equation (1)

$$D = \frac{K_B T}{6\pi\eta R_H}$$

Where K_B is Boltzmanns constant, η is the viscosity, T is the temperature and R_H the is hydrodynamic radius of the particle. The hydrodynamic radius is dependent on the surface structure, solvent medium and particle concentration. In our research work, analysis was performed at 25°C for different angles (70°, 90°, 110°, 130°) for sample volume approximately 0.8mL to 1 mL.

2.2.2.2 Small Angle X-ray Scattering (SAXS):

SAXS is a non-destructive method for investigating nanostructures in both liquids and solids. In a SAXS experiment the X-ray beam hits the nanostructured sample, for example proteins, macromolecules, or nanoparticle dispersions.

In general, the properties of a material are related to the structure and arrangement of domains on the nanoscale. To understand the basic relation between the size, shape, and arrangement of nanostructures and their macroscopic behavior it is necessary to accurately analyze these structures. There are several classical structural methods (many of them imaging methods), such as microscopy (AFM, TEM), which are used for characterizing the nanostructured materials. These methods, however, have the disadvantage that averaged, i.e. representative results of a sample can hardly be obtained. SAXS ideally a complementary microscopic method since it provides representative structural information about a large sample area.
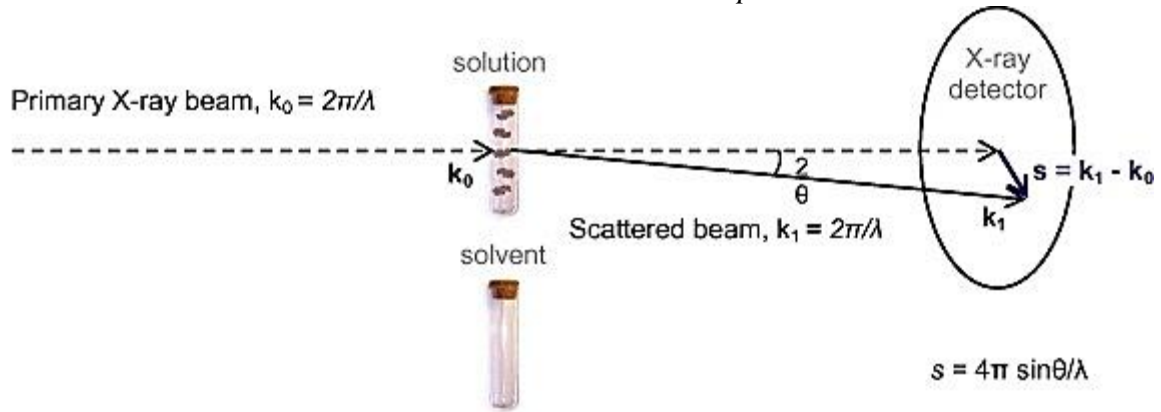
Figure 2.5: A typical Experimental Setup of Small Angle X-Ray Scattering (SAXS) [66]

The X-ray source emits an X-ray beam which interacts with the electrons of the sample and is scattered. The detected scattering pattern is characteristic for the nanostructures of the sample and can be used to determine important structural parameters like particle size, shape, internal structure, porosity, and arrangement (orientation).

The scattered X-rays can be recorded at different angles. In general, it can be said: The larger the particles of a sample, the smaller the scattering angle. In SAXS, the scattering pattern at small angles is analyzed, typically below 10 deg, to probe nano-sized particles and domains in a size ranging from approx. $D \sim 1$ to 100 nm, which scatter towards these small angles. Before scattering X-rays are transformed into a well-defined line-shaped or point-shaped beam. This process is called collimation. Each collimation type in a SAXS system is different for various applications.

A line-collimated beam has the advantage that it combines a high photon flux with a high scattering volume – which means measurement times can be dramatically shorter than point collimation. The drawback of a line-collimated beam is that it can only probe isotropic samples. Therefore, a line-shaped beam is preferable for analyzing weakly scattering samples, such as proteins and other soft matter.

A point-collimated beam can be used to also analyze anisotropic samples, such as fibers or porous solids. Point collimation allows you to probe small sample areas and determine their local nanostructure, with the drawback of long measuring times.
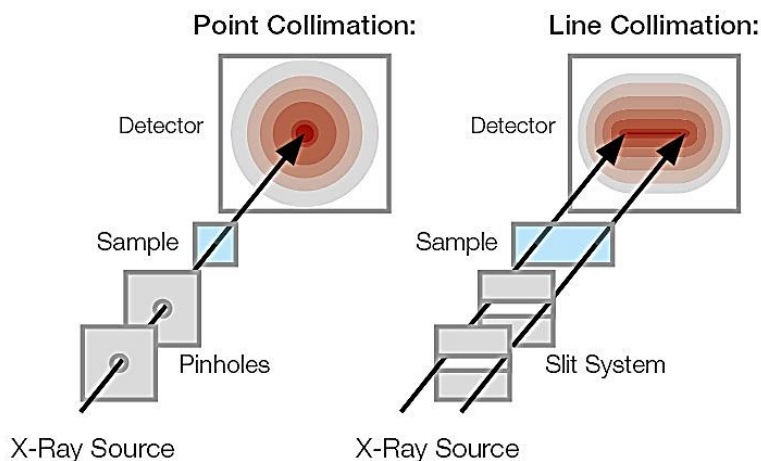
Figure 2.6: Point collimation and Line Collimation of Small Angle X-ray Scattering (SAXS) system [66]

SAXS is used to determine several parameters of nanostructured samples – the most common ones are shape, size, internal structure, crystallinity, porosity and orientation.

2.2.2.3 Transmission Electron Cryomicroscopy (CryoTEM):

Cryogenic TEM has been developed as a method to immobilize biological molecules in a hydrated state which can be maintained within the vacuum of an electron microscope [91]. The challenge of freezing biological material with a standard protocol is that the formation of ice crystals at best deforms and at worst destroys the sample. This will be even more noticeable at the small scale examined in TEM imaging, and so non-crystalline, vitreous ice is formed through rapid plunge freezing.

Samples are vitrified by plunge freezing into liquid ethane cooled down to liquid nitrogen temperatures (77k), forming non-crystalline ice. The faster cooling rate of ethane is more appropriate than liquid nitrogen. This is then transferred into the microscope with a specially engineered holder and the temperature maintained with a liquid nitrogen cooled dewar.

This technique was pioneered by Jacques Dubochet in the late 1980's [92]. This

was the first time anyone had viewed a vitrified biological specimen within the electron microscope, with the main breakthrough being the realization that a high defocus value was needed to visualize low electron contrast material [93]. This was the start of a new era in biological electron microscopy where high resolution close to that achieved by materials scientists was possible for sensitive biological molecules.

Due to the highly damaging nature of the electron beam, a low electron dose imaging protocol must be used in order to gain viable images. This technique has been used for high resolution structural biology to resolve the three-dimensional atomic structure of various proteins. In order to do this a technique called single particle Cryo-EM must be carried out. Many proteins are imaged (>5000), and because they can be assumed to be randomly orientated in the ice, the images can be classed into different orientations and treated like a tomographic tilt series. Although an image of a single protein seems inconclusive, when combined with thousands and analysed this way the results can be extremely informative. A comprehensive review of the imaging protocol and image reconstruction techniques has been presented by Orlova et. al. [94].

Near-atomic resolution has been reached by exploiting the icosahedral symmetry of viral proteins [62]. The DNA nanostructure has been studied at high resolution using cryo-TEM [95]. The DNA helix is visible with cryo-EM reconstruction and focal series, as illustrated in figure below.
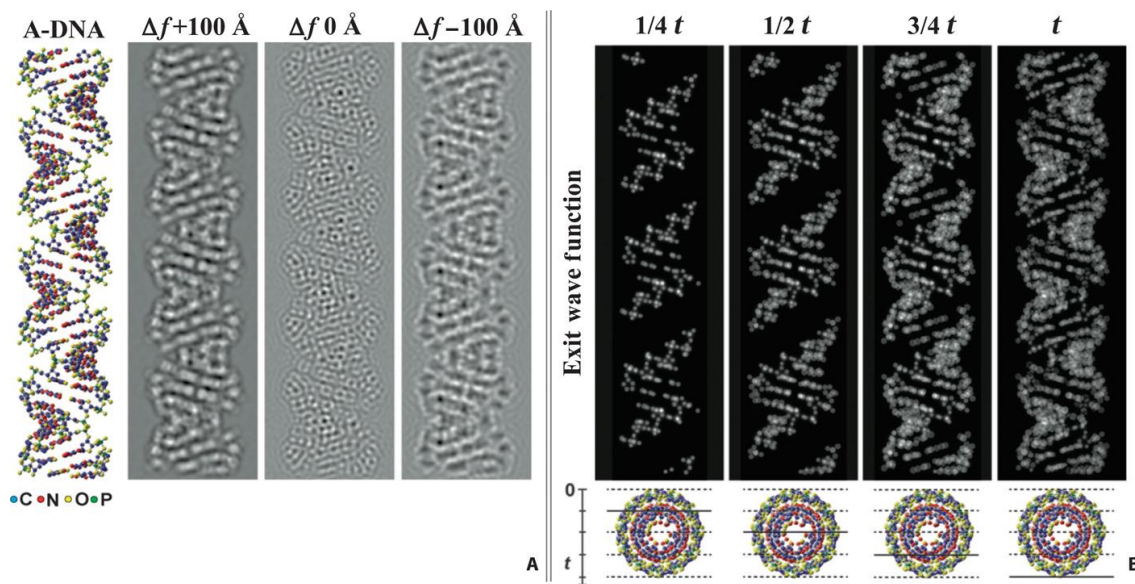
Figure 2.7: Atomic model of A-DNA and corresponding TEM image simulations calculated using three defocus (Δf) values [99].

This background of the figure shows some of the thousands of molecules needed for averaging to reconstruct and refine a model for the DNA. The fore-figure furthest to the right shows the refined helix structures.

2.2.2.3.1 Cryo-TEM Tomography:

An alternative method to obtain a three-dimensional image of biological molecules in the electron microscope is tomography. Electron tomography follows the same principles as that used in other imaging modalities (such as X-ray computed tomography). Projections of the same object is taken at a range of angles surrounding the object [96]. This is done in the electron microscope by tilting the specimen as the beam is fixed. The three-dimensional reconstruction is then based on the central slice theorem which states that 'a projection at a given angle is a central section through the Fourier transform of that object' [97], hence, performing an inverse Fourier transform on the collated Fourier transformed projections results in the reconstruction of the object in three dimensions. This has been done on cell sections as room temperature for the desmosome [98], resulting in a revelation in the understanding of the interaction of intermediate filaments and the rest of the cell. Cryo-STEM tomography of whole, unstained vitrified cells has also recently been demonstrated [99].

Tomography of single molecules is possible through cryo-TEM but is more challenging as the sample is more delicate, and the dose is higher per unit area of the sample, however, this has been performed on large molecules such as the herpes simplex virus [100] and immunoglobulins [101].

The reconstruction of the slices can be a computationally demanding process. It is helpful if there are reference points in the images which can be used to aid in registration between slices, these are known as fiducial markers. In electron microscopy, a highly electron scattering object is most useful as a fiducial marker, as it can easily be detected in an image; gold nanoparticles are ideal for this purpose [102].

2.2.2.4 Zeta-Potential

When suspended, many nanoparticles or colloidal particles have a surface load. Due to the interaction between the charged particle and the applied field, the electrons migrate when an electrical field is applied. The movement direction and velocity is a function of the particle charge, the medium of suspension, and the strength of the electric field. The velocity of the particles is then evaluated by watching the change of the Doppler in the dispersed light. The particle velocity on the shear plane that is zeta potential is proportional to the particle's electrical potential. This optical particle movement measurement under an applied field can thus be used to determine the zeta potential.
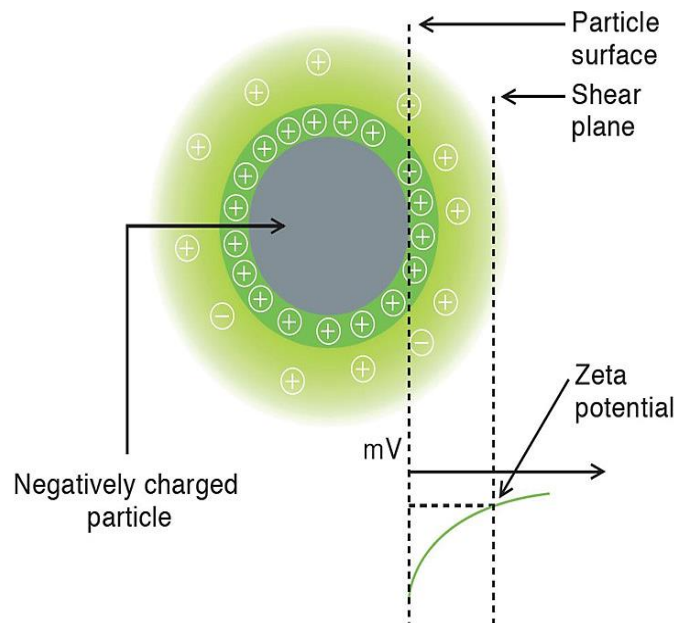
Figure 2.8 Representation of the electrical double layer on a negatively charged particle, highlighting the existence of Stern layer and sliding plane in the Diffuse layer. Positive electrode is shifting the adverse particle. [68]

Particle movement is known as electrophoresis under an applied electric field. The technique is known as the electrophoresis of laser Doppler. Particles of the sample are suspended in a liquid known as the refractive index n, the speed π and the dielectric constantπ. The sample is irradiated by wavelength π laser light. A power E electrical field is applied. The electrons are moving because of the electric field. Since the particles are moving, the dispersed angle light is evaluated, and the frequency change determines the particle velocity V. Mobility is then acquired as the velocity radio to the V / E electric field intensity. Mobility is then discovered using a Smulochowski model,

the most commonly used

$$U = \frac{\lambda \cdot Vd}{2 \cdot E \cdot n \cdot \sin(\theta/2)}$$

The following equation is used for the relationship between the calculated electrical mobility and zeta potential.

$$\zeta = \frac{U\eta}{\varepsilon f(ka)},$$

where ζ – Zeta potential, U – Electrical mobility, E – Electric field strength, ε – Solvent dielectric constant, n – Solvent refraction index, η – Solvent viscosity, f(ka) – henry coefficient

2.2.2.5 Nuclear Magnetic Resonance:

Nuclear magnetic resonance is defined as a condition when the frequency of the rotating magnetic field becomes equal to the frequency of the processing nucleus. If ratio frequency energy and a, magnetic field are simultaneously applied to the nucleus, a condition as given by the equation $v = \gamma H_0/2\pi$ is met. The system at this condition is said to be in resonance [v — frequency of radiation associated with transition from one state to the other; γ = proportionality constant and H_0 = magnetic field]

The nuclear magnetic resonance principle is based on atomic nuclei spins. The magnetic measurements rely on the spin of unpaired electron while the magnetic resonance measure the magnetic effect induced by protons and neutrons spinning. Both of these nucleons have inherent angular moments or spins and therefore behave as basic magnets.

In the hyper-fine structure of spectral lines, the presence of nuclear magnetism was disclosed. If the nucleus is positioned in the magnetic field with a certain magnetic moment, we can observe the phenomenon of space quantization and there will be a slightly distinct energy level for each permitted direction.

The hydrogen nucleus or protons can be considered as a positive charged

spinning unit, creating a small HO magnetic field along its spinning axis (as shown in Figure 2.9). If this nucleus is now positioned in an internal magnetic field H_0, it will naturally align either parallel A or antiparallel B with the internal field direction. The A, being of reduced energy, will be more stable.

As the nucleus flips from one direction to the other, the energy difference AE between two states will be absorbed or emitted.
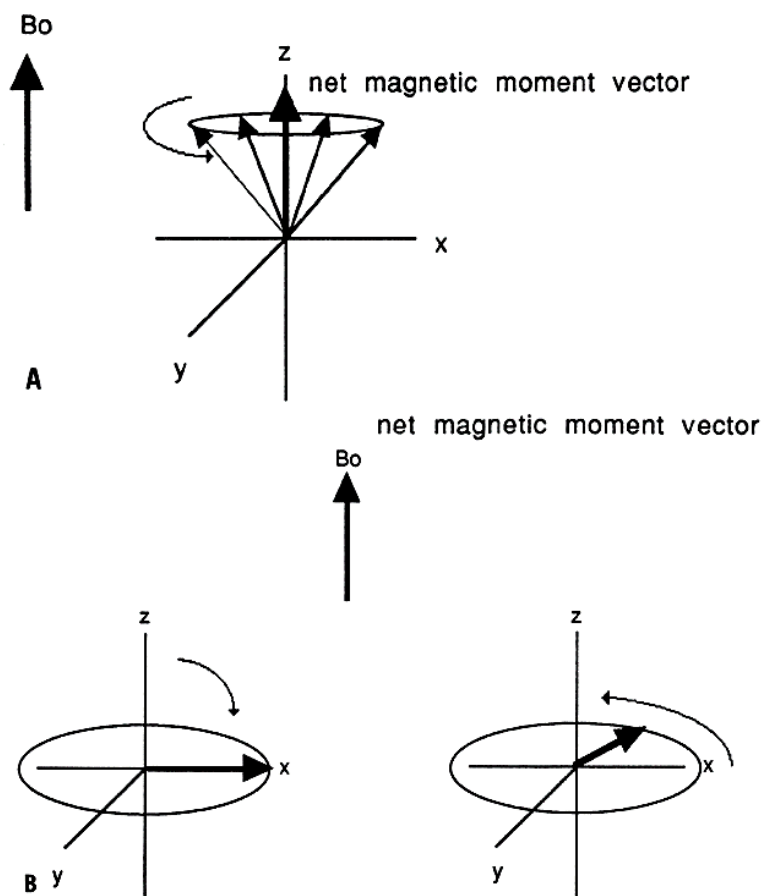
Figure 2.9: A. Diagram showing individual nuclei aligning with the main magnetic field (B0). The summation of the individual magnetic moments creates a net magnetic moment vector. The individual nuclei precess around the Z axis at a frequency proportional to the main magnetic field strength. B.Following a 90° RF excitation pulse, the net magnetic vector rotates into the transverse X-Y plane. On discontinuation of the RF pulse, the magnetic moment vector begins to precess in the X-Y plane.[108]

Then AE = hv

where v = a radiation frequency and h = Planck's constant

If correct frequency is applied to the sample containing hydrogen nuclie and sample is placed in the external field HQ, then low energy nuclie A will absorb AE = hv, and flips

to B. Thus, on flipping back down, they remit hv as a radiation signal which is picked up by the instrument.

In other words, if both radio frequency and magnetic field are simultaneously applied to the nucleus, transition from lower to higher level will occur when equation (1) will be equal to (2).

$\Delta E = \partial hH/2\pi \dots (1)$

$\Delta E = hv \dots (2)$

or $v = \delta H/2\pi \dots (3)$

δ = Gyromagnctic ratio, a constant characteristic of a particular nucleus.

Where ΔE = energy difference between two spin states, h = Planck's constt, v = frequency of resonance absorption, H = strength of applied magnetic field at nucleus. The system at this condition is said to be in resonance and hence the name nuclear magnetic resonance. The observed value of H is therefore a function of molecular environment of proton affording the signal.

Relaxation processes are defined as different types of radiation-less transitions by which a nucleus in an upper spin slate returns to a lower spin state. There are two types of relaxation processes such as Spin-spin Relaxation (It is affected by mutual exchange of spins by two processing nuclei in close proximity to each other) and Spin Lattice Relaxation. This process maintains an excess of nuclei in a lower state, which is the essential basic condition for the observation of nuclear resonance phenomenon.

In a NMR spectroscopy the sharp resonance lines are observed for stales of extended excitation, and broad lines are observed for short-lived excited stales. Both the processes, spin-spin relaxation and spin lattice relaxation contribute to he width of a spectral line. The atoms like O^{16} and C_{12} which have even number of protons and neutrons have no magnetic moment and hence refuse to give resonance signals. While atoms such as P^{21}, F^{19}, which have odd number of protons and even numbers of neutrons, if any, generate nuclear magnetic moments and "hence give resonance signals.

In our research work, we are interested in collecting ^{19}F-NMR spectra in order to demonstrate the presence of the super fluorinated probe in our nanocarriers. On the same

spectrometer, also ^{19}F relaxation times T1 and T2 were recorded at 305 K. The inversion recovery and the cpmg pulse sequences were used for the measures of T1 and T2, respectively. In the results section, chemical shifts are reported in parts per million (ppm). A solution of trifluoroacetic acid (TFA) in D_2O 36mM at known concentration with chemical shift set at ~ -75.5 ppm was added

Upon deduction of an estimate of the number of ^{19}F atoms in the standard, a proportion was made between the integral of the reference solution peak, that is, the area subtended by it, and the integral of the sample along with its corresponding fluorine atom content. Using MestreLab ® MNova Software, the integrals of both peaks were assessed. The standard solution was the reference role, so its integral was normalized to 1. The sample maximum region value then modulated accordingly. The amount of ^{19}F atoms in the volume contained in the NMR tube was obtained from the proportion between the integrals. This amount, however, referred to a sample of 400 μL, so it had to be scaled to its complete volume. Once the content of ^{19}F atoms was known throughout the resulting dispersion, it was divided by the number of fluorine atoms in a single PERFECTA molecule to obtain the final number of molecules of the probe and the corresponding moles. The latter was split by the original quantity of PERFECTA used in the formulation to estimate the contrast agent's encapsulation output.

The number of fluorine atoms are calculated using the following calculations:

$$integral\ value_{NMR\ sample} : 1 = {}^{19}Fatoms_{NMR\ sample} : {}^{19}Fatoms_{TFA}$$

$$\rightarrow {}^{9}Fatoms_{NMR\ sample} = {}^{19}Fatoms_{TFA} \cdot integral\ value_{NMR\ sample}$$

$$^{19}Fatoms_{Total\ sample} = \frac{volume_{Total\ sample}}{volume_{NMRsample}} \cdot {}^{19}Fatoms_{NMRsample}$$

$$PERFECTA\ molecules_{final} = \frac{{}^{19}Fatoms_{Total\ sample}}{36}$$

$$PERFECTA\ moles_{final} = \frac{PERFECTA\ molecules_{final}}{N^{\circ}_{Avogadro}}$$

$$PERFECTA\ moles_{initial} = \frac{PERFECTA\ weight_{initial}}{Molecular\ Weight}$$

$$Yield\ of\ encapsulation\ (\%) = \frac{PERFECTA\ moles_{final}}{PERFECTA\ moles_{initial}} \cdot 100$$

Chapter 3: Fluorinated DOPC-based liposomes

3.1 DOPC liposomes loaded with PERFECTA

3.1.1 Introduction

In recent years, the interest of research was addressed to the chemical synthesis of phospholipids in order to obtain a single component with well-defined structure and configuration properties. [41] In fact, as mentioned in section 1.3, synthetic phospholipids are purer and more stable than natural ones, even though they are also more expensive. Among synthetic phospholipids, 1,2-dioleoyl-sn-glycero-3-phosphocholine (DOPC) was selected in this thesis work since it is frequently used for liposomal formulations for its very low melting temperature (-17°C). [67] DOPC is a zwitterionic phospholipid synthetized *via* acylation of sn-Glycero-3-phosphocholine. [89] Studies noticed that liposomes prepared with mostly unsaturated phospholipids, like DOPC, proved to have higher load entrapping efficiency than those prepared starting from saturated phospholipids. [39]
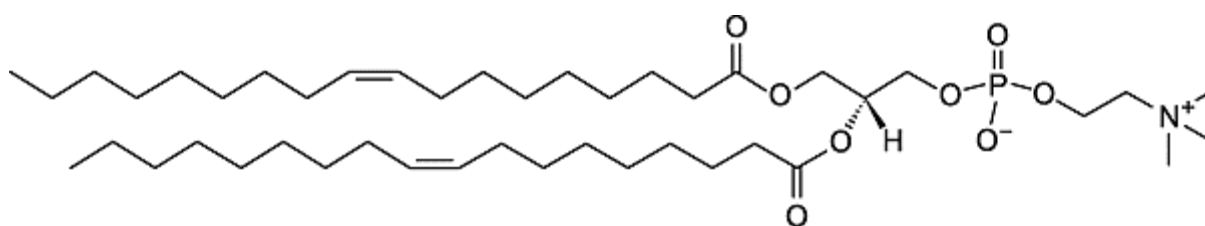
Figure 3.1 – Chemical structure of 1,2-dioleoyl-sn-glycero-3-phosphocholine (DOPC). [67]

In our research project, DOPC liposomes loaded with PERFECTA were prepared according to the thin-film hydration method, similarly to Lecithin liposomes in section 3.1.2.1. In the following sections, the performed work of optimization is described in detail. First of all, the optimization involved the determination of the best

PERFECTA/DOPC ratio in order to have the highest encapsulation. Secondly, also the preparation protocol and the post-processing techniques, which proved to play a relevant role in final entrapping efficiency, size and polydispersity, were improved.

3.1.2 Experiment

Firstly, 25mg of DOPC was taken in a round bottom flask and 10 mg of PERFECTA were solubilized in 1 mL of the solution of CHCl3:Solkane 5:1 volume ratio by means of bath sonication (7-10 minutes, room temperature, 59 kHz frequency, 100% power). Successively, the PERFECTA solution was poured onto the 25mg of of DOPC in a round bottom flask. DOPC dissolution was accelerated by vortexing. The solvents were then evaporated under vacuum and a translucent lipid film with white dots was observed on the walls of the flask. The thin film was dried under vacuum for 30 min. Successively, it was hydrated by adding 1 mL of 150mM of Nacl and vortexed for 20 minutes. The sample was bath sonicated for 15 minutes at 59 kHz and 40°C. Finally, an extra amount of 150mM Nacl equal to 500 µL was added in order to ensure complete hydration. The two operations of vortexing and bath sonication were alternatively repeated for three cycles.

The DOPC with PERFECTA sample was heated at 40°C in Thermoblock and extruded with two subsequent extrusions (21 passages each): firstly with 200 nm polycarbonate membrane, secondly with 100 nm membrane.

Dialysis was performed for the sample to ensure complete removal of the organic solvent. The Sample was poured in a dialysis membrane with molecular weight-cut-off (MWCO) of 2 kDa, previously wetted with the same solvent used in the sample hydration (150mM Nacl). Then, the closed membrane was submerged in 150 mL of the same dispersant and kept under gentle stirring overnight. DLS and ^{19}F-NMR measurements was performed after hydration, extrution and dialysis.

3.2 DOTAP/DOPC liposomes

3.2.1 Introduction

Cationic lipid chemistry is under continuous improvement and has been synthesized by more and more advanced molecules. [92] In comparison with ionizable lipids such as DODAP, cationic lipids are always charged positively, irrespective of the external pH. If they are self-assembled into liposomes, the presence of this net positive charge on the surface of the vesicles is responsible for the binding with negative nucleic acid phosphates. Among cationic lipids, N-(1-(2,3-dioleoyloxy)propyl)-N, N, N-trimethylammonium, is one of the most widely used since it is relatively cheap but also very efficient in *in vitro* and *in vivo* applications. [90] In addition, it is often coupled to produce lipoplexes with DOPC as a helper lipid. Therefore, the vast quantity of literature research on DOTAP / DOPC liposomes for gene delivery led to the belief that further tests on oligonucleotide binding would be simpler once PERFECTA encapsulation has been optimized on this type of system. [93, 94]
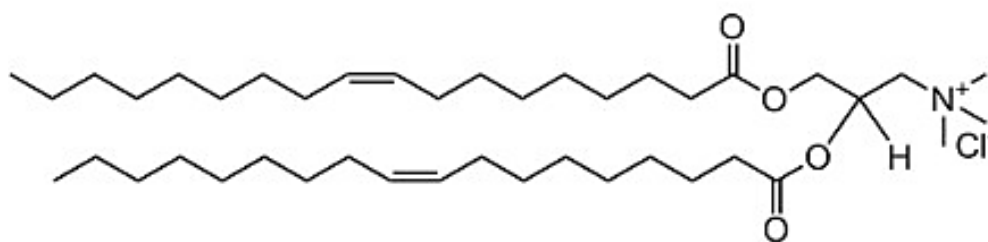
Figure 3.2 – Chemical structure of N-(1-(2,3-dioleoyloxy)propyl)-N,N,N-trimethylammonium chloride (DOTAP). [67]

In the following sections, DOTAP/DOPC liposomes were formulated with PERFECTA and the composition and protocol is described in the following sections.

3.2.2 Experimental

Firstly, 18.1 mg of DOPC and 6.9 mg of DOTAP was taken in a round bottom flask (molar ratio DOTAP/DOPC 3:7). The lipids were solubilized using 0.5 mL of a CHCl3:Solkane 5:1 volume ratio to each of the two flask and vortexed for few seconds for complete dissolution. The lipid solution from one flask was retrieved and added to the other flask and vortexed. 10 mg of PERFECTA was weighed in a vial. The lipid solution was added to the PERFECTA and bath sonicated (7-10 minutes, room temperature, 59 kHz frequency, 100% power). The solvents were then evaporated under vacuum and a translucent lipid film with white dots was observed on the walls of the flask. The thin film was dried under vacuum for 30 min. Successively, it was hydrated by adding 1 mL of 150mM of Nacl and vortexed for 20 minutes. The sample was bath sonicated for 15 minutes at 59 kHz and 40°C. Finally, an extra amount of 150mM Nacl equal to 500 µL was added in order to ensure complete hydration. The two operations of vortexing and bath sonication were alternatively repeated for three cycles.

The DOPC/DOTAP with PERFECTA sample was heated at 40°C in Thermoblock (a white precipitate is observed) and extruded with two subsequent extrusions (21 passages each): firstly with 200 nm polycarbonate membrane, secondly with 100 nm membrane.

Dialysis was performed for the sample to ensure complete removal of the organic solvent. The Sample was poured in a dialysis membrane with molecular weight-cut-off (MWCO) of 2 kDa, previously wetted with the same solvent used in the sample hydration (150mM Nacl). Then, the closed membrane was submerged in 150 mL of the same dispersant and kept under gentle stirring overnight. DLS and ^{19}F-NMR measurements was performed after hydration, extrution and dialysis.

3.3 Results and Discussion

We performed two different liposome formulations one with DOPC loaded with PERFECTA (molar ratio 0.31) and other formulation with DOTAP & DOPC loaded with PERFECTA (molar ratio 3:7). The preparation protocol included lipid solubilization in a chloroform and solkane solution and subsequent dissolution of the lipid solution to solid PERFECTA (10 mg). The organic solvents were then evaporated, and the deposited lipid film was hydrated by vortexing and bath sonication at 40 ° C in 1.5 mL of Nacl. The most effective post-processing techniques involved two cycles of extrusion, with 200 and 100 nm polycarbonate membranes, followed by overnight dialysis.

As already recognized from literature, the technique of thin-film hydration generates large and non-homogeneous multi-lamellar vesicles which require further treatment to become homogeneous small uni-lamellar vesicles. [110] Thus, for our formulation we used thin-film hydration technique. The liposome size was explored by measuring DLS. The sample was thus checked by DLS at the different stages of preparation. We performed four DLS readings at angles 70, 90, 100 and 110 for each test consisting of three sub-runs with a length of 10 seconds. Then we usually reported the hydrodynamic size value obtained by the cumulant fitting i.e. Z-Average size as averaged value of the particle's hydrodynamic radius. A second important number is the polydispersity index which is a measure of the width of the particle size distribution. Z-Averaged hydrodynamic radii and PDI values are reported in Table 4.1.

DLS results showed that samples were extremely polydispersed before extrusion and dialysis due to the formation of multilamellar vesicles, while a decrease was observed after these treatments. Conversely, as indicated in Table 4.1, it was unexpected that data fitting provided a small hydrodynamic size. The doubt of obtaining a dispersion of micelles instead of liposomes is arousing, as micelles are smaller because they are created from a single lipid layer, typically with the hydrophilic heads facing the water clustering together and the hydrophobic tails [23]. The small size of the liposomes might be due to the co-presence of empty liposomes, liposomes containing PERFECTA in the lipid bilayer and small micelles containing PERFECTA or PERFECTA particles surrounded by a lipid monolayer. For all these purposes, additional structural studies were conducted using SAXS and Cryo-TEM as

indicated in the following parts.
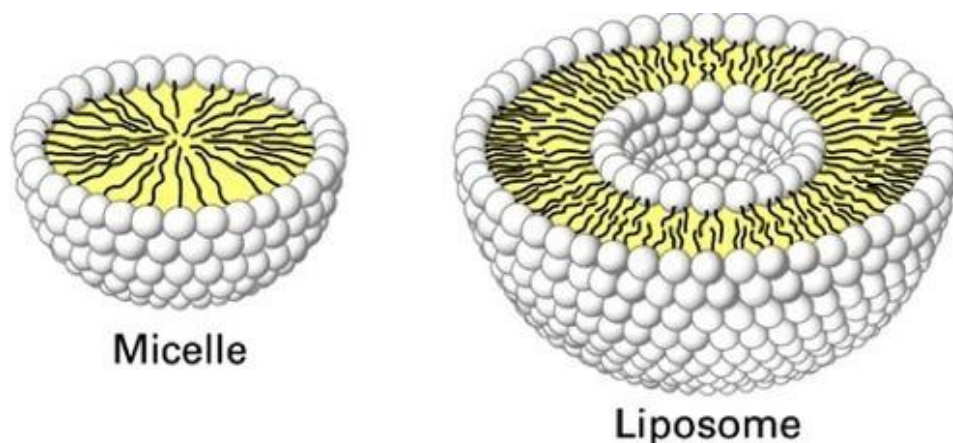
Figure 3.3: "Alternative particles based on lipids: micelle and liposome" [23]

Sample	PDI			$<R_H>$ [nm]	
	After hydration	*After extrusion*	*After dialysis*	*After extrusion*	*After dialysis*
A1	0.42	0.28	0.24	27± 5	27± 5
B1	0.38	0.29	0.21	36± 5	36± 5
C1	0.38	0.37	0.35	88± 4	88± 4
D1	0.25	0.27	0.22	53± 5	53± 5

Table 3.1 – The PDI and $<R_H>$ evaluated for A1 (DOPC liposomes loaded with PERFECTA with molar ratio 0.31), B1 (DOTAP/DOPC liposomes with PERFECTA formulated at the molar ratio 3:7), C1 (DOPC), D1 (DOTAP/DOPC) hydrated by using 150 mM of Nacl. The analysis was collected at each processing step.

Extrusion has been shown to be a useful method to reduce polydispersity and obtain a homogeneous dispersion from the information gathered. Before extrusion, heating the sample proved to be an efficient trick to reduce the effort needed. The lipid bilayer's mobility also generally improves by raising the temperature. [23] It would not be possible to extrude straight with a polycarbonate membrane with pores with a diameter of 100 nm due to the elevated pressure difference on the two opposite sides of the membrane. Both extrusion cycles played an important part as can be seen in each step by the PDI's continuously declining value. A more homogeneous dispersion led in a better adjustment of the rates of decomposition as a function of the scattering vector q square at various corners. For this reason, the linear fitting determination coefficient R2 approached the unit at each step more and more. This means

that at the end of the extrusion phase, the calculated value of the hydrodynamic radius becomes more accurate.

In addition, dialysis has resulted in an extra improvement of the final quality of the liposomes. Indeed, one of the primary issues in the manufacture of liposomes for medical apps is caused by organic solvent toxicity, which can cause severe health impacts, especially halogenated ones. Accordingly, tests were carried out to remove organic solvents under vacuum forming lipid film while purification was tried after preparing. Several methods for removing solvent traces from liposomes have been suggested in literature; among them, dialysis is one of the most used [23]. In our experiments, dialysis was performed overnight and a loss of roughly 20% in volume was generally observed.

In order to evaluate the impact of medicines and dispersants on them, a preliminary research on DOPC. DOTAP/DOPC liposomes was conducted without encapsulating PERFECTA. DLS sample measurements were registered in the Table 4.2 below after dialysis. From the results we observed a higher PDI value showing that the sample was polydisperse and a higher hydrodynamic radius could be due to the presence of aggregates that can be confirmed by the SAXS experiment and the results of the SAXS were discussed in the following sections.

A) *Correlation Function*

B) *Intensity-weighted aver*
averaged size distribution

C) *Decay coefficient fitting*

$$y = 8E+06x - 180.68$$
$$R^2 = 0.998$$

Figure 3.4 - DLS analysis of sample A1(DOPC loaded with PERFECTA) after dialysis. Graph A reports the correlation function and graph B the intensity-weighted averaged size distribution at different detection angles: 70°, 90°, 110°, 130°. Graph C shows the linear trend of the decay rates Γ as a function of the square of the scattering vector q.

A) *Intensity-weighted aver averaged size distribution (Radius and radius number weight)*

B) *Correlation function at 90⁰*
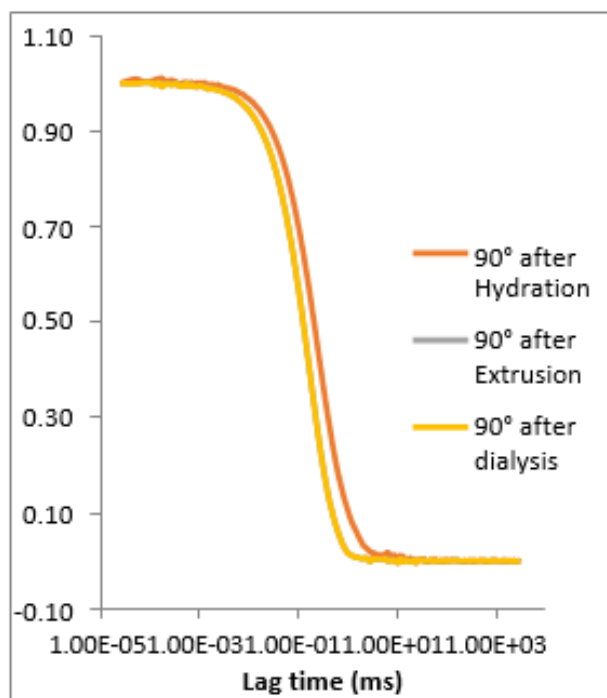
Figure 3.5 - DLS analysis of sample A1(DOPC loaded with PERFECTA) after dialysis. Graph A reports the intensity-weighted averaged size distribution at 90° for Radius and radius number weight after hydration, extrusion and dialysis. Graph B shows the correlation function at 90° after hydration, extrusion and dialysis.

A) *Correlation Function*

B) Intensity-*weighted aver*
averaged size distribution

C) *Decay coefficient fitting*

$y = 7E+06x - 463.64$
$R^2 = 1$

Figure 3.6 - DLS analysis of sample B1(DOPC & DOTAP with PERFECTA) after dialysis. Graph A reports the correlation function and graph B the intensity-weighted averaged size distribution at different detection angles: 70°, 90°, 110°, 130°. Graph C shows the linear trend of the decay rates Γ as a function of the square of the scattering vector q.

A) *Intensity-weighted aver averaged size distribution (Radius and radius number weight)*

B) *Correlation function at 90º*
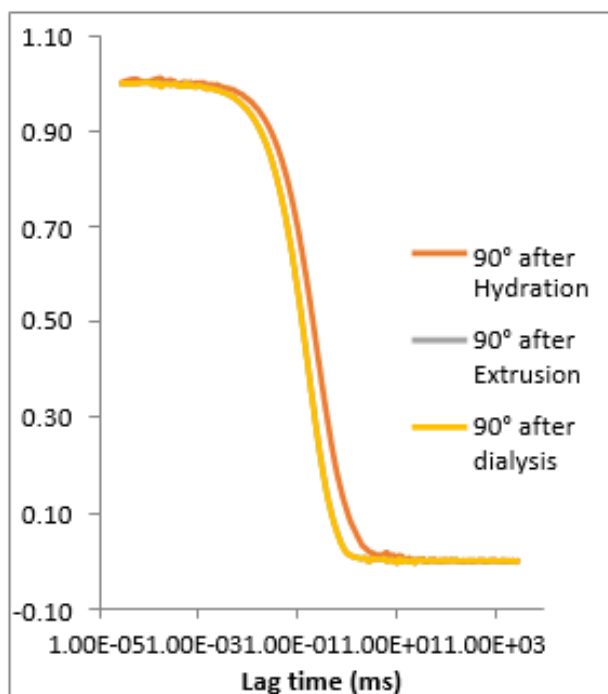
Figure 3.7 - DLS analysis of sample B1(DOTAP & DOPC loaded with PERFECTA) after dialysis. Graph A reports the intensity-weighted averaged size distribution at 90° for Radius and radius number weight after hydration, extrusion and dialysis. Graph B shows the correlation function at 90° after hydration, extrusion and dialysis.

A) *Correlation Function*

B) *Intensity-weighted aver averaged size distribution*

C) *Decay coefficient fitting*

$y = 3E+06x - 189.7$
$R^2 = 0.9982$
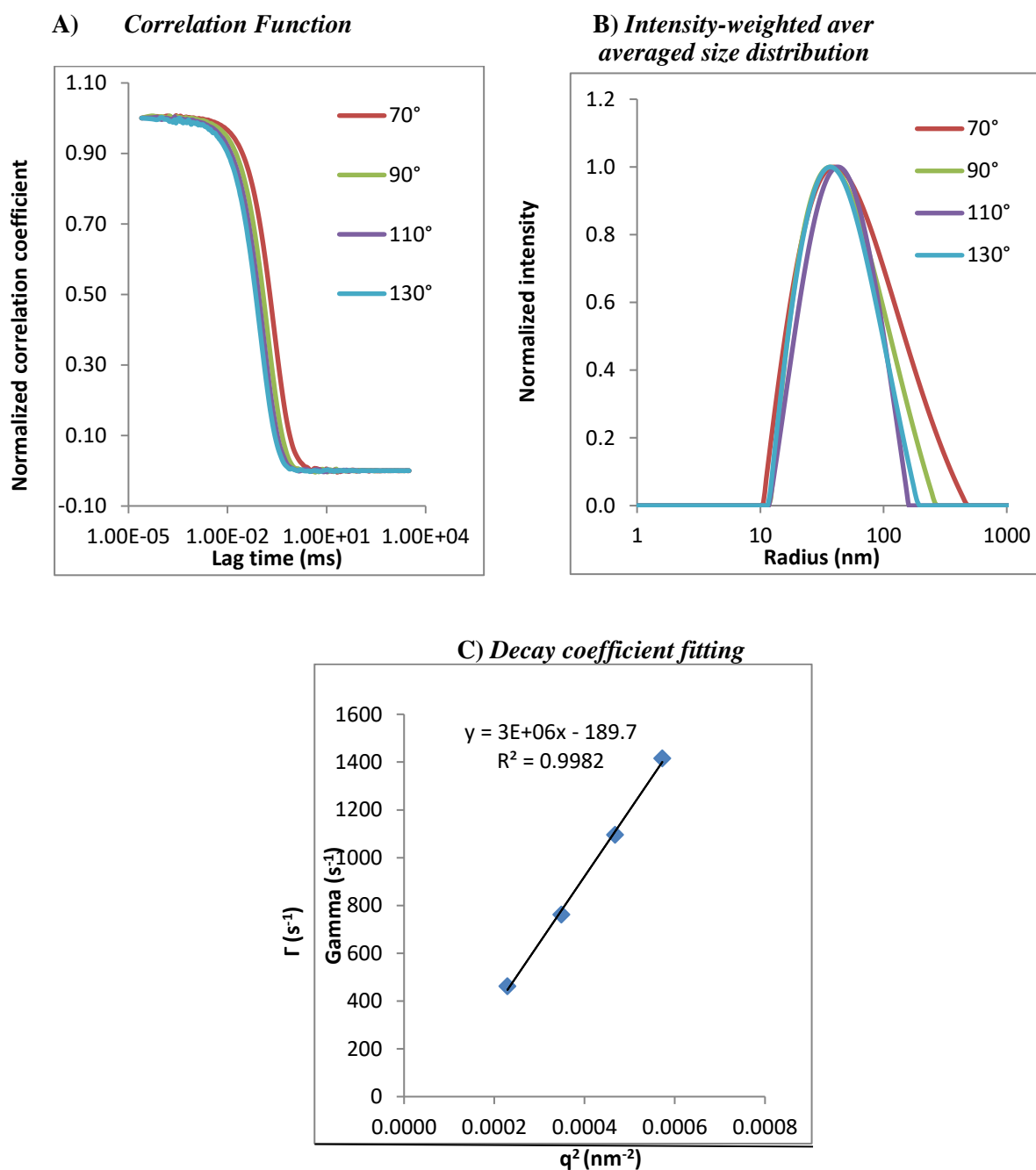
Figure 3.8 - DLS analysis of sample C1(DOPC without PERFECTA) after dialysis. Graph A reports the correlation function and graph B the intensity-weighted averaged size distribution at different detection angles: 70°, 90°, 110°, 130°. Graph C shows the linear trend of the decay rates Γ as a function of the square of the scattering vector q.

A) *Correlation Function*
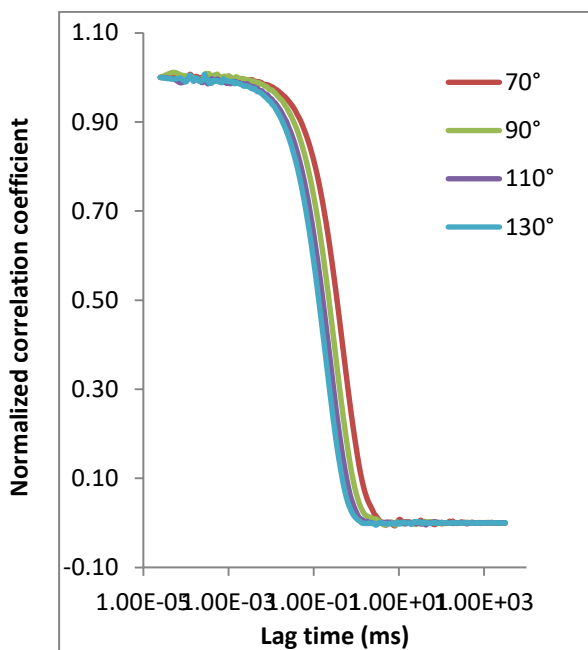
B) *Intensity-weighted aver averaged size distribution*

C) *Decay coefficient fitting*

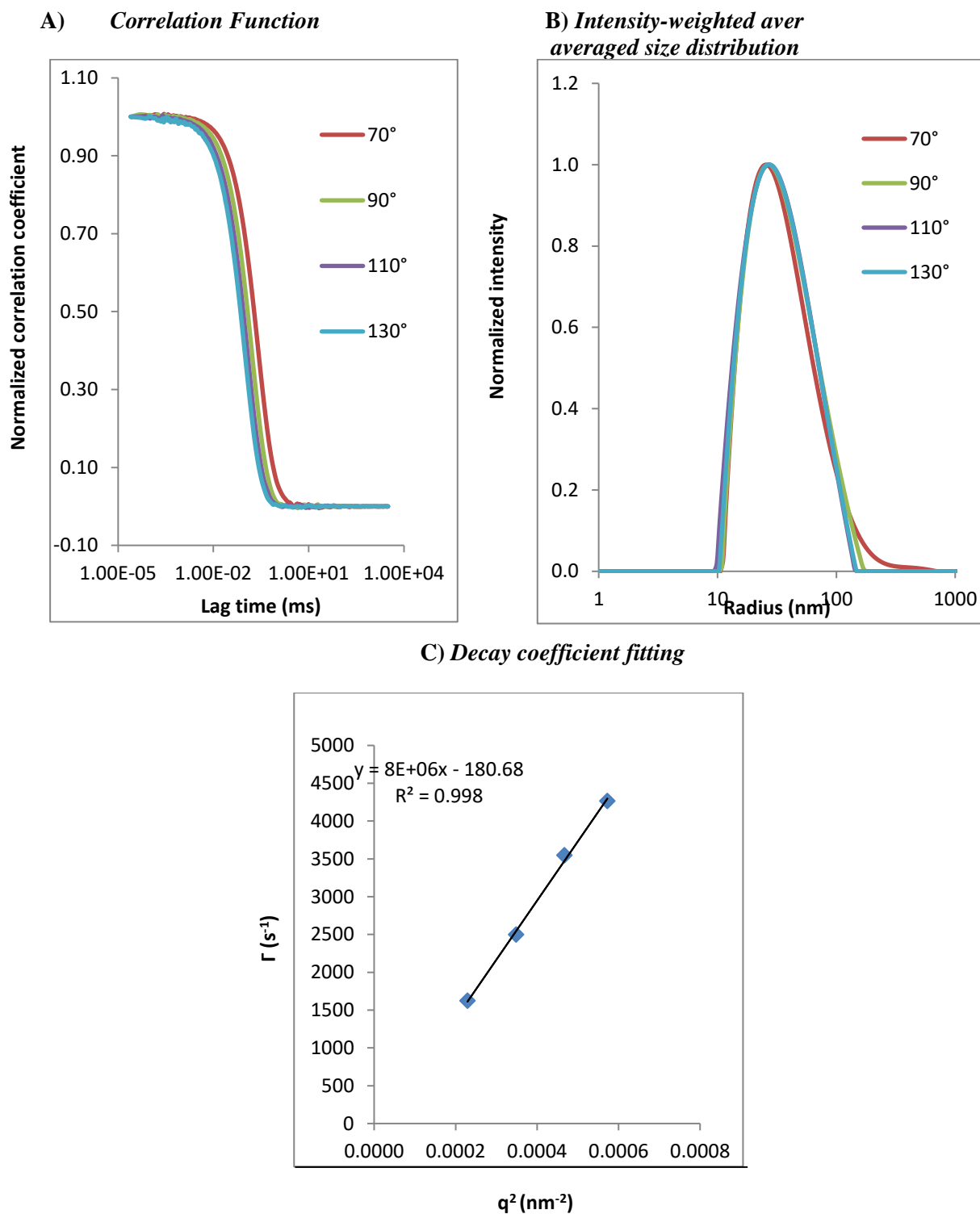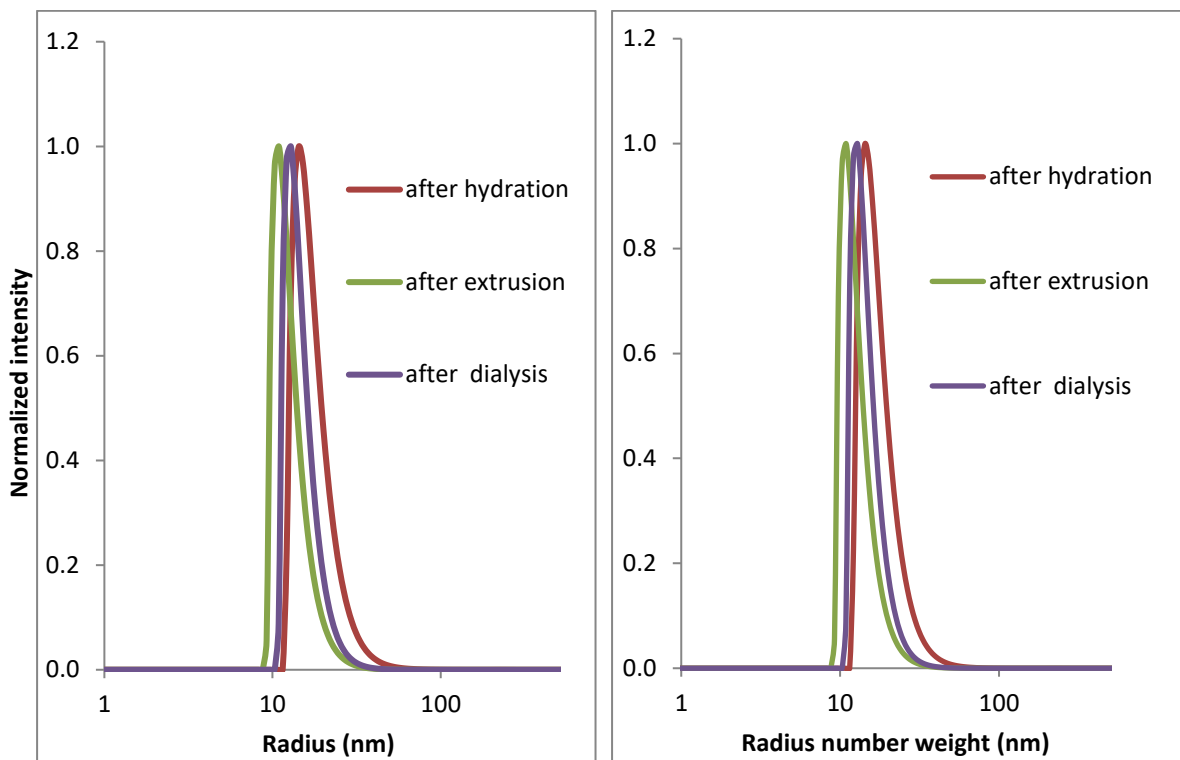$$y = 4E+06x - 139.58$$
$$R^2 = 0.9998$$

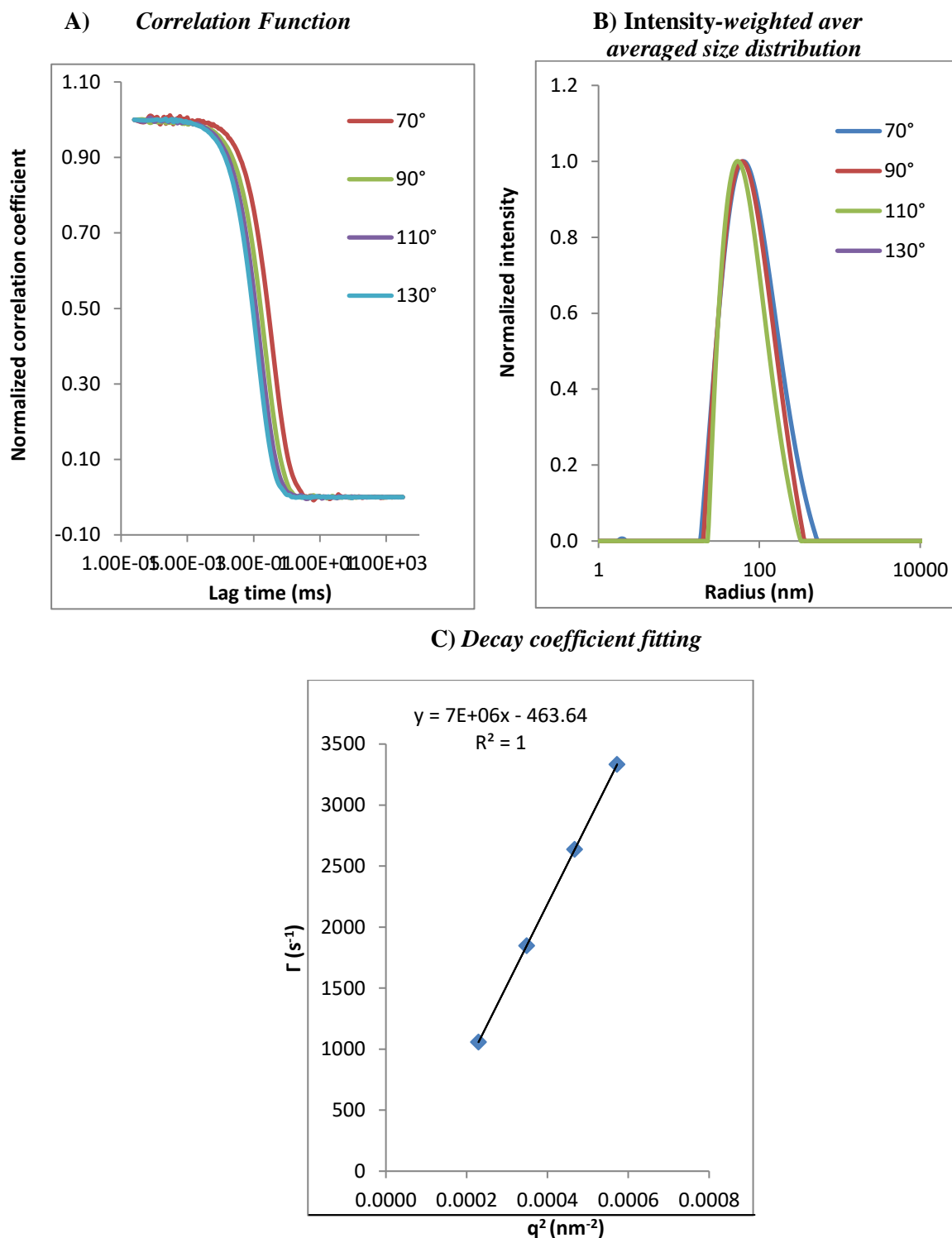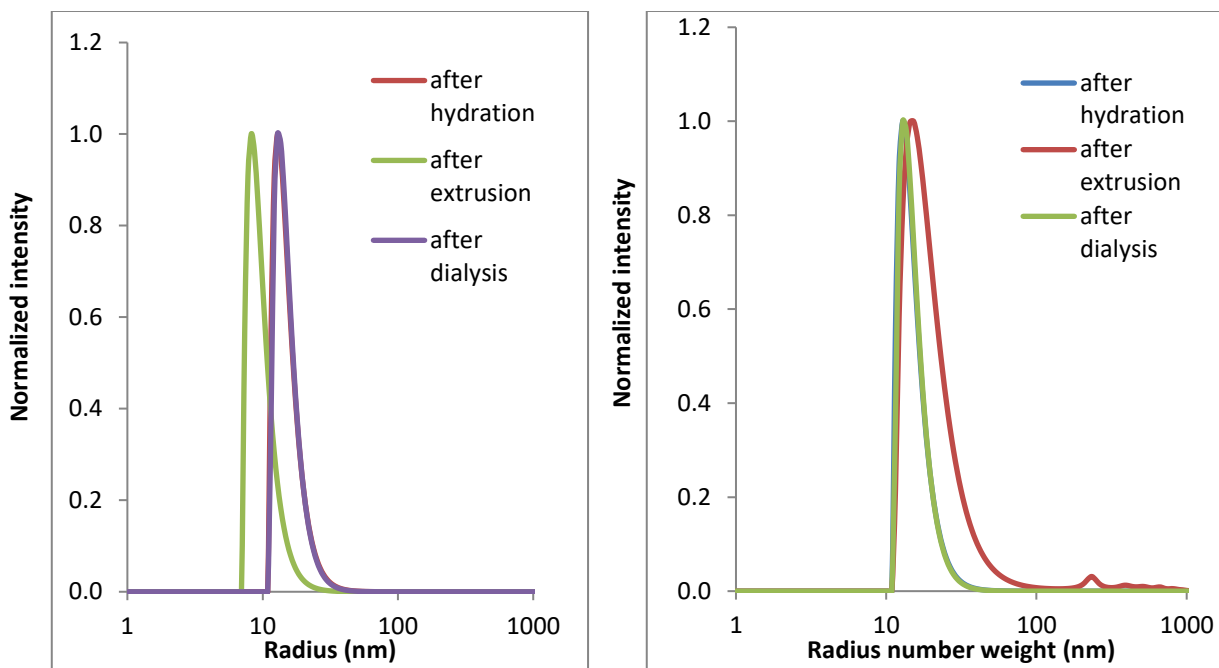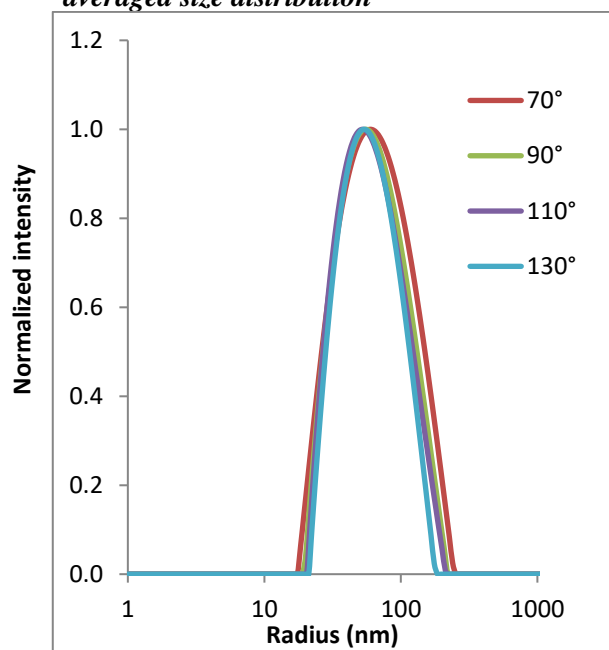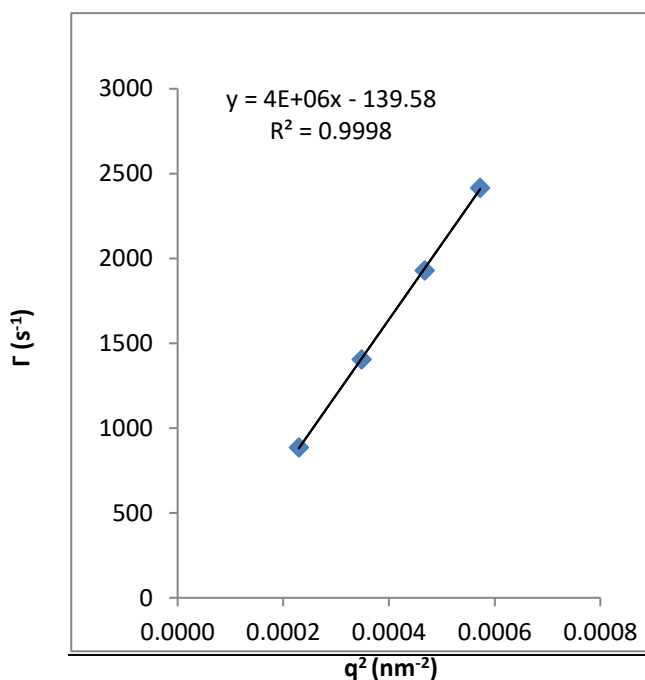**Figure 3.9 - DLS analysis of sample D1(DOTAP & DOPC without PERFECTA) after dialysis. Graph A reports the correlation function and graph B the intensity-weighted averaged size distribution at different detection angles: 70°, 90°, 110°, 130°. Graph C shows the linear trend of the decay rates Γ as a function of the square of the scattering vector q.**

When a DOPC lipid solution was dissolved in CHCl3:Solkane poured on solid

PERFECTA, there was a noticeable rise in the trapping effectiveness. Samples A1, A2 and A3 were prepared using the latter methodology and with the optimal initial PERFECTA / DOPC that was previously determined. The findings of ^{19}F-NMR showed a greater encapsulation in synthetic neutral liposomes of our superfluorinated sample. Comparison of DLS outcomes after extrusion and dialysis as well as estimation of PERFECTA loss due to extrusion and dialysis, expressed in terms of the remaining ^{19}F electrons and encapsulation yield, are recorded below for sample A1.

Sample	*solvent*	*^{19}F atoms (x 10^{19})*	*Yield of PERFECTA encapsulation [%]*
A1 (AFTER HRDRATION)	NaCl 150 mM	6.9x 10^{20}	319
A2 (AFTER EXTRUTION)	NaCl 150 mM	2.0x 10^{20}	93.
A3 (AFTER DIALYSIS)	NaCl 150 mM	1.4 x10^{20}	63.

Table 3.2: The number of ^{19}F atoms and corresponding yield of encapsulation estimated for sample A1 after hydration, extrusion and after dialysis treatment.
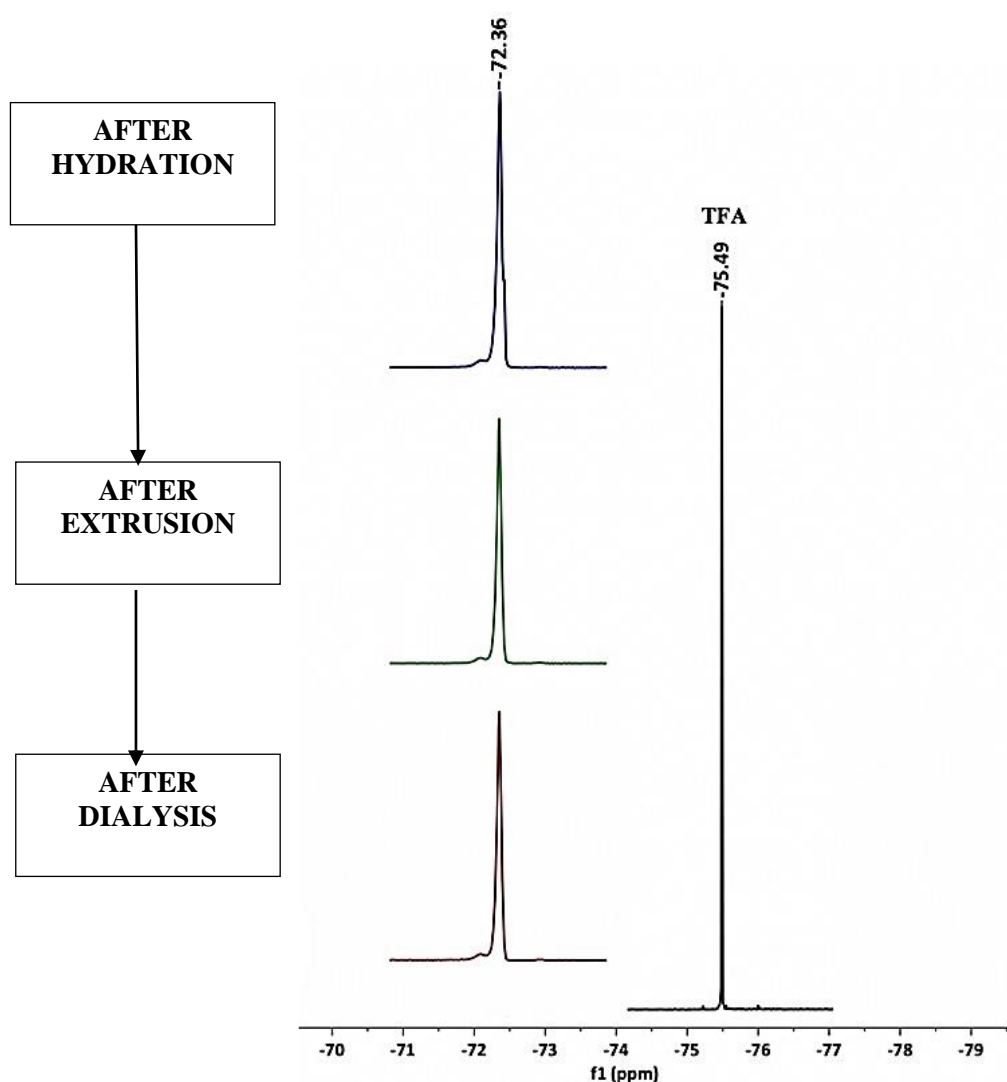
Figure 3.10 – ^{19}F-NMR spectra of the sample A1 is reported (on the left). The peak of PERFECTA, at -72.36 ppm, recorded after hydration, after extrusion and after dialysis respectively, has been compared to the peak of the TFA reference solution at -75.49 ppm

substantial enhancement in the PDI. Regarding the outcomes of the ^{19}F-NMR spectroscopy, they showed that at each phase of the post-processing methods there was a loss in the quantity of encapsulated contrast agent. The fact that extrusion causes the breakage and instant liposome reformation could explain it. Some of the superfluorinated molecules may be lost in this procedure. On the other side, dialysis may also require either removing some organic solvent residues or possibly small PERFECTA encapsulating micelles. Extrusion, in specific, meant a greater output decrease compared to dialysis. However, the final liposomes have a satisfactory encapsulation yield, with a high level of fluorine, sufficient for detection

of MRI. Finally, as relaxation times play a significant part in the sensitivity of ^{19}F-MRI, the ^{19}F-NMR relaxation behaviors of optimized DOPC liposomes loaded with PERFECTA, corresponding to sample A1, have been explored. [3] Small T1 and T1/T2 ratios are known to result in increased signal-to-noise ratios. For this reason, the most desirable conditions are short T1 and long T2. [6] Sample A1 showed values of T1 and T2 equivalent to 679 ms and 323 ms respectively, as recorded in Table 4.4. For our formulation, a comparable T1 value and a significantly greater T2 value were predicted for those acquired for the PERFECTA emulsion with Lecithin and Safflower Oil in the literature. [5] This demonstrates that our liposomes are highly suitable for MRI applications, with T1 and T2 values in the right range for providing valuable images at MRI.

sample	*T1 [ms]*	*T2 [ms]*
A1	679	323
PERFECTA emulsion	622	181

Table 3.3 – Relaxation times T1 and T2 evaluated for the sample A1. These data are compared to those obtained for the emulsion of PERFECTA reported in literature. [5]

As it is small and reproducible in size, it has elevated fluorine atoms content and excellent characteristics for ^{19}F-MRI, the advanced liposomal formulation has promising characteristics for theranostic applications. The experiments performed on adding a cationic component to the lipid mixture are described in the next sections in order to obtain, in addition to the properties, also a positive surface charge of the vesicles.

Sample (D1)	*PDI @90°*	*<R$_H$> [nm]*	*Zeta Potential [mV]*
After hydration	0.24	41.8 ± 4.2	61.1 ± 12.9
After Extrusion	0.22	45.3 ± 4.5	59.3 ± 13.9
After Dialysis	0.21	43.8 ± 4.4	61.1 ± 12.9

Table 3.4 – The PDI, <R$_H$> and Mean Zeta Potential of sample D1(DOTAP & DOPC loaded with PERFECTA) after hydration, extrusion and dialysis are reported.

As already noted for DOPC liposomes loaded with PERFECTA, it can be noted from Table 4.5 that the hydrodynamic radius of the samples was small even prior to extrusion. However, even before extrusion, the PDI also occurred to be quite small in this situation. As a result, the post-processing method only given a slight enhancement in polydispersity and fit for size determination. One possible reason for this phenomenon is to observe the formation of a precipitate at 40° C conducted prior to extrusion during the bath sonication. The larger liposomes probably precipitated, and they reduced the PDI of the resulting suspension by staying in the flask. The high ZP values before and after extrusion, however, confirmed that the labeled liposomes are still positively charged and stable, even when encapsulated with PERFECTA. Through dialysis, the sample was further purified. After dialysis, complete sample characterization was conducted, including assessment of ZP, ^{19}F-NMR, T1 and T2.

Zeta Potential Distribution
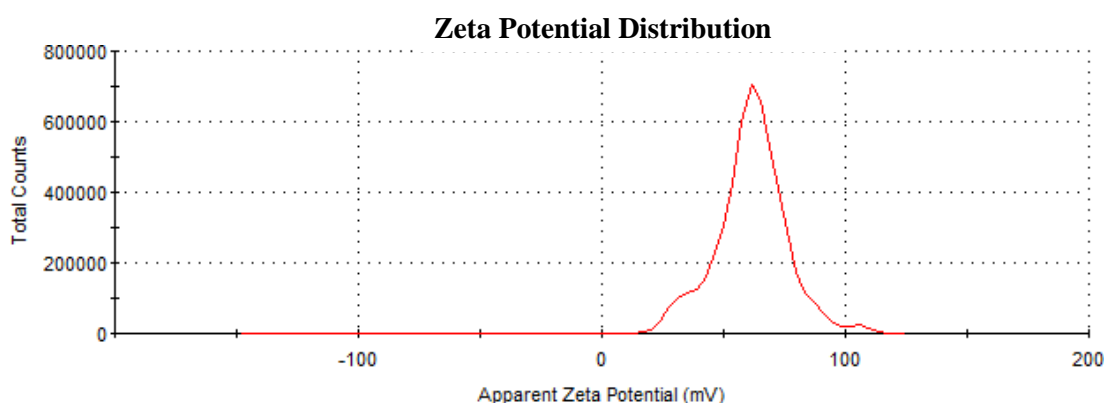
Figure 3.11 - Zeta potential distribution of sample B1 (DOTAP/DOPC loaded with PERFECTA) after dialysis.

Sample	solvent	^{19}F atoms (x 10^{19})	Yield of PERFECTA encapsulation [%]
D1 (AFTER HRDRATION)	NaCl 150 mM	1.6x 10^{20}	73.
D2 (AFTER EXTRUTION)	NaCl 150 mM	1.0x 10^{20}	46
D3 (AFTER DIALYSIS)	NaCl 150 mM	8.0x10^{19}	37

Table 3.5: The number of ^{19}F atoms and corresponding yield of encapsulation estimated for sample A1 after hydration, extrusion and after dialysis treatment.

Sample	^{19}F Atoms (10^{19})	Yield of encapsulation (%)	T1 [ms]	T2 [ms]
D1	8.0	37	597	323

Table 3.6 - Estimated values of the number of ^{19}F atoms, corresponding yield of encapsulation and relaxation times T1 and T2 of sample B1 after dialysis are reported.
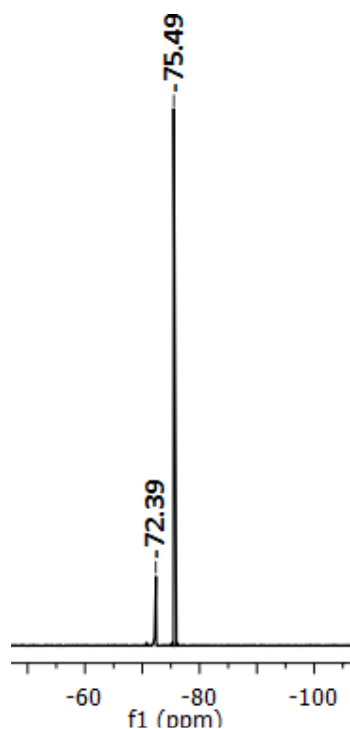
Figure 3.12 - ^{19}F-NMR spectra of sample B1 after dialysis. PERFECTA peak at -72.39 ppm has been compared to TFA reference solution peak at -75.49 ppm.

The collected dispersion ZP value was considerably high and positive, demonstrating stable and cationic liposomes. PERFECTA encapsulation yield was high enough, corresponding to a number of fluorine atoms well above the ^{19}F-MRI detection limit. Eventually, the T1 relaxation time was short enough and the T2 value was long enough to ensure high MR image resolution. As for fluorinated DOTAP / DOPC liposomes, the T2 value was the same as that obtained for DOPC liposomes in Table 4.8, whereas T1 was even lower (597 ms versus 679 ms). These data also demonstrated that the developed fluorinated DOTAP/DOPC liposomes are even more suitable for MRI applications respect to the PERFECTA emulsion reported in literature. [5]

Due to all the above-mentioned characteristics, DOTAP / DOPC liposomes labeled with PERFECTA and prepared according to the described protocol and composition (DOTAP / DOPC molar ratio 3:7 and total lipid concentration of 25 mg / mL) may be considered an optimal theranostic vesicle for gene complexation to be studied. Structural studies were done using SAXS and Cryo-TEM the results are discussed below.

A) Small-angle X-Ray Scattering Spectra
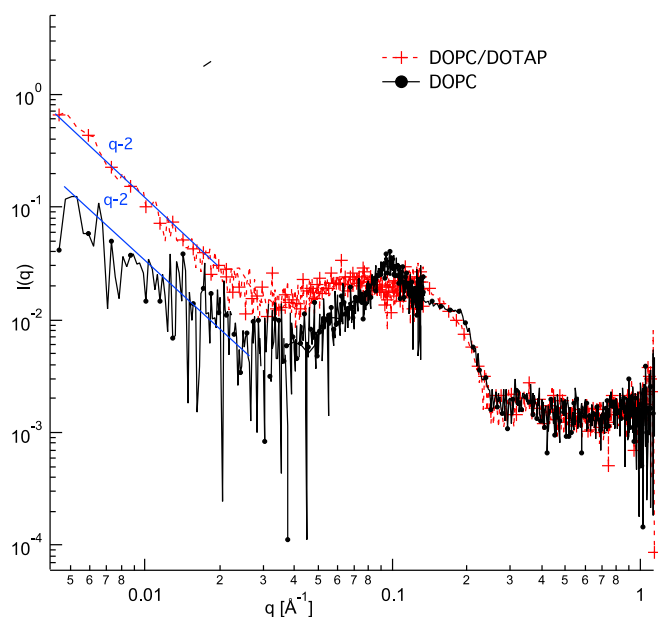
FIGURE 3.13: Small-angle X-rays Scattering spectra of DOPC (25mg) and DOPC-DOTAP liposomes (3:7 molar ratio containing 18.1 mg of DOPC & 6.9 mg of DOTAP)

Figure 3.13 shows the typical spectra of liposomes, the bump at intermediate q values is due to the presence of a lipid bilayer and the fact that it is more pronounced for DOPC formulation (with the appearance of a peak) is due to the presence of a certain amount of multi-lamellar vesicles. At low-q values it is observable the typical power law I(q) vs q^{-2}, fingerprint of the presence of a lipid bilayer.

Small-angle X-Ray Scattering Spectra
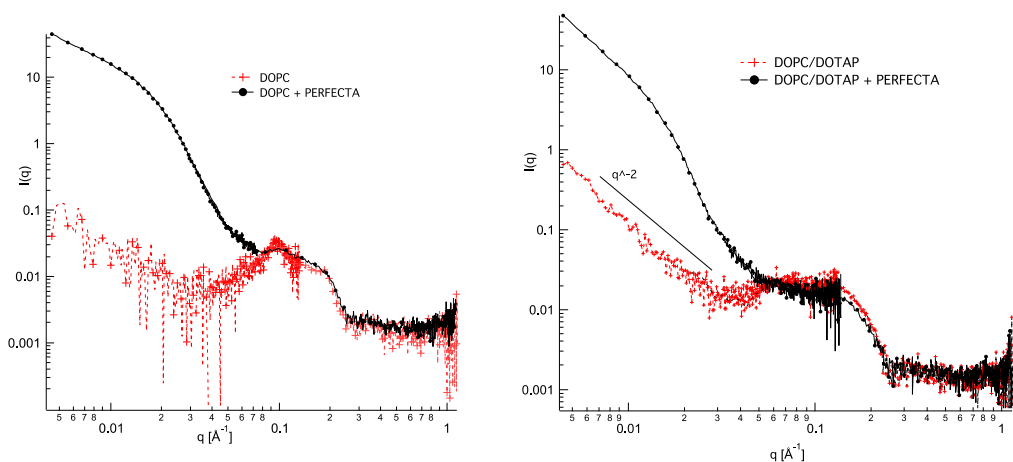
FIG 3.14: SAXS spectra of DOPC (25mg, molar ratio 0.31) and DOPC-DOTAP liposomes (3:7 molar ratio containing 18.1 mg of DOPC & 6.9 mg of DOTAP) prepared with PERFECTA (10mg) according to protocol.

Figure 3.14 shows the SAXS spectra of the liposome formulations upon addition of the fluorinated probe, PERFECTA. As it can be observed by the sharp change of slope at low-q values, PERFECTA addition induced a drastic ^{77} ication of the local structure of the aggregates. It was not possible to find a typical power law that can be related to a precise shape of the aggregates. This probably means that a distribution of different populations is present in the sample, empty liposomes co-exist with PERFECTA-lipid aggregates. From the SAXS results we observed that the q^{-2} power law was completely lost therefore the main population was represented by the NPs and not by the liposomes. Further studies were carried out using Cryo-TEM.

Cryo-TEM was a two-dimensional projection of three-dimensional objects. Liposomes were spherical, creating a dark circle with an even darker edge contour. This dark contour was derived from the dispersion of electrons in the portion of the beam that meets the largest stretch of liposomal wall. In face-to-face situation, a circular disk of comparable material was also depicted by a dark circular region, but without a rim in this situation. If the disk was small compared to the thickness of the liquid film, it will also be present in other directions regarding the direction of the electron beam, giving rise to elliptical predictions, all the way to a straight dark rod in complete edge-on perspective.

First, the thin areas were penetrated by far more electrons than the dense areas. Usually the picture at the holes ' rims will be very dark and very bright in the center. In order to achieve printable pictures, this impact must be compensated for in the image treatment.

Cryo-TEM Images

A)

B)

C)
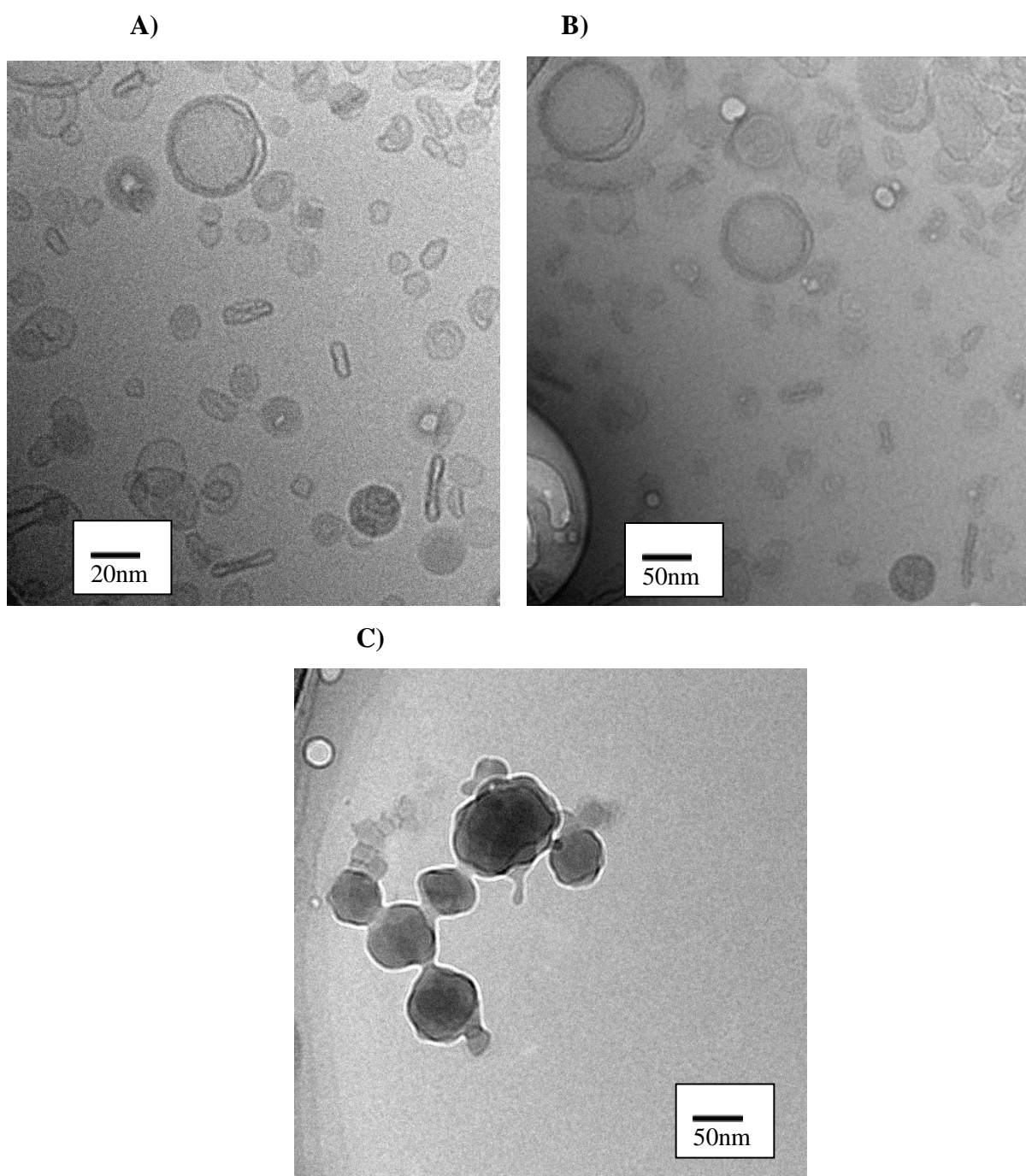
Figure 3.15 :The transmission electron microscopy (TEM) images were collected using JEM 3200FS field emission microscope (JEOL) operated at 300 kV in bright field mode with Omega-type Zero-loss energy filter. The images were acquired with GATAN DIGITAL MICROGRAPH software while the specimen temperature was maintained at -187 oC. The Cryo-TEM samples are prepared by placing 3 µL aqueous dispersion of sample on a 200 mesh copper grid with holey carbon support film (Holey Carbon-Cu,200mesh, 50 micron) and plunge freezed using vitrobot with 2s blotting time under 100% humidity.

From the outcomes of cryo-TEM we noticed that the dark circular regions are the PERFECTA nanoparticles probably coated by a monolayer of lipids while the lighter regions with a darker border are the empty liposomes without PERFECTA or may be with PERFECTA included in the bilayer. From the picture we also observed single wall liposomes all this likely implies that in the sample there was a distribution of various populations like empty liposomes coexist with PERFECTA-lipid aggregates, liposomes containing PERFECTA in the lipid bilayer and small micelles containing PERFECTA or PERFECTA particles surrounded by a lipid monolayer. However, from the SAXS results we observed that the q^{-2} power law was completely lost, the main population was represented by the NPs and not by the liposomes. Future studies focus on the gene transfer property of developed liposomes.

Conclusions

The aim of this research work was the development and optimization of innovative formulations of cationic liposomes carrying a new superfluorinated contrast agent, i.e. PERFECTA for in vivo imaging by ^{19}F-MRI. The cationic formulation was due to the need of deliver miRNA into the cells as therapeutics against ALS. ALS is a fatal neurodegenerative disease; it is proved that miRNA as a biomarker to study the mechanism of neural differentiation in ALS. miRNA are small non-coding RNAs that bind to the complementary target sequences is altered in the ALS patients, thus miRNA is determined to have a new therapeutic approach to the disease. However, cationic liposomes are usually formulated by using a lipid mixture of cationic and zwitterionic lipids, due to the high toxicity of the cationic lipid alone. Therefore, in our research work, neutral liposomes loaded with PERFECTA were firstly developed and then the cationic component was added in order to obtain positively charged formulations. In this work, we synthesized a liposome nanocarrier which consist of a mixture of both neutral (DOPC) with molar ratio 0.31 and cationic liposomes (DOTAP) with the molar ratio 3:7 to effectively transfer miRNA into neuronal cells and be trackable by ^{19}F-MRI with the help of superfluorinated contrast agent called PERFECTA, has high fluorine density, low toxicity, chemical stability which produces a single sharp NMR peak.

Liposomes are generally considered to be pharmacologically inactive with minimal toxicity, as they are composed of natural phospholipids (Koning and Storm, 2003; Metselaar and Storm, 2005; Ding et al., 2006; Hua and Wu, 2013). Liposomal formulations are characterized by properties such as particle size, charge, number of lamellae, lipid composition and surface modification, which govern their stability in vitro and in vivo. ^{19}F-MRI used as a complementary diagnostic technique to ^{1}H-MRI. ^{19}F-MRI provides non-invasive in-depth in vivo detection, higher sensitivity, real-time response, and can be coupled to ^{1}H-MRI to provide selectively high-contrast images of the nanovector in vivo.

The structure ensuring maximum trapping effectiveness was the one based on an original PERFECTA / DOPC molar proportion equivalent to 0.31, corresponding to 25 mg of DOPC for 10 mg of PERFECTA. The optimum preparation protocol included lipid solubilization in a chloroform and solkane solution and subsequent dissolution of the lipid solution to solid PERFECTA. The organic solvents were then evaporated, and the deposited lipid film was

Conclusions

hydrated by vortexing and bath sonication at 40 ° C in 1.5 mL of Nacl. The most effective post-processing techniques involved two cycles of extrusion, with 200 and 100 nm polycarbonate membranes, followed by overnight dialysis. The result was a monodispersed suspension of liposomes (PDI = 0.236), small and reproducible in size (<R_H> = 45 nm), with high fluorine atoms content (1.364x 10^{20}) and good properties for ^{19}F-MRI (T1=679 ms, T2=323 ms). The preparation protocol and the post-processing techniques were the same optimized for DOTAP/DOPC liposomes. This time the result was an almost homogeneous suspension of cationic liposomes (PDI = 0.21), with a positive surface charge (ZP = 61 mV), again small and reproducible in size (<R_H> = 54 nm), with less but still high fluorine atoms content (7.958$_x$ 10^{19}) and better properties for ^{19}F-MRI (T1=597 ms, T2=323 ms).

The SAXS spectra of the liposome formulations upon addition of the fluorinated probe, PERFECTA. As it can be observed by the sharp change of slope at low-q values, PERFECTA addition induced a drastic modification of the local structure of the aggregates. It was not possible to find a typical power law that can be related to a precise shape of the aggregates. This probably means that a distribution of different populations is present in the sample, empty liposomes co-exist with PERFECTA-lipid aggregates.

From the outcomes of cryo-TEM we can notice that the dark circular regions are the liposomes loaded with PERFECTA and the lighter regions are the liposomes without PERFECTA. From the picture we also observed single wall liposomes all this likely implies that in the sample there is a distribution of various populations, vacant liposomes coexist with PERFECTA-lipid aggregates. But from the SAXS results we observed that the q^{-2} power law was completely lost therefore the main population was represented by the PERFECTA NPs and not by the liposomes.

Overall, these results showed that pure liposomes are not a good system to encapsulate PERFECTA as most the superfluorinated probe seems to form different kind of aggregates with the lipids. Thus, even if these formulations are characterized by a good encapsulation yield and suitable relaxation parameters for 19F-MRI imaging, more efforts should be dedicated to obtaining a homogenous formulation with aggregates with the same size and shape.

[1] G. Whitesides and P. Alivisatos, "Fundamental Scientific Issues for Nanotechnology.," in *Nanotechnology Research Directions: IWGN Workshop Report.* , Dordrecht, Springer, 2000, pp. 1-24.

[2] T. J. Webster, "Nanomedicine: what's in a definition," *International Journal of Nanomedicine,* vol. I, no. 2, pp. 115-116, 2006.

[3] I. Fernandez-Piñeiro, I. Badiola and A. Sanchez, "Nanocarriers for microRNA delivery in cancer medicine," *Biotechnology Advances,* no. 35, pp. 350-360, 2017.

[4] I. Fernandez-Piñeiro, I. Badiola and A. Sanchez, "Nanocarriers for microRNA delivery in cancer medicine," *Biotechnology Advances,* no. 35, pp. 350-360, 2017.

[5] J. M. Caster, A. N. Patel, T. Zhang and A. Wang, "Investigational nanomedicines in2016: a review of nanotherapeutics currently undergoing clinical trials," *WIREs Nanomed Nanobiotechnol ,* vol. 9, 2017.

[6] L. Jin, X. Zeng, M. Liu, Y. Deng and N. He, "Current Progress in Gene Delivery Technology based on Chemical methods," *Theranostics,* vol. 4, no. 3, pp. 240-255, 2014.

[7] L. Sercombe, T. Veerati, F. Moheimani, S. Y. Wu, A. K. Sood and S. Hua, "Advances and Challenges of Liposome Assisted Drug Delivery," *Front. Pharmacol.,* vol. 6, p. 286, 2015.

[8] N. Pippa, S. Pispas and C. Demetzos, "The delineation of the morphology of charged liposomal vectors via a fractal analysis in aqueous and biological media: Physicochemical and self-assembly studies," *International Journal of Pharmaceutics,* vol. 437, pp. 264-274, 2012.

[9] S. Kargozar and M. Mozafari, "Nanotechnology and Nanomedicine: Start small, think big," *Materials Today: Proceedings,* no. 5, p. 15492–15500, 2018.

[10] U. S. N. N. Initiative, "National Nanotechnology Initiative," [Online]. Available: https://www.nano.gov. [Accessed October 2018].

[11] S. M. Janib, A. S. Moses and J. A. MacKay, "Imaging and drug delivery using theranostic nanoparticles," *Advanced Drug Delivery Reviews,* vol. 62, pp. 1052-1063, 2010.

[12] J. Xie, S. Lee and X. Chen, "Nanoparticle-based theranostic agents," *Advanced Drug Delivery Reviews,* vol. 62, pp. 1064-1079, 2010.

[13] S. D. Patil, D. G. Rhodes and D. J. Burgess, "DNA-based Therapeutics and DNA

Delivery Systems: A Comprehensive Review," *The AAPS Journal,* vol. 7, no. 1, 2005.

[14] G. Whitesides and P. Alivisatos, "Fundamental Scientific Issues for Nanotechnology.," in *Nanotechnology Research Directions: IWGN Workshop Report.* , Dordrecht, Springer, 2000, pp. 1-24.

[15] I. Fernandez-Piñeiro, I. Badiola and A. Sanchez, "Nanocarriers for microRNA delivery in cancer medicine," *Biotechnology Advances,* no. 35, pp. 350-360, 2017.

[16] J. M. Caster, A. N. Patel, T. Zhang and A. Wang, "Investigational nanomedicines in2016: a review of nanotherapeutics currently undergoing clinical trials," *WIREs Nanomed Nanobiotechnol ,* vol. 9, 2017.

[17] L. Jin, X. Zeng, M. Liu, Y. Deng and N. He, "Current Progress in Gene Delivery Technology based on Chemical methods," *Theranostics,* vol. 4, no. 3, pp. 240-255, 2014.

[18] D. Ma, "Enhancing endosomal escape for nanoparticle mediated siRNA delivery," *Nanoscale,* vol. 6, no. 6415–6425, 2014.

[19] S. Hossen, M. K. Hossain, M. K. Basher, M. N. H. Mia, M. T. Rahman and M. J. Uddin, "Smart nanocarrier-based drug delivery systems for cancer therapy and toxicity studies: A review," *Journal of Advanced Research,* 2018.

[20] W. Li and F. C. Szoka Jr, "Lipid-based Nanoparticles for Nucleic Acid Delivery," *Pharmaceutical Research,* vol. 24, no. 3, 2007.

[21] S. Bhattacharya and A. Bajaj, "Advances in gene delivery through molecular design of cationic lipids," *Chem. Commun.,* no. 31, pp. 4632-4656, 2009.

[22] J. N. Israelachvili, Intermolecular and surface forces, Academic press, 2011.

[23] N. Monteiro, A. Martins, Reis, R. L and N. M. Neves, "Liposomes in tissue engineering and regenerative medicine.," *J. R. Soc. Interface,* vol. 11, 2014.

[24] S. Hua and S. Y. Wu, "The use of lipid-based nanocarriers for targeted pain therapies," *Front. Pharmacol.,* vol. 4, no. 143, 21 November 2013.

[25] J. Li, X. Wang, T. Zhang, C. Wang, Z. Huang, X. Luo and Y. Deng, "A review on phospholipids and their main applications in drug delivery systems," *Asian Journal of Pharmaceutical Sciences,* vol. 10, no. 2, pp. 81-98, 2015.

[26] R. P. Singh, H. V. Gangadharappa and K. Mruthunjaya, "Phospholipids: Unique carriers for drug delivery systems," *Journal of Drug Delivery Science and Technology,* vol. 39, pp. 166-179, 2017.

[27] D. Pezzoli, A. Kajaste-Rudnitski, R. Chiesa and G. Candiani, "Lipid-Based Nanoparticles as Nonviral Gene Delivery Vectors," *Nanomaterial Interfaces in Biology,* pp. 269-279, 2013.

[28] M. A. Mintzer and E. E. Simanek, "Nonviral Vectors for Gene Delivery," *Chem. Rev.,* vol. 109, pp. 259-302, 2009.

[29] F. Xiong, Z. MI and N. Gu, "Cationic liposomes as gene delivery system: transfection efficiency and new application," *Pharmazie,* vol. 66, no. 158-164, 2011.

[30] E. Jang, E. Kim, H.-Y. Son, E.-K. Lim, H. Lee, Y. Choi, K. Park, S. Han, J.-S. Suh, Y.-M. Huh and S. Haam, "Nanovesicle-mediated systemic delivery of microRNA-34a for CD44 overexpressing gastric cancer stem cell therapy," *Biomaterials,* no. 105, pp. 12-24, 2016.

[31] Q. Xu, C.-H. Wang and D. W. Pack, "Polymeric Carriers for Gene Delivery: Chitosan and Poly(amidoamine) Dendrimers," *Curr Pharm Des,* vol. 16, no. 21, pp. 2350 ì-2368, July 2010.

[32] D. Ma, "Enhancing endosomal escape for nanoparticle mediated siRNA delivery," *Nanoscale,* vol. 6, no. 6415–6425, 2014.

[33] S. Hossen, M. K. Hossain, M. K. Basher, M. N. H. Mia, M. T. Rahman and M. J. Uddin, "Smart nanocarrier-based drug delivery systems for cancer therapy and toxicity studies: A review," *Journal of Advanced Research,* 2018.

[34] W. Li and F. C. Szoka Jr, "Lipid-based Nanoparticles for Nucleic Acid Delivery," *Pharmaceutical Research,* vol. 24, no. 3, 2007.

[35] Rowland, L.P.; Shneider, N.A. Amyotrophic lateral sclerosis. N. Engl. J. Med. 2001, 344, 1688–1700.

[36] O'Brien, J.; Hayder, H.; Zayed, Y.; Peng, C. Overview of microrna biogenesis, mechanisms of actions, and circulation. Front. Endocrinol. Lausanne 2018, 9, 402.

[37] Ludwig, N.; Leidinger, P.; Becker, K.; Backes, C.; Fehlmann, T.; Pallasch, C.; Rheinheimer, S.; Meder, B.; Stähler, C.; Meese, A.; et al. Distribution of miRNA expression across human tissues. Nucleic Acids Res. 2016, 44, 3865–3877.

[38] Mocellin, S.; Pasquali, S.; Pilati, P. Oncomirs: From tumor biology to molecularly targeted anticancer strategies. Mini Rev. Med. Chem. 2009, 9, 70–80.

[39] Aumiller, V.; Förstemann, K. Roles of microRNAs beyond development—

metabolism and neural plasticity. Biochim. Biophys. Acta. 2008, 1779, 692–696.

[40] Carissimi, C.; Fulci, V.; Macino, G. MicroRNAs: Novel regulators of immunity. Autoimmun. Rev. 2009, 8, 520–524.

[41] Bushati, N.; Cohen, S.M. MicroRNAs in neurodegeneration. Curr. Opin. Neurobiol. 2008, 18, 292–296.

[42] Rajgor, D. Macro roles for microRNAs in neurodegenerative diseases. Noncoding RNA Res. 2018, 3, 154–159.

[43] Rinchetti, P.; Rizzuti, M.; Faravelli, I.; Corti, S. MicroRNA Metabolism and dysregulation in amyotrophic lateral sclerosis. Mol. Neurobiol. 2018, 55, 2617–2630.

[44] Rothstein, J.D. Current hypotheses for the underlying biology of amyotrophic lateral sclerosis. Ann. Neurol. 2009, 65, S3–S9.

[45] Ilieva, H.; Polymenidou, M.; Cleveland, D.W. Non-cell autonomous toxicity in neurodegenerative disorders: ALS and beyond. J. Cell Biol. 2009, 187, 761–772.

[46] Wijesekera, L.C.; Leigh, P.N. Amyotrophic lateral sclerosis. Orphanet J. Rare Dis. 2009, 4, 3.

[47] Brown, R.H., Jr.; Al-Chalabi, A. Amyotrophic lateral sclerosis. N. Engl. J. Med. 2017, 377, 162–172.

[48] Chiò, A.; Logroscino, G.; Traynor, B.J.; Collins, J.; Simeone, J.C.; Goldstein, L.A.; White, L.A. Global epidemiology of amyotrophic lateral sclerosis: A systematic review of the published literature. Neuroepidemiology 2013, 41, 118–130.

[49] Logroscino, G.; Traynor, B.J.; Hardiman, O.; Chio', A.; Couratier, P.; Mitchell, J.D.; Swingler, R.J.; Beghi, E. Descriptive epidemiology of amyotrophic lateral sclerosis: New evidence and unsolved issues. J. Neurol. Neurosurg. Psychiatry 2008, 79, 6–11.

[50] Manjaly, Z.R.; Scott, K.M.; Abhinav, K.; Wijesekera, L.; Ganesalingam, J.; Goldstein, L.H.; Janssen, A.; Dougherty, A.; Willey, E.; Stanton, B.R.; et al. The sex ratio in amyotrophic lateral sclerosis: A population-based study. Amyotroph. Lateral Scler. 2010, 11, 439–442.

[51] Sutedja, N.A.; Fischer, K.; Veldink, J.H.; van der Heijden, G.J.; Kromhout, H.;

Heederik, D.; Huisman, M.H.; Wokke, J.J.; van den Berg, L.H. What we truly know about occupation as a risk factor for ALS: A critical and systematic review. Amyotroph. Lateral Scler. 2009, 10, 295–301.

[52] Andersen, P.M. Amyotrophic lateral sclerosis associated with mutations in the CuZn superoxide dismutase gene. Curr. Neurol. Neurosci. Rep. 2006, 6, 37–46.

[53] Ben Hamida, M.; Hentati, F.; Ben Hamida, C. Hereditary motor system diseases (chronic juvenile amyotrophic lateral sclerosis). Conditions combining a bilateral pyramidal syndrome with limb and bulbar amyotrophy. Brain 1990, 113, 347–363.

[54] Andersen, P.M.; Al-Chalabi, A. Clinical genetics of amyotrophic lateral sclerosis: What do we really know? Nat. Rev. Neurol. 2011, 7, 603–615.

[55] Bigio, E.H.; Weintraub, S.; Rademakers, R.; Baker, M.; Ahmadian, S.S.; Rademaker, A.; Weitner, B.B.; Mao, Q.; Lee, K.H.; Mishra, M.; Ganti, R.A.; Mesulam, M.M. Frontotemporal lobar degeneration with TDP-43 proteinopathy and chromosome 9p repeat expansion in C9ORF72: Clinicopathologic correlation. Neuropathology 2013, 33, 122–133.

[56] Rizzo, F.; Riboldi, G.; Salani, S.; Nizzardo, M.; Simone, C.; Corti, S.; Hedlund, E. Cellular therapy to target neuroinflammation in amyotrophic lateral sclerosis. Cell. Mol. Life Sci. 2014, 71, 999–1015.

[57] Volk, A.E.; Weishaupt, J.H.; Andersen, P.M.; Ludolph, A.C.; Kubisch, C. Current knowledge and recent insights into the genetic basis of amyotrophic lateral sclerosis. Med. Genet. 2018, 30, 252–258.

[58] Kawahara, Y.; Mieda-Sato, A. TDP-43 promotes microRNA biogenesis as a component of the drosha and dicer complexes. Proc. Natl. Acad. Sci. USA 2012, 109, 3347–3352.

[59] Lagier-Tourenne, C.; Polymenidou, M.; Cleveland, D.W. TDP-43 and FUS/TLS: Emerging roles in RNA processing and neurodegeneration. Hum. Mol. Genet. 2010, 19, R46–R64.

[60] Brooks, B.R.; Miller, R.G.; Swash, M.; Munsat, T.L.; World Federation of Neurology Research Group on Motor Neuron Diseases. El escorial revisited: Revised criteria for the diagnosis of amyotrophic lateral sclerosis. Amyotroph. Lateral Scler. Other Motor. Neuron Disord. 2000, 1, 293–299.

[61] Belliveau JW, Kennedy DN, Jr., McKinstry RC, Buchbinder BR, Weisskoff RM,

Cohen MS, Vevea JM, Brady TJ, Rosen BR (1991) Functional mapping of the human visual cortex by magnetic resonance imaging. Science 254:716-719.

[62] Heurtault, B.; Saulnier, P.; Pech, B.; Proust, J.-E.; Benoit, J.-P. Biomaterials 2003, 24, 4283-4300.

[63] Charrois, G. J. R.; Allen, T. M. Biochim. Biophys. Acta 2004, 1663, 167-177.

[64] Gregoriadis, G. FEBS Letters 1973, 36, 292-296.

[65] Davidson, R. N.; Croft, S. L.; Scott, A.; Maini, M.; Moody, A. H.; Bryceson, A. D. Lancet 1991,337, 1061-1062.

[66] Guaglianone, P.; Chan, K.; Delaflor-Weiss, E.; Hanisch, R.; Jeffers, D.; Sharma, D.; Muggia, F. Invest. New Drugs 1994, 12, 103-112.

[67] Torchilin, V. P. Nature Rev. 2005, 4, 145-160.

[68] Safinya, C. R. Curr. Opin. Structural Biol. 2001, 11, 440-448.

[69] Meidan, V. M.; Glezer, J.; Amariglio, N.; Choen, J. S.; Barenholz, Y. Biochim. Biophys. Acta 2001, 1568, 177-182.

[70] Gregoriadis G, Perrie Y (2010) Liposomes. Encycl Life Sci, pp: 1-8.

[71] Mayhew E, Rustum YM, Szoka F, Papahadjopoulos D (1979) Role of cholesterol in enhancing the antitumor activity of cytosine arabinoside entrapped in liposomes. Cancer Treat Rep 63: 1923-1928.

[72] Çagdas M, Sezer AD, Bucak S (2014) Liposomes as potential drug carrier systems for drug delivery. Nanotechnol Nanomater 2014: 1-50.

[73] Li J, Wang X, Zhang T, Wang C, Huang Z, et al. (2014) A review on phospholipids and their main applications in drug delivery systems. Asian J Pharm Sci 10: 81-98.

[74] Bozzuto G, Molinari A (2015) Liposomes as nanomedical devices. Int J Nanomed 10: 975-999.

[75] Taylor KMG, Morris RM (1995) Thermal analysis of phase transition in liposomes behaviour. Thermochim Acta 248: 289-301.

[76] Dölle S, Lechner BD, Park JH, Schymura S, Lagerwall JPF, et al. (2012) Utilizing the Krafft phenomenon to generate ideal micelle-free surfactant-stabilized nanoparticle suspensions. Angew Chemie 51: 3254-3257.

[77] Hagmann WK. The many roles for fluorine in medicinal chemistry. J Med Chem.

2008;51:4359-69.

[78] Heidelberger C, Chaudhuri NK, Daneberg P, Mooren D, Griesbach L, Duschinsky R. Fluorinated pyrimidines, a new class of tumour-inhibitory compounds. Nature. 1957;179:663-6.

[79] Holland GN, Bottomley PA, Hinshaw WS. 19F r[87]ic resonance imaging. J Mag Res. 1977;28:133-6.

[80] Janjic JM, Ahrens ET. Fluorine-containing nanoemulsions for MRI cell tracking. Wiley Interdiscipl Rev Nanomed Nanobiotech. 2005;1:492-501.

[81] Ahrens ET, Flores R, Xu H, Morel PA. In vivo imaging platform for tracking immunotherapeutic cells. Nature Biotechnol. 2005;23:983-7.

[82] Ruiz-Cabello J, Barnett BP, Bottomley PA, Bulte JWM. Fluorine 19F MRS and MRI in biomedicine. NMR in Biomed. 2011;24:114-29.

[83] Kamm YJL, Heerschap A, van den Bergh EJ, Wagener DJT. 19F-magnetic resonance spectroscopy in patients with liver metastases of colorectal cancer treated with 5-fluorouracil. Anti-Cancer Drugs. 2004;15:229-33.

[84] Wang X, Chen J, Wang D, Dong S, Hao J, Hoffmann H. Monitoring the different micelle species and the slow kinetics of tetraethylammonium perfluorooctane-sulfonate by 19F NMR spectroscopy. Advances in Colloid and Interface Science. 2017; DOI:10.1016/j.cis.2017.05.0169.

[85] Drouza C, Dieronitou A, Hadjiadamou I, Stylianou M. Investigation of phenols activity in early stage oxidation of edible oils by electron paramagnetic resonance and 19F NMR spectroscopies using novel lipid vanadium complexes as radical initiators. J Agric Food Chem. 2017;65:4942-51.

[86] Hu H, Katyayan KK, Czeskis BA, Perkins EJ, Kulanthaivel P. Comparison between radioanalysis and 19F Nuclear Magnetic Resonance Spectroscopy in the determination of mass balance, metabolism, and distribution of pefloxacin. Drug Metab Dispos. 2017;45:399-408.

[87] Vints I, Gatenyo J, Rozen S. Fluorination of aryl boronic acids using acetyl hypofluorite made directly from diluted fluorine. J. Org. Chem. 2013;78:11794-7.

[88] Gatenyo J, Hagooly Y, Vints I, Rozen S. Activation of a CH bond in polypyridine systems by acetyl hypofluorite made from F2. Organic & Biomol Chem. 2012;10:1856-60.

[89] Liu Z, Shibata N, Takeuchi Y. Novel methods for the facile construction of 3,3-disubstituted and 3, 3-spiro-2H,4H- -benzo[e]1,2-thiazine-1,1-diones: synthesis of (11S,12R, 14R)-2-fluoro-14-methyl-11-(methylethyl)spiro[4H-benzo[e]- 1, 2-thiazine-

3,2'-cyclohexane]-1,1-dione, an agent for the electrophilic asymmetric fluorination of aryl ketone enolates. J Org Chem. 2000;65:7583-7.

[90] Vora HU, Rovis T. N-Heterocyclic carbene catalyzed asymmetric hydration: direct synthesis of alpha-protio and alpha- -deuterio alpha-chloro and alpha-fluoro carboxylic acids. J Am Chem Soc. 2010;132:2860-61. S. Naeem, L.-V. Kiew, L. Y. Chung, S. F. Kiew and M. B. Misran, "A Comparative [88] ach for the Preparation and Physicochemical Characterization of Lecithin Liposomes Using Chloroform and Non-Halogenated Solvents," *Journal of Surfactants and Detergents*, vol. 18, no. 4, 2015.

[91] J. Dubochet, M. Adrian, J-J Chang, J. Lepault, and A. W. McDowall. Cryoelectron microscopy of vitrified specimens. In Cryotechniques in Biological Electron Microscopy, pages 114–131. Springer, 1987.

[92] M. Adrian, J. Dubochet, J. Lepault, and A. W. McDowall. Cryo-electron microscopy of viruses. 1984.

[93] C. Mory, C. Colliex, and J. M. Cowley. Optimum defocus for STEM imaging and microanalysis. Ultramicroscopy, 21(2):171–177, 1987.

[94] E. V. Orlova and H. R. Saibil. Structural analysis of macromolecular assemblies by electron microscopy. Chemical reviews, 111(12):7710–7748, 2011.

[95] T. Kato, R. P. Goodman, C. M. Erben, A. J. Turberfield, and K. Namba. High-resolution structural analysis of a DNA nanostructure by cryoEM. Nano letters, 9(7):2747–2750, 2009.
J. Frank. Electron tomography: methods for three-dimensional visualization of structures in the cell. Springer Verlag, 2006.

[96] P. A. Midgley and M. Weyland. 3D electron microscopy in the physical sciences: the development of Z-contrast and eftem tomography. Ultramicroscopy, 96(3):413–431, 2003.

[97] W. He, P. Cowin, and D.L. Stokes. Untangling desmosomal knots with electron tomography. Science, 302(5642):109, 2003.

[98] S. G. Wolf, L. Houben, and M. Elbaum. Cryo-scanning transmission electron tomography of vitrified cells. Nature methods, 11(4):423–428, 2014.

[99] K. Grunewald, P. Desai, D.C. Winkler, J.B. Heymann, D.M. Belnap, W. Baumeister, and A.C. Steven. Three-dimensional structure of herpes simplex virus

from cryo-electron tomography. Science, 302(5649):1396, 2003.

[100] L. Bongini, D. Fanelli, F. Piazza, P. De Los Rios, S. Sandin, and U. Skoglund. Freezing immunoglobulins to see them move. Proceedings of the National Academy of Sciences of the United States of America, 101(17):6466, 2004.

[101] A. A. Sousa, M. A. Aronova, Y. C. Kim, L. M. Dorward, G. Zhang, and R. D. Leapman. On the feasibility of visualizing ul 89 ll gold labels in biological specimens by STEM tomography. Journal of structural biology, 159(3):507–522, 2007.

[102] I. Tirotta, A. Mastropietro, C. Cordiglieri, L. Gazzera, F. Baggi, G. Baselli, M. G. Bruzzone, I. Zucca, G. Cavallo, G. Terraneo, F. Baldelli Bombelli, P. Metrangolo and G. Resnati, "A superfluorinated molecular probe for highly sensitive in vivo 19F-MRI," *J. Am. Chem. Soc.,* vol. 136, no. 24, pp. 8524-8527, 2014.

[103] Z. Huang, X. Li, T. Zhang, Y. Song, Z. She, J. Li and Y. Deng, "Progress involving new techniques for liposome preparation," *Asian Journal of Pharmaceuticalsciences,* no. 9, pp. 176-182, 2014.

[104] G. Bozzuto and A. Molinari, "Liposomes as nanomedical devices," *International Journal of Nanomedicine,* vol. 10, pp. 975-999, 2015.

[105] Y. P. Patil and S. Jadhav, "Novel methods for liposome preparation," *Chemistry and Physics of Lipids,* vol. 177, pp. 8-18, 2014.

[106] Y. Barenholzt, S. Amselem and D. Lichtenberg, " new method for preparation of phospholipid vesicles (liposomes) - french press," *FEBS Letters,* vol. 99, 1979.

[107] C.-H. Huang, "Phosphatidylcholine vesicles. Formation and physical characteristics," *Biochemistry,* vol. 8, no. 1, p. 344–352, 1969.

[108] R. A. Parente and B. R. Lentz, "Phase behavior of large unilamellar vesicles composed of synthetic phospholipids," *Biochemistry,* vol. 23, pp. 2353-2362, 1984.

[109] F. Olson, C. A. Hunt, F. C. Szoka, W. J. Vail and D. Papahadjopoulos, "Preparation of liposomes of defined size distribution by extrusion through polycarbonate membranes," *Biochimica et Biophysica Acta (BBA) - Biomembranes,* vol. 557, pp. 9-23, 1979.